Mapping change of functional forest traits and diversity using airborne laser scanning in the canton Aargau 2014-2019

GEO 511 Master's Thesis

Author
Charis Gretler
13-938-410

Supervised by
PD Dr. Felix Morsdorf
Prof. Dr. Ross Purves
Dr. Daniel Kükenbrink (daniel.kuekenbrink@wsl.ch)

Faculty representative
Prof. Dr. Meredith Christine Schuman

05.09.2022
Department of Geography, University of Zurich

Abstract

Forests contribute substantially to ecosystem functions and services making their ecological quality valuable. Due to climate change, monitoring diversity is becoming increasingly important to record a possible decline. High functional diversity has been related to a decreasing vulnerability to disturbances like diseases, storms and insect attacks. Remote sensing and especially LiDAR are promising methods to assess functional traits and diversity in forests and have been linked to plant diversity and ecosystem functioning. However, large-scale and multitemporal analyses using LiDAR datasets are just at the beginning. This thesis aims to assess functional forest traits and diversity metrics out of ALS data and to compare them between the years 2014 and 2019. Three morphological traits, namely canopy height, foliage height diversity and plant area index were estimated for the entire forest area of the canton Aargau under defoliated conditions. Then, functional richness and divergence were computed out of the traits. For three subregions of the canton, occlusion in the lower canopy was computed to assess if traits and diversity metrics are influenced. More complex derivations of ALS point clouds, e.g. plant area index, richness or divergence, were found to be more sensitive to external influences like different sensor and flight settings and occluded fractions of the canopy volume. Various spatial patterns of the derived traits and diversity metrics were mapped, e.g. a decrease or smaller increase in steep and high altitude regions. Richness values showed a very large global increase of 123%, which cannot solely be attributed to biotic changes, but is rather caused by the sensitivity to sensor-related factors. The results demonstrate how the development of robust methods for trait and diversity estimations is important. The incorporation of sensor and flight parameters into the estimation methods is crucial for improved performance in multitemporal analyses using ALS point clouds.

Contents

List of Figures

List of Tables

1 Introduction

Forests do not only fulfill important ecosystem services, protective and utility functions but also make a significant contribution to biodiversity as they form a relevant part of the biosphere. Approximately one third of Switzerland is forested and more than 60% of the species found in the country live in this ecosystem (Geiger et al., 2012). Due to climate change and human activity, biodiversity is declining globally which could diminish said ecosystem services (Zheng et al., 2021). Its decline is gradual, thus is hardly noticed by society (Geiger et al., 2012).

Although a positive trend in the ecological quality of forests has been observed in recent decades, there are deficits in Swiss forest biodiversity. For example, the under-representation of diverse structures, too little old and dead wood lead to a decrease in rare and endangered light- and heat-loving species (Geiger et al., 2012). For this reason, it is important to monitor and control biodiversity parameters.

At least three primary attributes of ecosystems have been recognized to constitute the biodiversity of an area: composition, structure and function (McElhinny et al., 2005; Noss, 1990). Compositional and structural features had been the main part of biodiversity inventories. But with the emergence of function biogeography, functional features are studied increasingly today (e.g. Helfenstein et al., 2022; Schneider et al., 2017; Zheng et al., 2021). Plant functional traits and diversity have been demonstrated to show a positive relationship between plant diversity and ecosystem functioning (Schneider et al., 2017). Functional diversity measures the range and distribution of what organisms do in communities and ecosystems and hence recognizes the complementarity and redundancy of species that co-occur. Thus it is assumed to better predict ecosystem productivity and vulnerability compared to species diversity (Schleuter et al., 2010).

High functional diversity has been linked to high productivity of plant communities, enhanced tree growth and ecosystem stability. Furthermore, areas with high diversity showed increased responsiveness to dynamic environmental conditions and were less vulnerable to insect attacks, diseases, fire, and storms (Schneider et al., 2017).

Functional diversity can be retrieved from different sets of functional traits that can be morphological, physiological or phenological (Helfenstein et al., 2022; Homolová et al., 2013). In this thesis we use morphological traits to derive the diversity metrics, therefore morphological functional diversity – i.e. functional richness and divergence – are referred to as functional diversity. Morphological traits are linked to the availability of light and other factors

such as the growth rate of individual trees, the productivity of the ecosystem and also the specific habitat for canopy-dwelling organisms (Ishii et al., 2004; Moles et al., 2009; Zheng et al., 2021).

Many trait-based studies exist in forested ecosystems but these studies are usually ignoring variation in tree functional traits within species as they assess trait variation and functional diversity using the combined information of species abundances and their mean traits. Therefore, mapping traits and diversity continuously can fill existing data gaps. Recent improvements in remote sensing methods allow assessing morphological functional traits directly providing a continuous map of functional diversity over a larger area (Homolová et al., 2013; Schneider et al., 2017). Especially light detection and ranging (LiDAR) with airborne laser scanning (ALS) systems are considered promising in assessing forest canopy structure variables, i.e. canopy height or plant area index (Kükenbrink et al., 2017).

Large-scale ALS acquisitions are getting more common in central Europe (Bornand, 2020, p. 3). This opens up the possibility of making multitemporal analyses of forest structure. The main objective of this Master's thesis is to map functional traits and diversity to the large area of the entire canton of Aargau and to compare two points in time - 2014 and 2019. The functional diversity mapping approach used in this thesis was introduced by Schneider et al. (Schneider et al., 2017). Morphological traits are estimated out of a LiDAR dataset that describe the canopy architecture (horizontally and vertically) and the light availability which gives important evidence of competitive light use and ecosystem productivity (Schneider et al., 2017). Out of these traits, functional diversity metrics can be calculated. The results show the possibilities and limitations of the functional diversity mapping approach by Schneider et al. (Schneider et al., 2017) at a larger scale and in a multitemporal analysis.

Occlusion has been identified as a source of uncertainty in LiDAR measurements and change detection analyses. Dense canopy tops can prevent the laser pulse from reaching lower layers in forests in ALS measurements (Korpela et al., 2012; Kükenbrink et al., 2017). The occlusion mapping approach introduced by Kükenbrink et al. (2017) uses a voxel traversal algorithm (Amanatides and Woo, 1987) to trace ALS laser pulses through a predefined voxel grid. The resulting occlusion map will be used as an explanatory variable for detected changes in the functional diversity and trait maps.

With the help of the LiDAR data, the aim is to record whether and how structural changes have taken place in the protected forest areas in the canton of Aargau. A fraction (6% as of 2015) of the total forest area is protected where natural processes have priority and no management is carried out to promote forest biodiversity (Kanton Aargau: Departement Bau Verkehr und Umwelt, 2021; Wittwer, 2016). We thus also want to compare the forested areas in the natural forest reserves to the unprotected forest areas.

The following research questions are used to guide our objectives:

1. What are the possibilities and limitations of functional diversity mapping when applied over a large area and over two points in time?
2. Further, does this approach allow:
   a. to observe structural change in forests of the canton Aargau between 2014 and 2019?
   b. to observe differences in forest structures between protected and unprotected forest areas and to detect trends within these 5 years?
3. What is the potential of using occlusion mapping in a multitemporal analysis of functional traits and diversity?

We expect the functional diversity mapping to be well applicable to the area of the canton Aargau. A possible limitation of the approach could be that the neighborhood used for calculating functional richness and divergence must be kept at a smaller scale due to the computational expenses of the large area. Also, the different sensors and flight geometries of the LiDAR acquisitions could lead to difficulties in the comparison of the measured morphological traits between both years.

We expect minor changes to be visible between 2014 and 2019. Since the forest will not renew itself completely within 5 years and there will only be a correspondingly large increase in woody material, we do not expect the changes to be too large as we are focusing on morphological traits. The largest changes are expected to come from logging or storm damage.

The nature reserves were established in places where a forest was identified as being particularly worthy of protection. Therefore, we expect slightly higher diversity metrics in the protected forest areas.

Especially in areas with high occlusion, differences between 2014 and 2019 not being explainable by other variables – e.g. topographic variables like slope, aspect, etc. – are expected. Therefore, we predict the occlusion maps to help in explaining differences between 2014 and 2019.

2   Material and Methods

2.1   Study area

The study area includes the entire canton of Aargau. It is located in the north of Switzerland and has a total area of 1403 km^2. This makes it the tenth-largest canton in Switzerland.
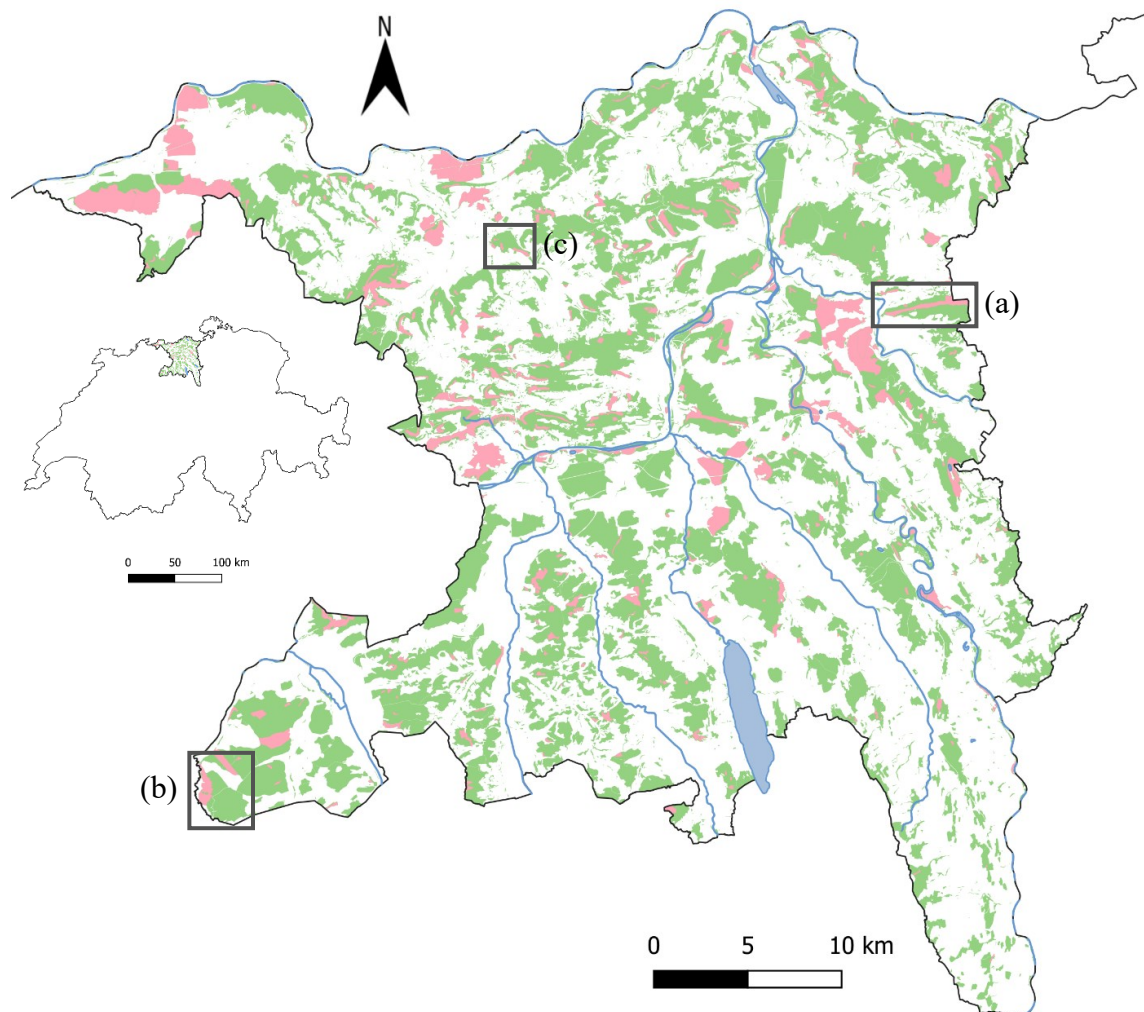
Figure 2.1: Overview of the study area (right) and where it is located in Switzerland (left).The forest reserves are indicated with light red polygons and the unprotected forest areas appear in a light green color (geodata source: swisstopo, 2022a). The locations of the three subregions, Laegern (a), Unterwald (b), and Frickberg (c), are marked with grey rectangles.

Approximately 500 km^2 is forest, which makes up about 35% of the canton's area. Most of the forests (63%) are pure or mixed deciduous forests. The predominant tree species are beech

with 32% and spruce with 26% of the forest stand (Kanton Aargau: Departement Bau Verkehr und Umwelt, 2018).

Most of the forests in Aargau belong to the biogeographical region of Aargauer Mittelland. These forests are somewhat less rich in deciduous trees than the forests belonging to the Aargauer Jura region. The forests of the Aargauer Mittelland are slightly less elevated and slightly less steep than the forests in the Aargauer Jura.

A survey by the National Forest Inventory (NFI) defined the ecologically most valuable forest areas. Since 1996, these areas have been protected to promote forest biodiversity (Wittwer, 2016). In the canton of Aargau, 40 natural forest reserves have been designated. These are large-scale forest areas (at least 20 hectares) in which no timber harvesting or forest management is allowed. Natural processes have priority, and no measures of any kind are carried out (Kanton Aargau: Departement Bau Verkehr und Umwelt, 2021).

As of 2015, around 6% of the forest area belongs to a forest reserve and is subject to a contractually agreed renunciation of use. The protected forests are richer in deciduous trees and, concerning the current stocking, also closer to nature than the unprotected forests. The most important key figures are listed in the table. (Kanton Aargau: Departement Bau Verkehr und Umwelt, 2018)

Table 2.1: Overview of the forested area of the canton Aargau.

		Forest area [ha]	Percentage of total forest in Aargau	Percentage of deciduous dominated forest area in Aargau
Biogeographical region	*Aargauer Jura*	8'342	17 %	61 %
	Aargauer Mittelland	40'728	83 %	73 %
Forest reserves and unprotected forest	*Forest reserve*	2'944[1]	6 %[1]	65 %
	Unprotected forest	46'125[1]	94 %[1]	39 %
Public and private forest	*Public forest*	38'415	78 %	61 %
	Private forest	10'655	22 %	72 %

---

[1] As of 2015

To be able to identify and discuss small-scale changes, three subregions were selected (see Figure 2.1). The subregions are the forest of Laegern, the forest in the southeast of the canton called Unterwald, and the forest of Frickberg. These three study areas were chosen because they are diverse in their attributes and spread over the canton Aargau. Every study area contains protected and unprotected forest areas and two of them, Laegern and Unterwald, are close to a NFI plot. Table 2.2 depicts the site locations and portrays the main attributes of the test areas.

Table 2.2: Overview of the main attributes of the subregion sites Laegern, Unterwald, and Frickberg.

	Laegern	**Unterwald**	**Frickberg**
Altitude [m.a.s.l.]	~450-910	~550	~480-800
Topographic characteristic	steep hill	flat	hill
Forest type	mainly deciduous and mixed forest	mainly coniferous	mainly deciduous
Area [m²]	4'390'923	4'582'052	1'621'979

2.2   Data

2.2.1   Airborne laser scanning data

For the years 2014 and 2019, three ALS datasets containing the entire area of the canton were available and provided by the Canton Aargau, Departement Bau, Verkehr und Umwelt, Abteilung Wald. The data was acquired in 2014 under leaf-off (defoliated) and leaf-on (foliated) conditions. The leaf-off data were collected from 18.03.2014 - 04.04.2014 with an LMS-Q680i RIEGL scanner. The leaf-on data was acquired from 19.06.2014-25.07.2014 with the same scanner. In 2019, only leaf-off data was collected from 23.03.2019 – 21.04.2019 with an LMS-VQ780i RIEGL scanner. All aerial surveys in 2014 and 2019 were carried out by Milan Geoservice GmbH (Kamenz, Germany).

Table 2.3: Summary of the specifications for all ALS data acquisitions in the canton of Aargau in 2014 and 2019.

	2014		2019
ALS parameter	Leaf-off	Leaf-on	Leaf-off
Acquisition date	February/March 2014	June/July 2014	March/April 2019
ALS sensor	LMS-Q680i		LMS-VQ780i
Operating platform	Airplane		
Area of coverage [km²]	~1400		
Mean operating altitude above ground [m]	600	700	1250
Scanning method	Rotating polygon mirror		
Pulse detection method	Full-waveform processing		
Scan angle [°]	±15	±15	±30
Mean point density [pts/m2]	16	30	30.8
Pulse footprint [cm]	30	35	31
Pulse repetition frequency [kHz]	300		1000
Beam divergence [mrad]	0.5		0.25
Laser wavelength [nm]	NIR		

2.2.1.1 *Preprocessing*

The raw full-waveform data was processed involving the following steps and were executed by Milan Geoservice GmbH (2020, 2014):

- Extraction of discrete laser returns into a local coordinate system using the software RiAnalyze (RIEGL)
- Transformation of the point cloud into the Swiss Cartesian coordinate system
  - 2014 data: CH-1903 (LV03)
  - 2019 data: CH-1903+ (LV95)
- Flight strip adjustment
- Filtering using the software TerraScan (TerraSolid) and classification of the point cloud into ground and vegetation
- Creation of a digital terrain model (DTM) with 0.5m resolution using the software TerraScan (TerraSolid)
- Due to the large amount of data, the LiDAR data and the DTM were divided into 1000 x 1000 m tiles.

The finished data were provided as LAS files containing a three-dimensional point cloud with planimetric coordinates, ellipsoidal heights, terrain-corrected heights, echo type, and intensity values. The DTM is provided in the GeoTIFF format.

2.2.2 Other data

The forest mixture proportion map containing the percentage coverage of broadleaved and coniferous trees is provided by the national forest inventory NFI (Waser and Ginzler, 2021), last updated on 6 April 2018. The mix rate is modeled using remote sensing methods and has a 10 m resolution.

The forest polygons were provided by Aargauisches Geografisches Informationssystem (AGIS), Departement Bau, Verkehr und Umwelt, Abteilung Wald. We used the data from 1 September 2019 for this project (AGIS, 2019).

Other general geodata like the borders of the canton as well as all rivers and lakes of the canton Aargau were provided by swisstopo (2022a), last updated 1 January 2015.

2.2.2.1 Topographic variables

All topographic variables, i.e. slope, altitude, and aspect were calculated using the digital terrain model provided by the LiDAR acquisition of 2019. Slope and aspect were computed using the *terra* package for R (Hijmans, 2022; R Core Team, 2022) (*terrain()* function) according to Horn (1981). Both variables are calculated using 8 neighboring cells with a 2 m resolution and output a theoretical range of 0-360° (aspect) and 0-90° (slope).

2.2.3 Forest mask

As the LiDAR data is very large, it was important to clip the LiDAR point clouds to the forest extent before processing to reduce computational power and processing time. Two forest masks were used for this project. A fine mask was created to clip the LiDAR data before calculating the functional diversity metrics and all forest traits. A very coarse mask was used to clip the ALS data before the voxel traversal algorithm. The LAS files were clipped using the software LAStools (Isenburg, 2021). The generation of these masks is outlined in detail in the following two subsections.

2.2.3.1 Mask for functional diversity metrics

Additionally to the reduction of computational power and time, to calculate functional richness and divergence, the forest boundary must be well defined as both metrics use neighborhood operations. Morphological richness is especially sensitive to outliers, therefore all non-forest pixels needed to be excluded by assigning the value *NaN*.

To achieve this, the data containing *"Waldareale"* forest polygons was obtained from the canton of Aargau. It is a derivative of the static forest boundary converted to polygons. We used the updated forest polygons from 1 September 2019 for both LiDAR datasets to use the same forest extent and have comparable results.

2.2.3.2   *Mask for Voxel Traversal Algorithm*

To reduce the computational effort for the Voxel Traversal Algorithm, the ALS dataset of the entire Canton was clipped by a forest mask. It was created in QGIS (QGIS.org, 2022) using the vector dataset of the forest area *"Waldareale"*. It is the same dataset as above.

The Voxel Traversal Algorithm traces the laser pulse until it hits the ground. To ensure that the algorithm can use the entire pulse as input, the dataset has to include a buffer that is large enough to cushion all pulses of larger scan angles. There is the possibility that a pulse is sent out outside of the forest and still hits the ground inside the forest (see Figure 2.2). For this reason, we chose a buffer of 20 meters around the forest to ensure that the complete pulse is included in the input dataset.
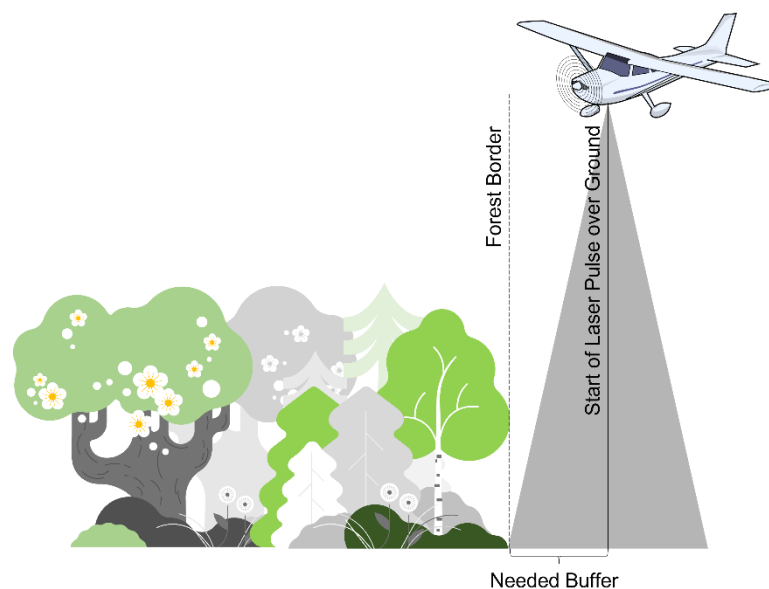
Figure 2.2: Possible ALS geometry at forest borders.

2.3 Functional traits and diversity metrics

2.3.1 Functional traits

It is crucial to choose appropriate traits to calculate functional diversity metrics. These traits should not be too highly correlated to each other and represent different facets of forest properties (Zheng et al., 2021). To assess functional richness and divergence, three morphological forest traits were chosen. We used the same morphological traits as Schneider et al. (Schneider et al., 2017) which are canopy height (CH), foliage height diversity (FHD), and plant area index (PAI).

These three morphological traits are relevant for plant ecosystem function and can be assessed with airborne remote sensing methods (Homolová et al., 2013; Schneider et al., 2017, 2014). Our selected morphological traits relate to the three primary components of variation in canopy space: canopy height, vertical layering and openness (Fahey et al., 2019). These structural axes have been linked to ecosystem functioning and are commonly used to differentiate between vegetation types. They have also been used to characterize the structural diversity of the canopy (Coops et al., 2016; Zheng et al., 2021). Figure 2.3 represents the conceptual model of the canopy structure introduced by Fahey et al. (2019).
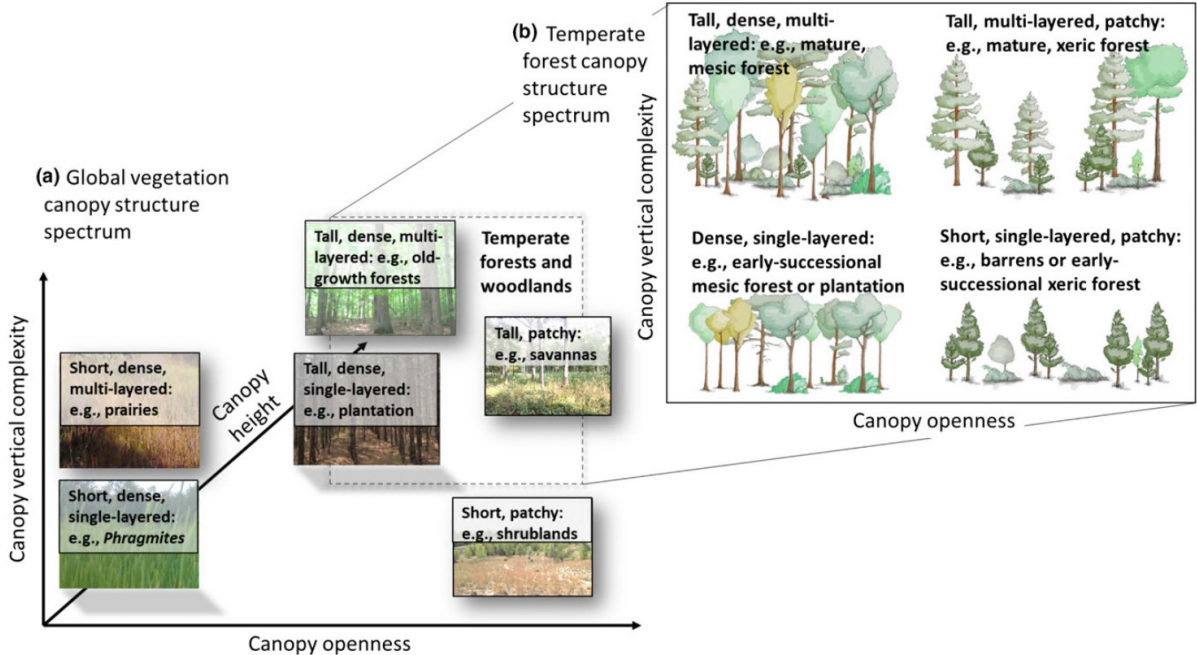
*Figure 2.3: Conceptual model of the canopy structure space illustrating **(a)** the global spectrum and **(b)** the temperate forest structure spectrum (illustration by Fahey et al. (2019)).*

2.3.1.1 Canopy height

Plant height has been shown to possess a central role in plant ecological strategy, as it determines how well a plant can compete for light which affects the carbon gain strategy of a species (Moles et al., 2009; Stahl et al., 2014). Furthermore, CH has been related to various species' abundances (Coops et al., 2016).

CH is one of the most common derivatives of ALS data because it is easy to measure and shows high accuracy with less bias compared to field-based measurements (Coops et al., 2016). With these advantages and its high relevance for ecosystem functioning, CH is an important trait for structural diversity. It represents the first axis of the canopy structure spectrum by Fahey et al. (2019). We calculated it as the vertical distance between the highest laser return representing the canopy top and the corresponding ground defined by the DTM. CH was derived from the LiDAR point cloud data on a grid with a 2 m resolution.

2.3.1.2 Foliage height diversity

FHD functions as a metric of variation and the number of canopy layers, representing the canopy vertical complexity, which forms the second axis of the canopy structure model (Fahey et al., 2019; Schneider et al., 2017). It is a trait most often used to describe stand structure through its vertical complexity (McElhinny et al., 2005; Tanabe et al., 2001). FHD has been related to biomass growth, biodiversity and habitat suitability (Seidel et al., 2016). It has been the first where a quantitative relationship was found between a structural element and a measure of faunal diversity (McElhinny et al., 2005): MacArthur and MacArthur (1961) reported a positive relationship between bird species diversity and FHD.

FHD was calculated using the Shannon-Wiener index as follows:

$$FHD = -\sum_i p_i \cdot \log_e p_i, \tag{1}$$

where p_i is the proportion of the foliage and stems lying in the ith layer. We used a 1 m vertical interval and excluded the lowest 3 m (NFI definition of minimal forest height) to separate the understory from the canopy. FHD was mapped on a 2 x 2 m grid.

Because FHD relates to how different the layers are in density and how many layers exist, it is expected to have some correlation to CH. CH defines the maximum layers possible with respect to the vertical interval.

McElhinny et al. (2005) denote FHD as a metric with a certain ambiguity, as no standard method has been established and the chosen layer thickness has often been arbitrary. In this thesis, we compare two datasets with each other, therefore our traits are used in a relative manner that mitigates said problem. A different vertical resolution only changes the magnitude of observed change (see Appendix Figure A.1), which also has been found by Leiterer et al. A 1 m vertical resolution was also used in studies by Seidel et al. (2016) and Tanabe et al. (2001).

2.3.1.3 *Plant area index*

When describing canopy structural characteristics, the plant area index (PAI) is an important morphological trait. Chen et al. (1991) defined PAI of a stand as "half the total area of leaves and woody materials per unit ground area". In forests, PAI is retrieved rather than the leaf area index (LAI) due to the existence of woody structures (Liu et al., 2021) and corresponds to the term *effective leaf area index (LAI$_e$)* (Solberg et al., 2009). LAI, a much-studied variable, is considered an important climate and biodiversity variable, as it influences photosynthesis, transpiration and rain interception (Bojinski et al., 2014; Liu et al., 2021; Skidmore et al., 2015).

Estimating the LAI or PAI respectively has been a challenge. Passive sensors have problems distinguishing influences from ground vegetation, shading and saturation at high LAI values, especially in coniferous forests (Solberg et al., 2009). Synthetic aperture radar (SAR) shows different problems, such as variable moisture conditions and rugged terrain that influence the trait estimation (Solberg et al., 2009). ALS was found as an alternative to said methods based on the Beer-Lambert law which showed promising results for PAI estimation compared with ground-based methods (Arnqvist et al., 2020).

Different approaches to computing the PAI are available, all of them having some advantages and disadvantages. Because we compare two LiDAR datasets with each other being recorded with different sensors, a robust method in PAI estimation is needed. Otherwise, a comparison cannot be conducted. Three approaches have been tested for our two datasets, where all methods are based on the Beer-Lambert law of light extinction.

1. Ray-tracing approach (RTA) by Kükenbrink et al. (Kükenbrink et al., 2015), implemented in MATLAB

2. First returns ratio approach (FR) without ray-tracing by de Almeida et al. (2019), implemented in the *leafR* (de Almeida et al., 2022) package in *R*

3. Scaled returns ratio (SR) approach by Arnqvist et al. (2020), implemented in MATLAB and Python

1. Ray-tracing approach (RT)

Kükenbrink et al. (Kükenbrink et al., 2015) use a voxel-based PAI estimation, where the scene is divided into a three-dimensional voxel grid. Each laser pulse is traced through the voxel grid, using a voxel traversal algorithm (the same as in Chapter 2.4). The number of pulses traversing the voxel with a laser return (N_{hit}) and without (N_{miss}) was recorded. By using the N_{hit} and N_{miss}, the penetration rate of the laser pulse through the voxel can be estimated and using the Beer-Lambert law of light extinction, the PAI can be estimated:

$$PAI = -\frac{1}{k} \cdot ln\left(\frac{N_{miss}}{N_{miss} + N_{hit}}\right), \qquad (2)$$

where k is the extinction coefficient defined by:

$$k = \frac{G(\theta, \theta_L)}{cos\,\theta} \qquad (3)$$

The leaf normal angle (θ_L) and the incidence angle (θ) of the pulse are affecting the projection of foliage area (G).

2. First returns ratio approach (FR)

De Almeida et al. (2019) used a similar approach but worked under the assumption that all pulses are vertically incident. With this, no computationally expensive voxel traversal algorithm was needed, as the passage of the laser pulses was tracked solely within the voxel columns. PAI is computed as follows:

$$PAI = \sum PAD, \qquad (4)$$

where PAD (plant area density) is the vertical distribution of plant elements in the *i*th canopy layer applying the MacArthur-Horn equation:

$$PAD_i = ln\left(\frac{pulses.in_i}{pulses.out_i}\right) \cdot \frac{1}{D_z} \cdot \frac{1}{k} \qquad (5)$$

D_z is the vertical resolution of the canopy layer, *pulses.in$_i$* are the number of pulses entering the voxel and *pulses.out$_i$* are the number of pulses passing through the voxel. Here, only first returns can be considered because the MacArthur–Horn approach works under the assumption that each pulse represents an independent canopy probe. Therefore, the number of emitted pulses has to be equal to the number of reflections. This leads to disregarding a large part of the dataset. Furthermore, it is expected to have a high site-to-site variability due to the method being sensitive to the ratio of the lidar footprint and the mean gap size in the canopy (Arnqvist et al., 2020).

3.   *Scaled returns ratio approach (SR)*

Arnqvist et al. (2020) proposed an approach combining two methods. The first one is an improved method first introduced by de Almeida et al. (2019). They tried their FR approach on a dataset using all returns not only the first returns in their supplementary material, which enables to use the entire dataset. On the other hand, this approach has the disadvantage that it has a poor theoretical background and needs further improvement. Arnqvist et al. (2020) modified the approach by using the scan angle in their computation.

The second approach is the method by Hopkinson and Chasmer (2009) which incorporates intensity values. The method presumes that the intensity values depend on the vegetation density from a vertical forest section and that the albedo for ground and vegetation is equal (Arnqvist et al., 2020). The main advantage is that it uses all returns and avoids many of the FR drawbacks. Its disadvantage is the assumption that the albedo for ground and vegetation is identical which is most problematic in not-so-dense forests.

By combining the two methods above, it is possible to combine their respective strengths and mitigate many of their problems. It estimates PAI values by the following four steps. First, it identifies all returns and scales them according to their intensities. The mathematical expression of the individual beam scaling is as follows:

$$r_s = \frac{I_{i_r}}{\sum_{i_r=1}^{N_r} I_{i_r}}, \qquad (6)$$

where r_s is the rescaled intensity of the i_rth return of the pulse, where the original intensity is I_{i_r}. The scaling factor is the sum of all intensities between the first and the maximal return

number (N_R) of the pulse. After the intensities are scaled, the approach estimates the ratio of incoming and outgoing radiation in a second step:

$$\frac{\sum_{i=1}^{k} R_i}{\sum_{i=1}^{k+1} R_i} = \frac{\sum_{i=1}^{k} r_{s_i}}{\sum_{i=1}^{k+1} r_{s_i}}, \tag{7}$$

where R is the radiation reflected at height z. Thirdly, it calculates PAD using the following equation:

$$\overline{PAD}\Delta z = -\frac{\cos \theta_1}{\mu} \, ln \left(\frac{\sum_{i=1}^{k} R_i}{\sum_{i=1}^{k+1} R_i}\right), \tag{8}$$

where θ_1 is the pulse-specific scanning angle of incoming radiation and μ is the extinction coefficient with a default of $\mu = 0.5$, as a spherical distribution of the reflecting vegetation surfaces is assumed. The PAI is then calculated using Eq. (4) in the last step.

Due to this weighting, the SR method is either equivalent to the FR method or the Hopkinson and Chasmer (2009) method when there is a first return only dataset or only one pulse over the binning area is available, respectively.

Suitability for our ALS data

The RT showed promising results when tested on the ALS datasets of 2014 and 2019. We used a 2 x 2 m resolution with 0.5 m vertical binning. The main drawback of the approach is the long computational time of the voxel traversal algorithm.

The FR has the advantage of being faster which is important because we need to compute the PAI for a large study area. However, using only the first returns and maximal scan angle of 5° for both years made the disadvantage of the FR method visible: The filtering of our point cloud resulted in large gaps without laser returns in the study area because we did not have enough pulses to cover the entire study area after filtering. For this reason, the FR method cannot be used with our datasets.

Because of the large amount of processing time of the RT approach and the FR approach being unsuitable for our datasets, we decided to use the SR approach. It considers many of the standard recorded attributes of ALS data (Arnqvist et al., 2020): position (x, y, z), intensity (I), return number (i_r), number of returns per pulse (N_R), ground classification, scanning angle (θ_1) and is thus less affected by the different sensors.

μ can be adapted to fit the PAI to improve the estimation of the area of interest. We left it on default because no reliable ground estimates were available for 2014 and 2019 and we are focusing on differences between the two points in time. PAD is calculated for 0.5 m height intervals on a 2 x 2 m grid, where the resulting PAI matches the resolution of the other two calculated traits, i.e. CH and FHD.

2.3.1.4 Functional trait post-processing

The three morphological traits are clipped to the exact forest borders. Additionally, the upper and lower extremes were removed to keep only the 1st and 99th percentile as shown in the histograms. Lastly, the traits needed to be linearly rescaled to values between 0 and 1 to be used as input for the functional richness and divergence algorithm.

2.3.1.4.1 Temporal normalization

Despite having relatively robust methods for determining the morphological traits, a systematic bias between 2014 and 2019 FHD and PAI is detected. Since FHD and PAI are dependent on pulse density and sensor instrument, a normalization between the two recording times had to be carried out to ensure that the traits and the resulting diversity metrics are comparable. CH being the simplest and most accurate trait was not affected and no temporal normalization had to be done. A simpler and a more complex approach for the temporal normalization were tested and are described in the following sections.

We changed the morphological traits of 2014, not 2019, because a larger uncertainty of these values is expected due to lower pulse density and flight strip overlaps. Our first and simpler approach assumes the global mean of each trait not to change between 2014 and 2019. This allows us to still observe local changes in trait distribution but has the drawback that global change is not observable anymore. A correction factor f was calculated for each trait which was then used to normalize:

$$T_{14corr} = T_{14orig} * f_\mu, \qquad f_\mu = T_{\mu19orig}/T_{\mu14orig} \qquad (9)$$

where T_{14orig} is the value of the uncorrected trait 2014, f_μ is the mean correction factor and T_{14corr} is the normalized trait used for further computation of the functional diversity metrics. $T_{\mu19orig}$ is the mean of the uncorrected trait 2019 and $T_{\mu14orig}$ the mean of 2014.

A more complex approach was also tested. On the ground of the Swissgrid switching substation known as Star of Laufenburg (see Appendix Figure A.14), many masts, lines, etc. that have a tree-like structure are observable. They were used as persistent scatterers since these pylons did not change in the 5 years between the recording dates. We estimated two correction factors to achieve almost identical boxplots of the trait in the area. Then they can be used to normalize the trait maps of the entire canton. The following equation was applied:

$$T_{14corr} = T_{14orig} * f + i \,, \tag{10}$$

where f and i are the correction factors estimated from the trait values at the Swissgrid station. This method has the advantage that a global mean change of the trait is allowed and compared to the first method not only corrects the mean of the trait but also its dispersion.

Unfortunately, the corrected FHD and PAI trait values are not satisfactory, because they showed impossible values in far away regions in the study area, indicating that the estimated f and i factors are not applicable over the entire area of the canton Aargau. More persistent scatterers distributed over the entire study area might help to improve the correction factor estimate. This would need to be subject of further studies.

We tried to improve the temporal normalization outcome of the global mean method by using Eq. (10) also on the global mean, but the results still are less promising than with Eq. (9) based on visual inspection of histograms, boxplots, and difference maps.

2.3.2   Functional diversity

For the detection of the effects biodiversity has on ecosystem functioning and services, functional diversity has been recognized as an effective diversity measure that allows the observation of ecosystem functioning using remotely sensed data (Helfenstein et al., 2022, p. 2). Functional diversity is defined as the diversity of traits where they are used to describe the diversity of species niches in trait space (Ahmed et al., 2018, p. 487). The functional diversity indices can use one functional trait (one-dimensional) or multiple functional traits (multi-dimensional/multivariate) as input. It is recommended to prefer multivariate indices, thus they are used more often. As we used the approach by Schneider et al. (2017), a set of three traits were selected and a multidimensional space is created in which each point represents a species, individual or pixel where each coordinate corresponds to a measured trait. (Ahmed et al., 2018; Schleuter et al., 2010)
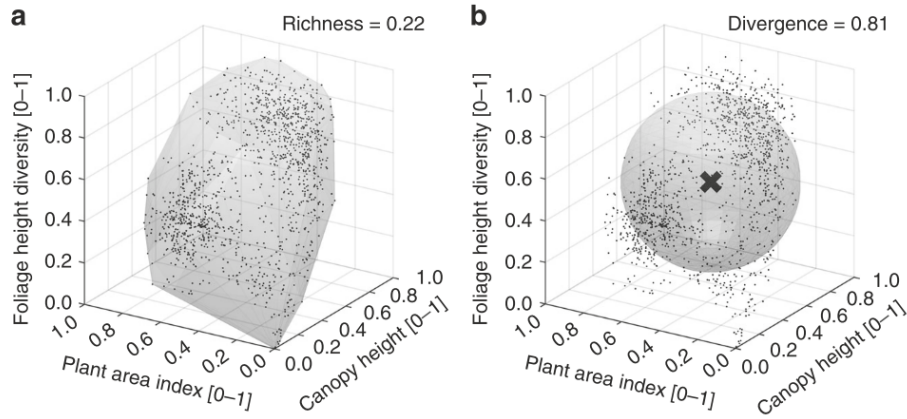
*Figure 2.4: Two aspects of functional diversity in a three-dimensional trait space based on morphological forest traits (canopy height, foliage height diversity and plant area index). The shaded volumes refer to **(a)** functional richness and **(b)** functional divergence of a circular area with a radius of 120 m. (illustration by Schneider et al. (2017))*

Different multivariate functional diversity indices represent different aspects of trait distributions and can be used as a subsidiary (Zheng et al., 2021). The two chosen indices are functional richness and functional divergence. Schneider et al. (2017) also computed functional evenness, which is not considered in this thesis because functional divergence and evenness both describe adequately how the samples are spread within the community niche (Helfenstein et al., 2022). The more complex metric could not be examined because of the long computation times for the large study area.

Functional richness measures the community niche extent using the convex hull of the occupied functional space (Figure 2.4, a). Its disadvantage may be a strong influence by outliers.

Functional divergence measures the community niche density which describes how sample points are spread with respect to the center of gravity (Figure 2.4, b) (Helfenstein et al., 2022; Schneider et al., 2017; Villéger et al., 2008). Divergence is calculated based on Villéger et al. (2008):

$$\Delta|d| = \sum_{i=1}^{S} \frac{1}{S} \cdot \left| dG_i - \overline{dG} \right|, \tag{11}$$

$$FDiv = \frac{\overline{dG}}{\Delta|d| + \overline{dG}} \tag{12}$$

It is calculated using the number of pixels S mapped in the functional space where dG_i is the Euclidean distance between the ith pixel and the center of gravity (dG). For example, FDiv = 1 would mean that all pixels lie on a sphere around the center of gravity. Lower values of functional diversity are achieved if the pixels lie dispersed in the trait space. An example of the behavior of functional richness and divergence is depicted in Figure 2.5.

(a) Functional Richness (*FRic*)
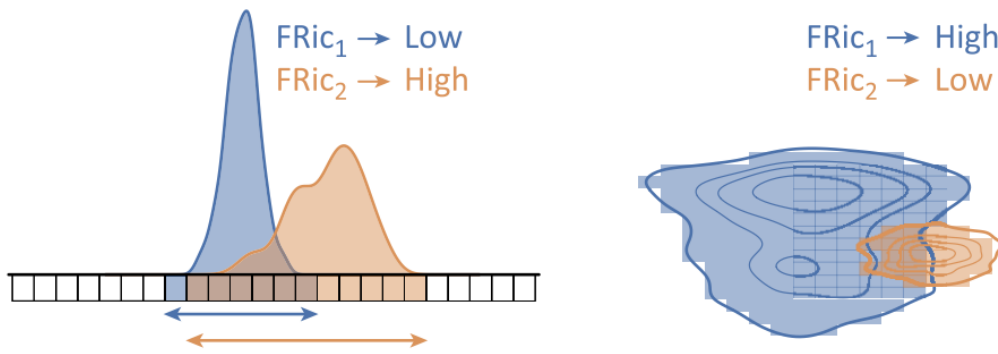
(b) Functional Divergence (*FDiv*)
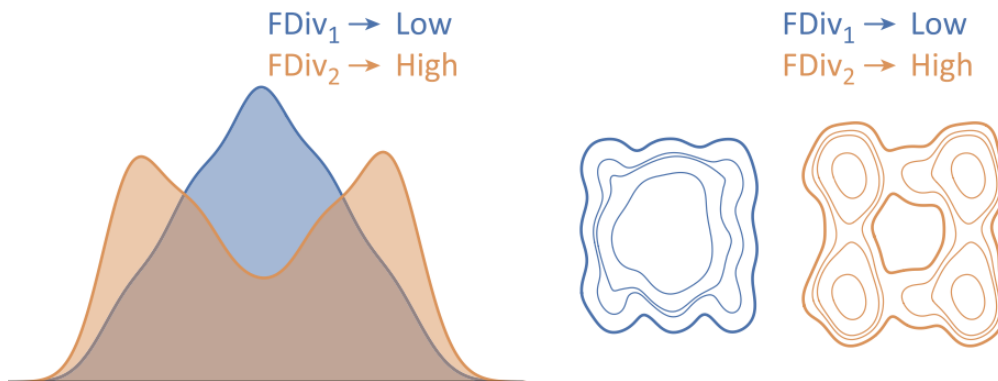
*Figure 2.5: Concepts of functional diversity in a two-dimensional trait space illustrating differences (low/high) between **(a)** functional richness and **(b)** functional divergence. (adapted from Carmona et al. (2016))*

2.4   Occlusion mapping

When working with ALS data, especially when estimating complex forest traits, a major source of uncertainty has been found in the view obstruction of dense canopy tops (Korpela et al., 2012; Kükenbrink et al., 2017). This results in the laser pulse not reaching lower parts of the canopy leading to an incomplete dataset. The occluded part of the forest canopy is not evident when analyzing the point cloud. To assess the occurring occlusion, Kükenbrink et al. (2017) developed a method to calculate the occlusion of an ALS dataset, which is used in this thesis.

Each laser pulse is traced to reconstruct its path via ray-tracing. For this ray-tracing, a voxel traversal algorithm introduced by Amanatides and Woo (1987) is used. It is a computationally inexpensive way to trace the laser pulse through a partitioned 3D space.

Space is divided into voxels which are rectangular cubes. Then, each laser pulse is traced through this voxel grid. A pulse is represented as a vector:

$$\vec{x} = \vec{p_0} + \vec{td} \, , \tag{13}$$

where the distance along the vector $\vec{d}$ to reach the point $\vec{x}$ is defined by t. The voxel traversal algorithm has two stages, the initialization, and the incremental traversal phase. During the initialization phase, the voxel where the laser pulse first intersects the voxel grid is identified and its x, y, and z indices are stored. The stepping in x-, y-, and z-direction (1 or -1) is defined by the ray crossing the voxel boundaries according to the signs of the x, y, and z components of $\vec{d}$. In the incremental traversal phase, the value of t at the crossing of the voxel border is determined for each of the three dimensions. The minimum value defines how far the ray can travel without leaving the voxel. Lastly, also for all dimensions, the length (units of t) the ray must travel to reach the width of the voxel is determined. A more detailed explanation of the voxel traversal algorithm can be found in Amanatides and Woo (1987). The pulse diameter is assumed to be infinitesimally small to simplify the process. The implications of this assumption are considered to lead to only a small overestimation of the occlusion (Kükenbrink et al., 2017).

For each voxel, the number of hits (N_{hit}), the number of misses (N_{miss}), and the number of occluded (N_{occ}) rays are recorded. If a traversed voxel has a laser return inside, N_{hit} is increased by 1, if it has no return inside, N_{miss} is increased. If a voxel is traversed after the pulse's last return, N_{occ} is increased. If the pulses reach the voxel grid border or the terrain (defined by the DTM), the voxel traversal algorithm is stopped.

After all pulses are traced through the voxel grid, a voxel classification is established. Possible classes are *observed voxels* that have a laser return inside, *empty voxels* which do not have a return inside, *occluded voxels*, which are hidden from the sensor, and *unobserved voxels*, which are unobserved by the laser sensor and are never traversed by the voxel traversal. The classification is depicted in Table 2.4.

Table 2.4: Classification of voxel cells after Kükenbrink et al. (2015) and Bienert et al. (2010).

	Number of		
	Returns (N_{hit})	Penetrations (N_{miss})	Occlusions (N_{occ})
Observed	>0	≥0	≥0
Empty	=0	>0	≥0
Occluded	=0	=0	>0
Unobserved	=0	=0	=0

Occluded voxels would have been traversed by the pulses, but all energy has already been reflected due to interactions with the forest canopy. Unobserved voxels can occur at the border of the flight swath or when the pulse density is too low.

We chose a voxel size of 0.5 m due to the fact the ALS dataset is recorded under leaf-off conditions. With a larger voxel size, it would not be possible to observe a big part of the occlusion in our dataset. As the last step, the occlusion 3D map was processed to represent the fraction of occluded canopy volume over the surface area (2 x 2 m grid) that matched the trait and functional diversity maps.

Initially, the entire canton Aargau was supposed to be mapped. It became clear that the computational expense to ray-trace 1403 km^2 is immense although the ray-tracing algorithm used is relatively economical. The large area combined with a relatively small grid made it very hard to follow through. We parallelized the process using the ScienceCluster by S^{3}IT where each tile covering an area of 1 km^2 was submitted in a separate job. Unfortunately, many tiles did not run smoothly, and it was not possible to debug all of them. Thus, occlusion maps are only computed for the three subregions Laegern, Unterwald, and Frickberg.

2.5 Comparison of trait and diversity maps

In the first step, the trait and diversity maps are grouped by different aspects, slopes, forest mix rates, and altitudes and displayed in a set of boxplots. The forest reserves and the unprotected forest areas are contrasted with each other to detect differing trait and diversity distributions. Also, both recording years are compared to each other. The tables below depict the classification of the topographic and forest variables. The classified maps can be found in Appendix Figure A.10.

Table 2.5: Aspect classification.

Value	Description	Aspect [°]
1	North	315-44
2	East	45-134
3	South	135-224
4	West	225-314

Table 2.6: Forest mix rate classification after Brändli et al. (2020).

Value	Description	Deciduous tree mix rate [%]
1	pure coniferous	0-10
2	mixed coniferous	11-50
3	mixed deciduous	51-90
4	pure deciduous	91-100

Table 2.7: Slope classification after KA5 (Sponagel, 2005).

Value	Description	slope [°]
1	flattish	<2
2	weakly inclined	2-<5
3	medium inclined	5-<10
4	heavily inclined	10-<20
5	steep	>20

Table 2.8: Altitude classification. A vertical bin height of approximately 100 m is chosen, resulting in 6 altitudinal belts from 255-910 m.a.s.l.

Value	altitude [m.a.s.l.]
1	255-350
2	351-450
3	451-550
4	551-650
5	651-750
6	751-910

Table 2.9: Occlusion classification.

Value	Description	Occluded canopy volume [%]
1	no occlusion	<5
2	low occlusion	5-<25
3	medium occlusion	25-<50
4	heavy occlusion	>50

Table 2.10: Occlusion change classification.

Value	Description	Value Occlusion map 2019- 2014
1	no occlusion change	-0.05-<0.05
2	low occlusion change	-0.25-<0.05 & 0.05-<0.25
3	medium occlusion change	-0.5-<0.25 & 0.25-<0.5
4	large occlusion change	< -0.5 & > 0.5

2.5.1 Analysis of variance

To test whether the trait and diversity metrics can be explained by the topographic and forest variables, and above all, if occlusion influences the outcomes of traits and diversity metrics, we conducted an analysis of variance with a type-I sum of squares, like Schneider et al. (2017) and followed their workflow. Due to high computational expenses and not having the occlusion map for the entire canton, not the entire area of the canton Aargau could be investigated. The test areas are the region of Laegern, the region in the southeast of the canton Unterwald, and the region of Frickberg.

We aggregated the data to a 30 m x 30 m grid using the mean. This is the size we used to compute the diversity metrics, where the moving window had a radius of 30 m. We had the traits, CH, FHD, and PAI and the diversity metrics, richness and divergence, and the associated change maps as the dependent variables which are all continuous. The independent variables were altitude, slope, forest mix rate, occlusion, and point density as continuous variables and aspect as the only categorical variable like Schneider et al. (2017). We used the aspect classification from Table 2.5 but reduced the categories such that only northern, southern, and other slopes remained. In the aggregation process, a simple majority was used for the variable aspect.

Because we work with spatial data, we had to cope with spatial autocorrelation. A spatial simultaneous autoregressive error model estimation was used to fit a generalized linear model (Chun and Griffith, 2013; Schneider et al., 2017). We used the function *errorsarlm* of the *spatialreg* package in R (Bivand and Piras, 2015). It has the form:

$$y = X\beta + u, \quad u = \lambda W u + \varepsilon, \tag{14}$$

where y is the vector of the dependent variable, X a matrix of the independent variables, β is the parameter vector of regression coefficients, λ is the spatial error parameter, W is a fixed spatial weights matrix and ε is the error of the regression model.

We investigated if the traits and diversity metrics can be explained by altitude, slope, aspect, forest mix rate, occlusion, and point density. As a next step, we explored if the mapped change of the traits can be explained by occlusion and point density. To explain the change of richness and divergence, we also used the change maps of the individual traits as explanatory variables, additionally to occlusion and point density, to see if certain traits have a larger influence on FRic and FDiv than others. In Table 2.11, the used regression equations are depicted.

Table 2.11: Equations used in the generalized linear model.

CH2014	~ altitude + slope + aspect + forest_mix + occlusion2014 + pt_density2014	
FHD2014	~ altitude + slope + aspect + forest_mix + occlusion2014 + pt_density2014	
PAI2014	~ altitude + slope + aspect + forest_mix + occlusion2014 + pt_density2014	*Traits and diversity metrics 2014*
FRic2014	~ altitude + slope + aspect + forest_mix + occlusion2014 + pt_density2014	
FDiv2014	~ altitude + slope + aspect + forest_mix + occlusion2014 + pt_density2014	
CH2019	~ altitude + slope + aspect + forest_mix + occlusion2019 + pt_density2019	
FHD2019	~ altitude + slope + aspect + forest_mix + occlusion2019 + pt_density2019	
PAI2019	~ altitude + slope + aspect + forest_mix + occlusion2019 + pt_density2019	*Traits and diversity metrics 2019*
FRic2019	~ altitude + slope + aspect + forest_mix + occlusion2019 + pt_density2019	
FDiv2019	~ altitude + slope + aspect + forest_mix + occlusion2019 + pt_density2019	
CH_diff	~ occlusion_diff + pt_density_diff	
FHD_diff	~ occlusion_diff + pt_density_diff	*Trait change*
PAI_diff	~ occlusion_diff + pt_density_diff	
FRic_diff	~ CH_diff + FHD_diff + PAI_diff + occlusion_diff + pt_density_diff	*Diversity change*
FDiv_diff	~ CH_diff + FHD_diff + PAI_diff + occlusion_diff + pt_density_diff	

3 Results

3.1 General traits and diversity metrics

Three morphological traits were computed for the entire forested study area of the canton Aargau. We estimated CH, FHD, and PAI using the leaf-off ALS point clouds recorded in March/April 2014 and February/March 2019. The traits were mapped on a 2 x 2 m grid.

All maps are available at *https://drive.switch.ch/index.php/s/SpW9PPUFv0SW8qD*.

3.1.1 Functional traits

The average normalized CH $\pm$ standard deviation (values between 0 and 1, where 0 is the lowest canopy height (*2014:* CH_{min} = 0.21 m, *2019:* CH_{min} = 0.04 m) and 1 is the maximum canopy height (*2014:* CH_{max} = 42.35 m, *2019:* CH_{max} = 43.20 m)) was 0.49±0.23 and 0.47±0.24 in 2014 and 2019 respectively. FHD showed a mean of 0.56±0.18 and 0.56±0.25, PAI 0.28±0.14 and 0.28±0.17. Global statistics of all traits before normalization are visible in Appendix Table A.1. The CH and FHD mean values of protected forest areas are slightly higher compared to unprotected forest areas. PAI mean values are similar in 2014 and 2019 (see Table 3.1).

Table 3.1: Global statistics of functional traits for nature reserves (NR) and unprotected forest areas (UF) 2014 and 2019 after normalization.

		CH		FHD		PAI	
		2014	*2019*	*2014*	*2019*	*2014*	*2019*
Mean value	*NR*	0.5	0.49	0.57	0.58	0.28	0.27
	UF	0.49	0.47	0.56	0.56	0.28	0.28

The resulting histograms of all traits after normalization from 2014 and 2019 are depicted in Figure 3.1. While CH had similar distribution and maxima in 2014 and 2019, FHD and PAI showed differences between both years. In 2014, FHD had its maximum at ~0.8 and PAI at ~0.45. In 2019, FHD peaked at ~0.75 and PAI at ~0.3 and their dispersion was wider.
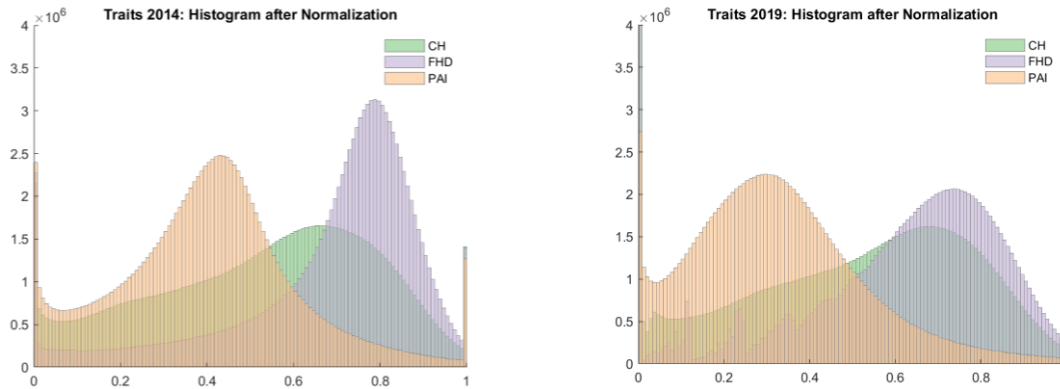
Figure 3.1: Morphological trait histograms of 2014 (left) and 2019 (right) after normalization.

3.1.2 Functional diversity metrics

In 2014 and 2019, functional richness values showed a mean and standard deviation of 0.09±0.04 and 0.19±0.09, respectively, and were thus much larger than in 2014. Functional divergence showed more constant values for both years, their mean and standard deviation values were 0.69±0.02 and 0.7±0.03. Divergence had the same mean values in nature reserves and unprotected forest areas, but functional richness revealed higher means in both years in the unprotected forest (see Table 3.2).

Table 3.2: Global statistics of functional diversity metrics for nature reserves (NR) and unprotected forest areas (UF) 2014 and 2019.

		Minimal value		Mean value		Maximal value	
		NR	*UF*	*NR*	*UF*	*NR*	*UF*
FRic	*2014*	0.00	0.00	0.08	0.09	0.36	0.44
	2019	0.00	0.00	0.17	0.20	0.56	0.65
FDiv	*2014*	0.51	0.48	0.69	0.69	0.91	1.00
	2019	0.53	0.51	0.70	0.70	0.87	0.92

3.1.3 Correlations between traits and diversity metrics
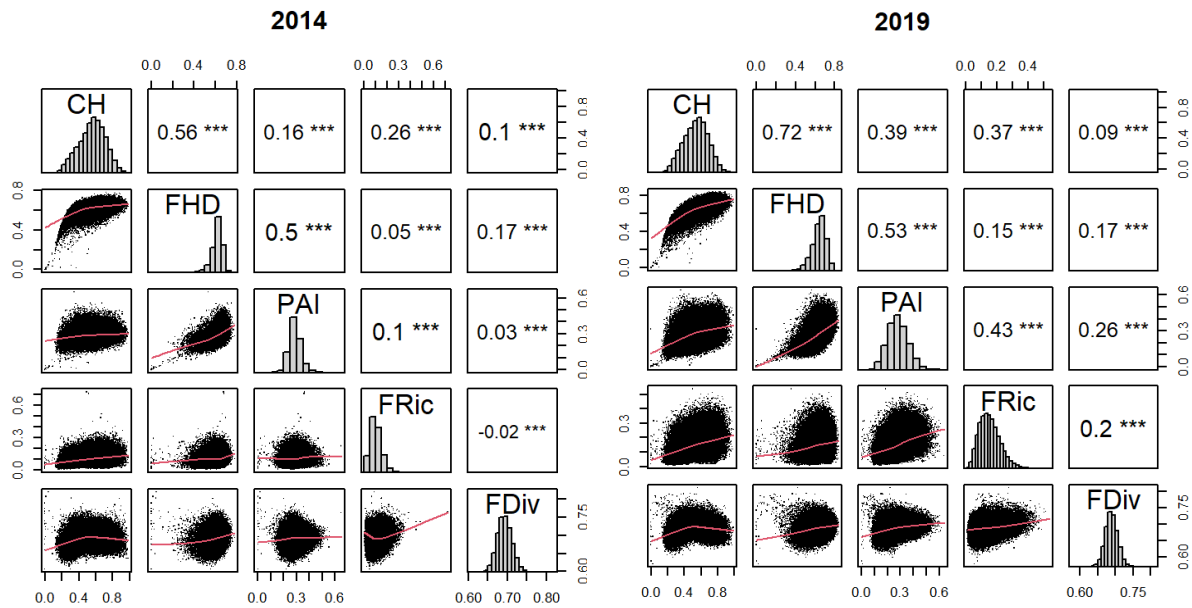
Figure 3.2: Correlation matrix of functional traits with scatterplots (lower panel) and histograms (diagonal panel). Correlation coefficients (upper panel) are scaled according to significance (*** = significance level 0.001).

All traits were significantly positively correlated (see Figure 3.2). In 2014, CH and FHD were correlated with $r = 0.56$, in 2019 with $r = 0.73$. The correlation between CH and FHD was relatively high, as expected, and in 2019 it was even a bit higher than in 2014. CH and PAI were correlated with $r = 0.16$ and $r = 0.39$ in 2014 and 2019, respectively. Therefore, they showed a weak to medium correlation in both years. CH and PAI had the largest difference in correlation between both study years, where the correlation was much stronger in 2019 than in 2014. FHD and PAI correlated with $r = 0.50$ in 2014 and $r = 0.53$ in 2019 and thus were displaying the least increase in correlation.

FRic and FDiv showed only weak correlations between each other (*2014: r = -0.02, 2019: r = 0.2*) and the functional traits. In 2019, the correlations were stronger between the traits and FRic and FDiv. PAI and FRic correlated the most in 2019 ($r = 0.43$), while in 2014 their correlation was much weaker ($r = 0.1$). PAI and FDiv did have a much lower correlation in 2014 ($r = 0.1$) compared to 2019 ($r = 0.43$).

3.2   Spatial patterns

3.2.1   Functional traits

In Figure 3.3, the three morphological traits are mapped as a red, green, and blue color composite with our normalized traits (similar to the mapping in Schneider et al. (2017)). Red areas are defined as CH > FHD, CH > PAI, green areas show trait values of FHD > CH and FHD > PAI, and blue areas as PAI > CH, PAI > FHD.
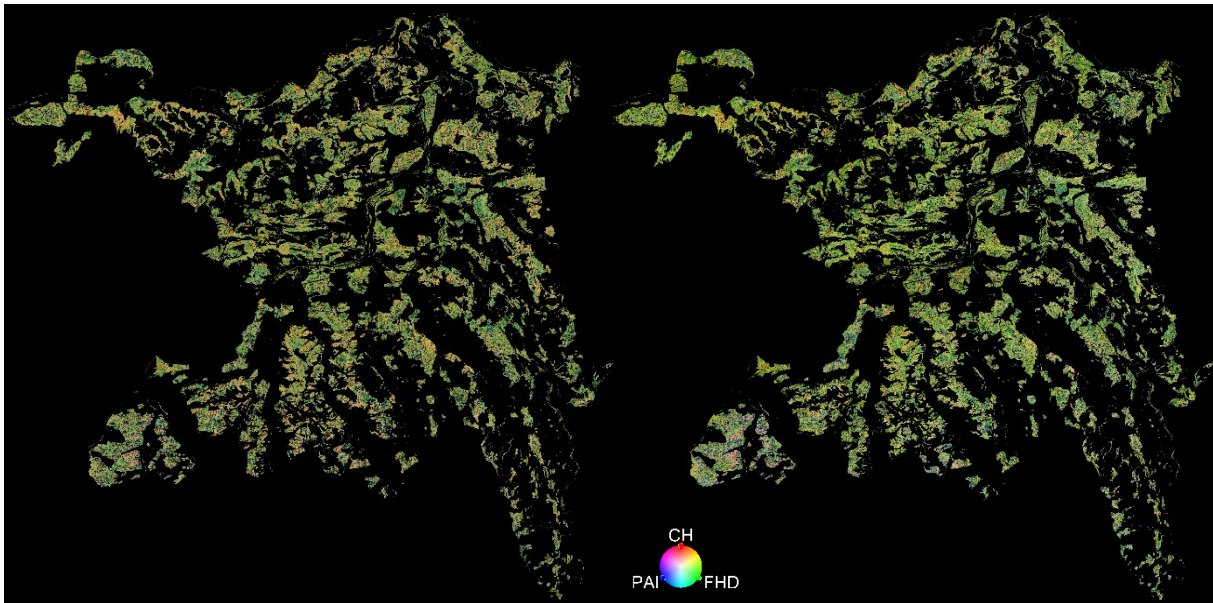
Figure 3.3: RGB composites of the morphological traits of 2014 (left) and 2019 (right) in the entire study area. Higher resolution images can be found in the Appendix in Figure A.2 and Figure A.3.

Throughout the canton, green to yellow colors were dominant (see Figure 3.3). They indicate high vertical layering, medium to high canopy height, and fairly low density. In the southwest, around the area of Vordemwald, a leaning towards the blue and reddish colors was observable. These colors imply high PAI values with low to medium canopy height and rather low vertical layering. In the southwestern part of the canton, conifer trees were much more common or even dominated the forested areas. In the north-western part of Jurapark, more yellow patches were prominent which are representing medium to high canopy and vertical layering with relatively low density. These general observations were similar in 2014 and 2019, except for blueish-green hues: When comparing the RGB composites of both study years, blueish regions from 2014, especially at the Laegern ridge, appeared in a greener hue in 2019 which means that high PAI values have become less prominent whereas FHD showed higher values compared to CH and PAI. Otherwise, the RGB composites were fairly similar in both years.

In Figure 3.4, CH mapped over the entire canton is depicted in 2014 and 2019. The corresponding difference map is visible in Figure 3.5. Canopy height values showed high and low patterns distributed all over the canton. CH generally showed relatively small local changes and pixels showing a slight increase can be observed all over the canton. FHD and PAI maps can be found in Appendix Figure A.4 to Figure A.7. FHD displayed relatively homogenous values in 2014 and also in 2019. FHD values were more dispersed in 2019. Highest FHD was observed around Kettenjura, southern Aargau, and eastern Aargau but was still relatively homogenous across the canton. Variation and change in FHD values can be better observed at smaller scales and are discussed in the following sections. Higher PAI values were estimated in the southern canton, where more coniferous trees are located. At the Tafeljura, in the northern part of Jurapark, a decrease in PAI was observed while the change on the Kettenjura is much smaller. A slight increase was detected in the southern part of Aargau where *NaN*-value-pixels were found much more than in other areas. These are pixels where the algorithm could not estimate a PAI value resulting in a *NaN* (not a number) pixel. In the northeastern part of the canton, a striping pattern is visible showing more *NaN*-values.

In the subsequent section, the three subregions are used to observe spatial patterns on smaller scales of the ALS-derived functional traits and diversity metrics. The functional trait maps of the subregions are investigated and the computed functional diversity maps are examined.
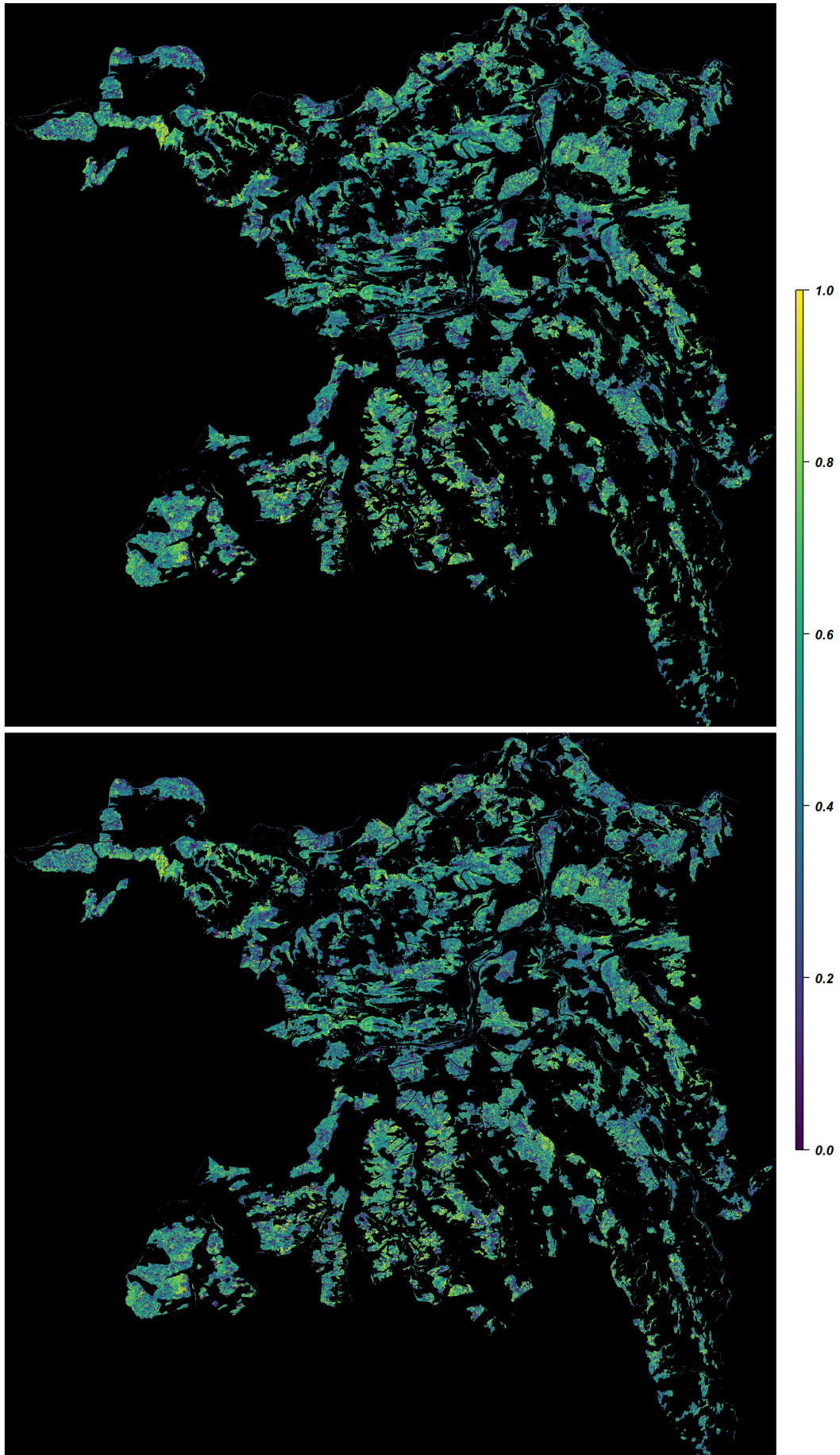
Figure 3.4: Canopy height maps of the canton Aargau of 2014 (top) and 2019 (bottom).
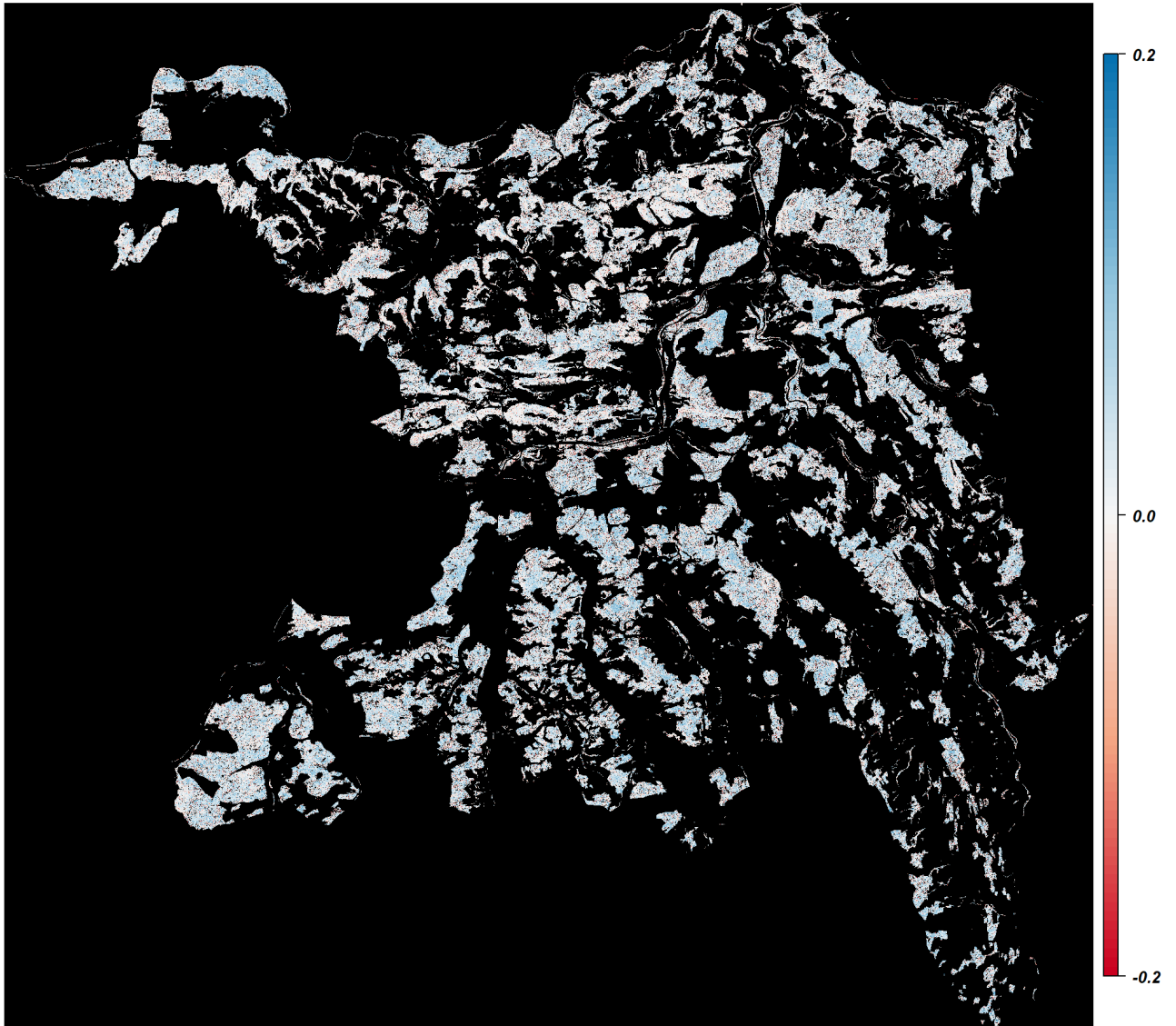
Figure 3.5: Difference map of canopy height between the years 2014 and 2019. Red pixels indicate higher values in 2014, blue pixels show higher values in 2019.

At Laegern, the canopy height distribution was similar in both years. The largest trees were found on the northern slopes and below the ridge on the southern side with tree heights of >35 m. The biggest change was observed in the lower northern part of Laegern, where larger forest patches showed a strong decrease in canopy height. A slight increase in CH was visible throughout the subregion. FHD values showed more dispersion and higher values in 2019 compared to 2014, as mentioned under Chapter 3.1.1. But now, when examining the subregions, a more pronounced decrease towards the Laegern ridge was observed. A strong decrease in vertical layering appeared mostly in the same areas as the CH decrease. There was almost no increase in the steep regions along the ridge. On the northern slope, a slight striping effect in the north-south direction and slightly higher FHD values were noticeable. As with FHD, PAI values were moderately higher in 2019. The most increase was visible on the southern slopes, where the density in 2019 was larger than on the northern slopes. Again, the same patches of decreasing values were visible as with CH and FHD. Higher PAI values appeared mainly in the southeastern part, where more coniferous trees were growing.

In the Unterwald subregion, the highest trees appeared in the western part with some smaller patches of large trees in the center and the southeast. A decrease was visible all over Unterwald with some large patches in the southeastern part. FHD values were again in a medium range and the 2019 decrease corresponds well with CH reduction. PAI 2014 showed a slight striping in the center of Unterwald which is discussed under Chapter 4.3. Higher values in PAI appeared in 2019 but there were also large areas with a density decrease, especially in the western part of Unterwald. PAI showed many *NaN*-values in Unterwald.

In the subregion Frickberg, as in Laegern and Unterwald, tree heights were fairly similar in both years, with some patches showing a large decrease in CH. The largest trees were found in the northeastern and southern slopes where low trees were prominent on top of Frickberg. Generally, CH was very diverse. Patches with low FHD values corresponded to also very low canopy height, but FHD values appeared very uniform in a medium range, again with a slight increase in 2019. The patches with the largest decrease of FHD corresponded again with areas of CH decrease. PAI values were highest where coniferous trees were located. As opposed to Laegern, there was almost no density increase between 2014 and 2019. PAI values decreased most notably on the upper slopes facing south and in the same areas where CH and FHD decreased between the two recording dates.

Laegern
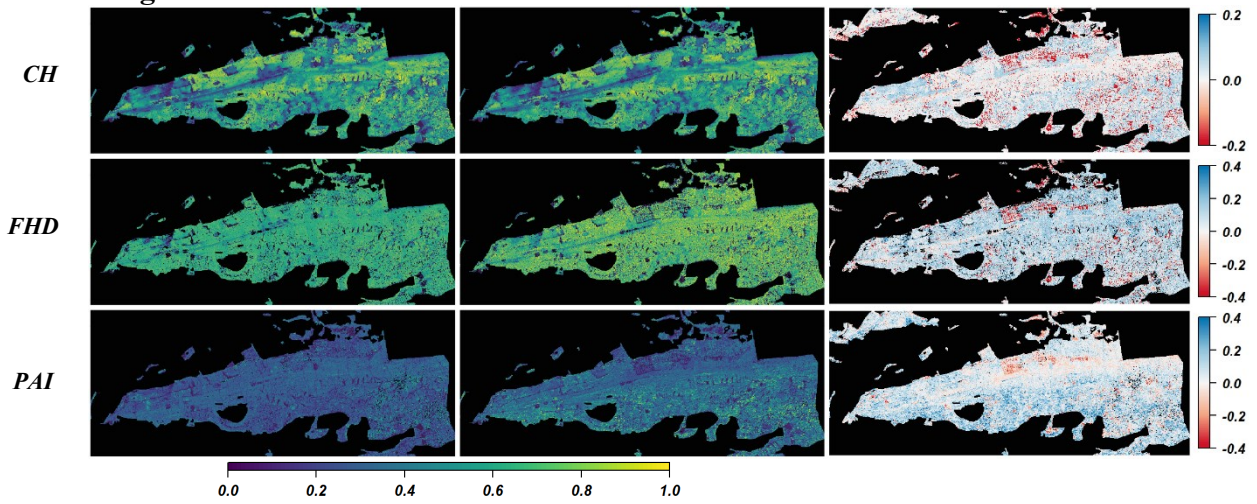
Figure 3.6: Functional traits of Laegern in 2014 (left), 2019 (middle), and their change map (right). CH is in the top row, FHD in the middle row, and PAI in the bottom row. In the right column, red pixels indicate higher values in 2014, blue pixels show higher values in 2019.

Unterwald
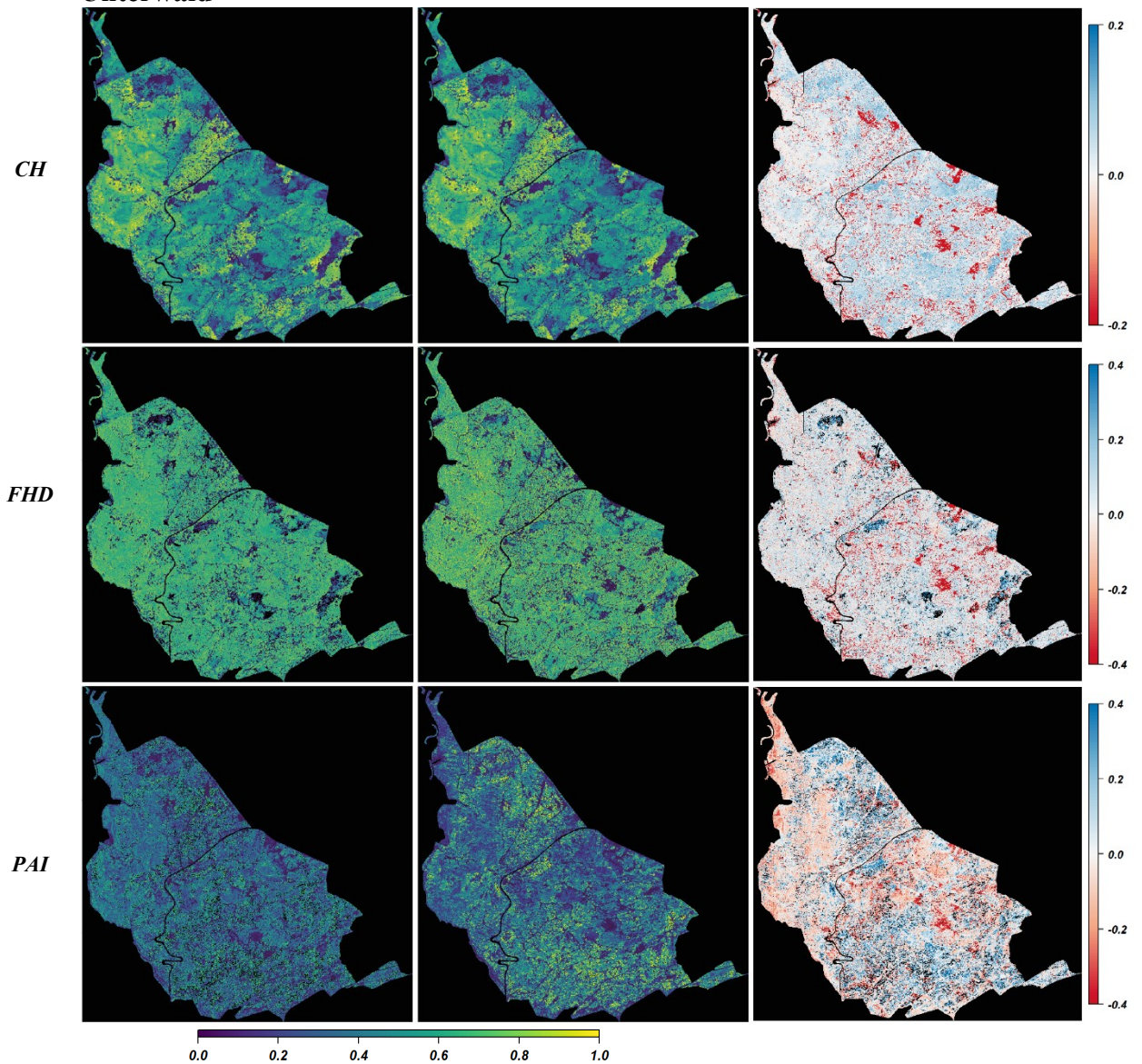
Figure 3.7: Functional traits of Unterwald in 2014 (left), 2019 (middle), and their change map (right). CH is in the top row, FHD in the middle row, and PAI in the bottom row. In the right column, red pixels indicate higher values in 2014, blue pixels show higher values in 2019.

Frickberg
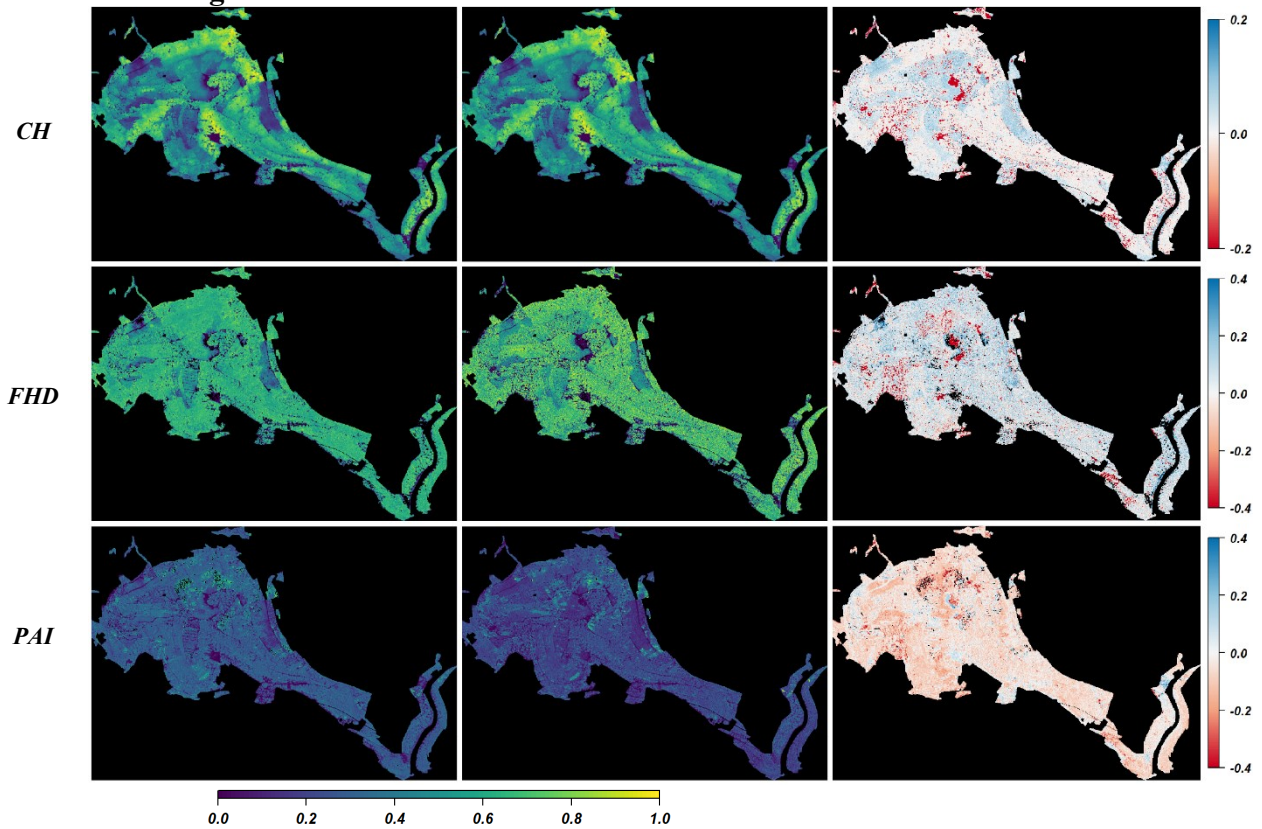
Figure 3.8: Functional traits of Frickbeg in 2014 (left), 2019 (middle), and their change map (right). CH is in the top row, FHD in the middle row, and PAI in the bottom row. In the right column, red pixels indicate higher values in 2014, blue pixels show higher values in 2019.

3.2.2 Functional diversity metrics
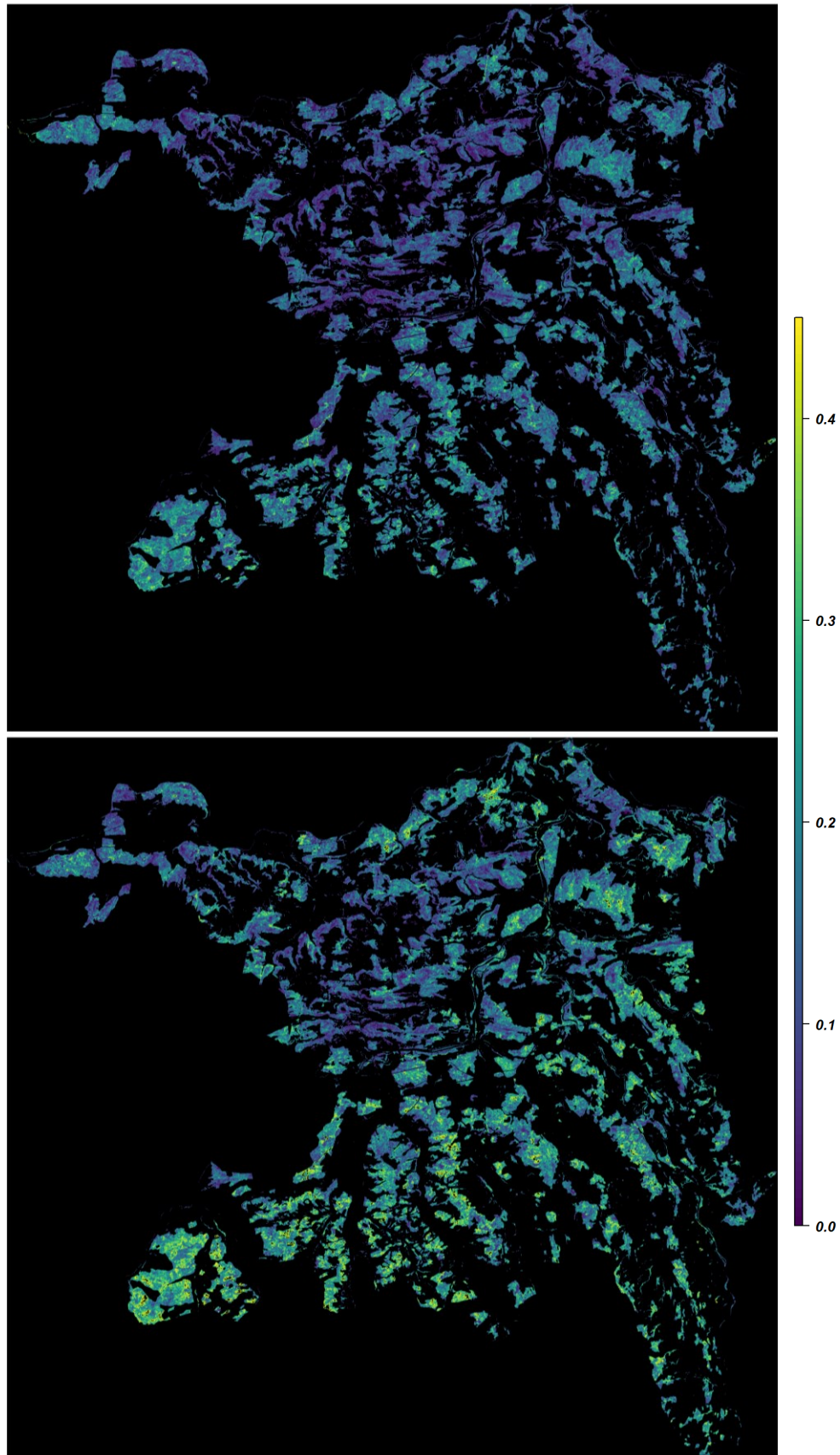
Figure 3.9: Functional richness maps of the canton Aargau of 2014 (top) and 2019 (bottom).

Functional richness showed strong patterns across the study area (see Figure 3.9). The highest values of 2014 and 2019 were observed along the southern and eastern borders of the canton. High richness values in the southern part of the canton showed up at the same places where a high abundance of conifer trees was present. The lowest richness was found in the Jurapark, especially along the Kettenjura. There, the difference map showed also the strongest decrease (see Figure 3.10). A decrease in FRic values was observed mostly along the southern slopes of the Jura and on top of the mountains. It was highly noticeable that FRic showed much lower values in 2014 than in 2019, where the mean increased by around 123 %.

Figure 3.10: Classified difference map of functional richness. It is classified using its mean (μ_{FRic} = 0.110). Values within one standard deviation of the observed change in occlusion are beige, within two standard deviations are light red/blue up to four which are dark red/blue. Red pixels indicate higher values in 2014, blue pixels show higher values in 2019 compared to the mean.

Functional divergence was distributed relatively equally over the entire study area, where high and low values were visible across the entire canton (see Appendix Figure A.8 and Figure A.9). Increasing divergence was found mostly in the southern part of the canton, while a decrease was visible mostly in the region of Jura. The largest decrease was found in the northern and center parts of the Fricktal.

In Figure 3.11, the computed diversity maps of the three subregions are depicted. At Laegern, the lowest richness pixels were located on the ridge and the northern slope. The highest richness values appeared on the southern slope in areas where coniferous trees were dominating. Furthermore, very high richness values were observed in the southeast of the large clearing. Comparing 2014 and 2019, these were also the regions with the highest increase in richness. Divergence values were more diverse and showed more local patterns. Low values occurred all across the region but were most prominent south below the ridge next to the clearing. There, high trees (>35 m) were common. The largest decrease in divergence happened north and south along the ridge. Otherwise, the negative change was relatively small but more prominent than the positive change. The strongest increase was visible in the southeast of the clearing, at the same location as the increase in richness.

In Unterwald, high richness values occurred mostly in three relatively large patches in both years. The biggest one in the center of the forest was where high canopy values were measured. The other two were more in the south of Unterwald. In these three areas, the increase in richness in 2019 was more pronounced than in the rest of Unterwald. Areas with decreasing richness were also observed as patches with decreasing values of CH, FHD, and PAI (see Figure 3.7). As in Laegern, divergence values were fluctuating much more in small areas. Larger patches of high values corresponded to the high richness patches. There has not been a large change over big forest patches between 2014 and 2019. As opposed to Laegern, an increase in divergence was more prominent.

In Frickberg, high richness areas were located on similar sites in both years, in the north-east edge of the forest and the steep areas facing south. In these regions, richness increased the most. Richness decreased only in a small area which is also visible in the change maps of CH, FHD, and PAI (see Figure 3.8). Divergence patterns were again small-scaled. Compared to Laegern, divergence decreased much more. There were only small areas with increasing divergence. They were located around patches of losses of CH, FHD, and PAI.
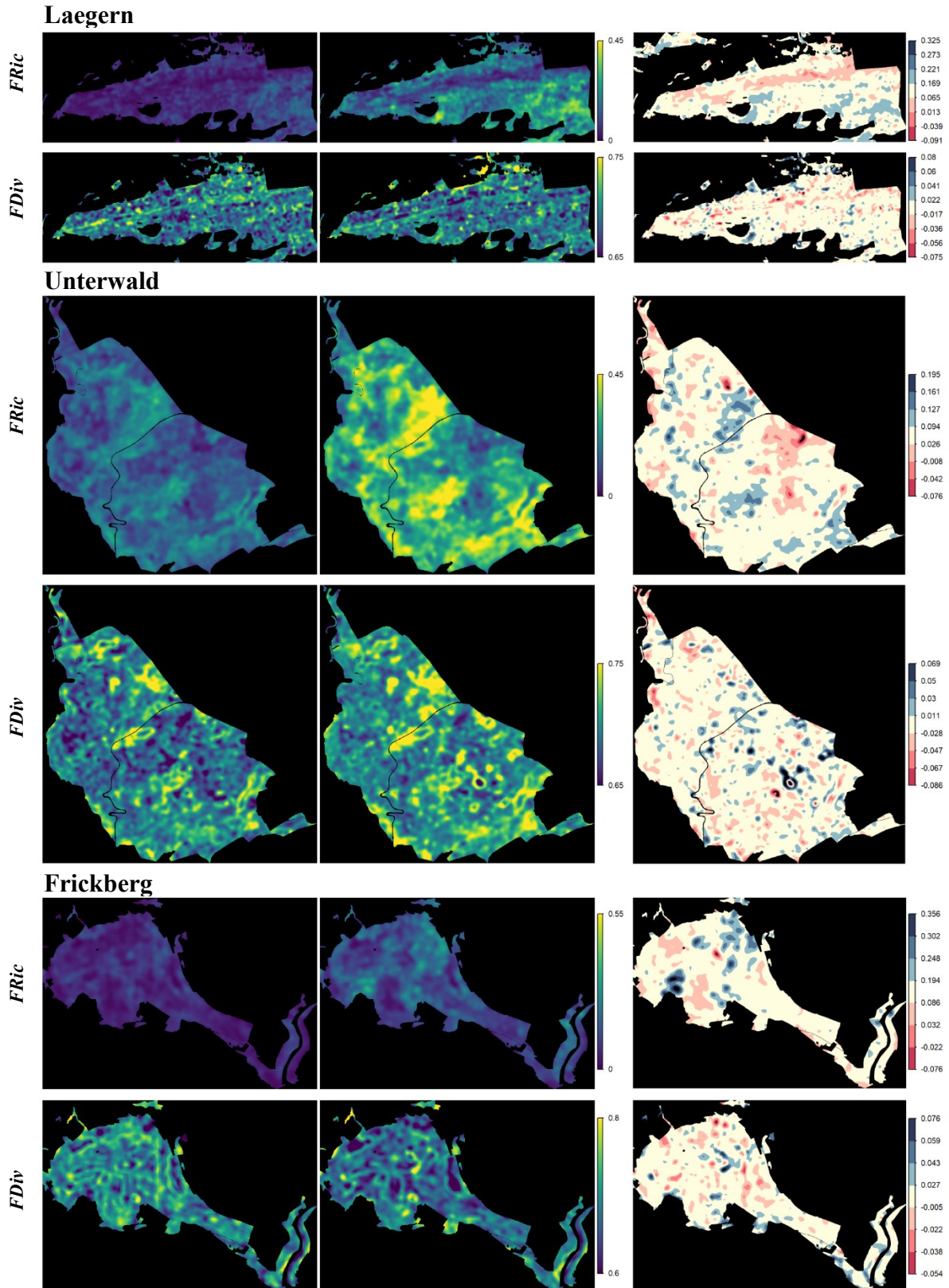
Figure 3.11: Functional richness and divergence maps of the three subregions Laegern (top), Unterwald (middle), and Frickberg (bottom) of 2014 (left), 2019 (middle), and their change maps (right). In the right column, the classified difference maps of all areas are visible. They are classified using their mean (Laegern: $L\mu_{FRic} = 0.117$, $L\mu_{FDiv} = 0.002$, Unterwald: $L\mu_{FRic} = 0.140$, $L\mu_{FDiv} = 0.011$, Frickberg: $L\mu_{FRic} = 0.060$, $L\mu_{FDiv} = -0.008$). Values within one standard deviation of the observed change in occlusion are beige, within two standard deviations are light red/blue up to four which are dark red/blue. Red pixels indicate higher values in 2014, blue pixels show higher values in 2019 compared to the mean.

Summarizing this subchapter, canopy height generally increased slightly over the study region. FHD values were more uniform and did not show as distinctive patterns as CH. PAI had its highest values in regions with evergreen conifers growing. Patches of strong decrease of the functional traits were found in the same places.

Looking at functional diversity metrics, richness showed higher values in regions with a higher fraction of coniferous trees. Also, in such areas, the observed increase was largest. Conversely, regions with low richness values experienced the largest decrease. Divergence patterns were small-scale and must be examined in smaller areas (like we did for the three subregions). The largest small-scaled divergence increases were found around patches where the functional traits showed a strong decrease. Still, bigger patterns of divergence change were observed in Jura, where the values decreased, and in southern Aargau, where more increasing divergence values were visible.

3.3 Topographic and forest parameters

Functional traits and diversity metrics were compared graphically using boxplots. Various classes of topographic and forest parameters were used to compare different characteristics of the study area. The classification can be found in Table 2.5 to Table 2.10. The boxplots were split to show differences between the years and protected and unprotected forest areas. Additionally, a type one ANOVA was conducted for each subregion.

3.3.1 Functional traits

The functional trait boxplots are depicted in Figure 3.12 which show the trait values in different topographic and forest classes. CH was lowest in altitudes below 450 m.a.s.l. Unprotected and protected areas showed similar heights in all classes. A slight decrease was observable, especially in lower areas. Tree height did not seem to change depending on aspect, but the steeper the ground was, the higher the canopy got. This was very similar in protected and unprotected forest areas. Pixels with coniferous trees showed higher canopy height values and smaller ranges, which fit the observation described by Davison et al. (2020).

Exact differences in FHD were harder to observe. Generally, the range of FHD in 2019 was larger in all classes and more bottom outliers were visible than for CH. Protected and unprotected areas were fairly similar but there were still some trends visible in the plots: FHD was mostly increasing in 2019 in higher altitudes. Furthermore, as with CH, FHD increases with the slope in both years and steeper pixels had slightly more vertical layering in 2019 than in 2014.

The interquartile range of the PAI values was located on the lower end of the observed values which means that they were distributed in a right skew except for coniferous areas, where the distribution was more centered. In almost all classes, there were still some outliers in high values after normalization. Protected and unprotected areas below 650 m.a.s.l. had lower medians in 2019 while in higher regions the medians were similar in both years. In aspect and slope classes, the boxplots were very similar for protected and unprotected forest areas: 2019 PAI medians were lower than in 2014. PAI slightly increased with steeper slopes, but no clear differences were observable between the aspect classes. Forest mix classes showed a change in distribution the more deciduous the pixels were. The interquartile range was decreasing in both years and contained lower values indicating a larger skew of the distribution.
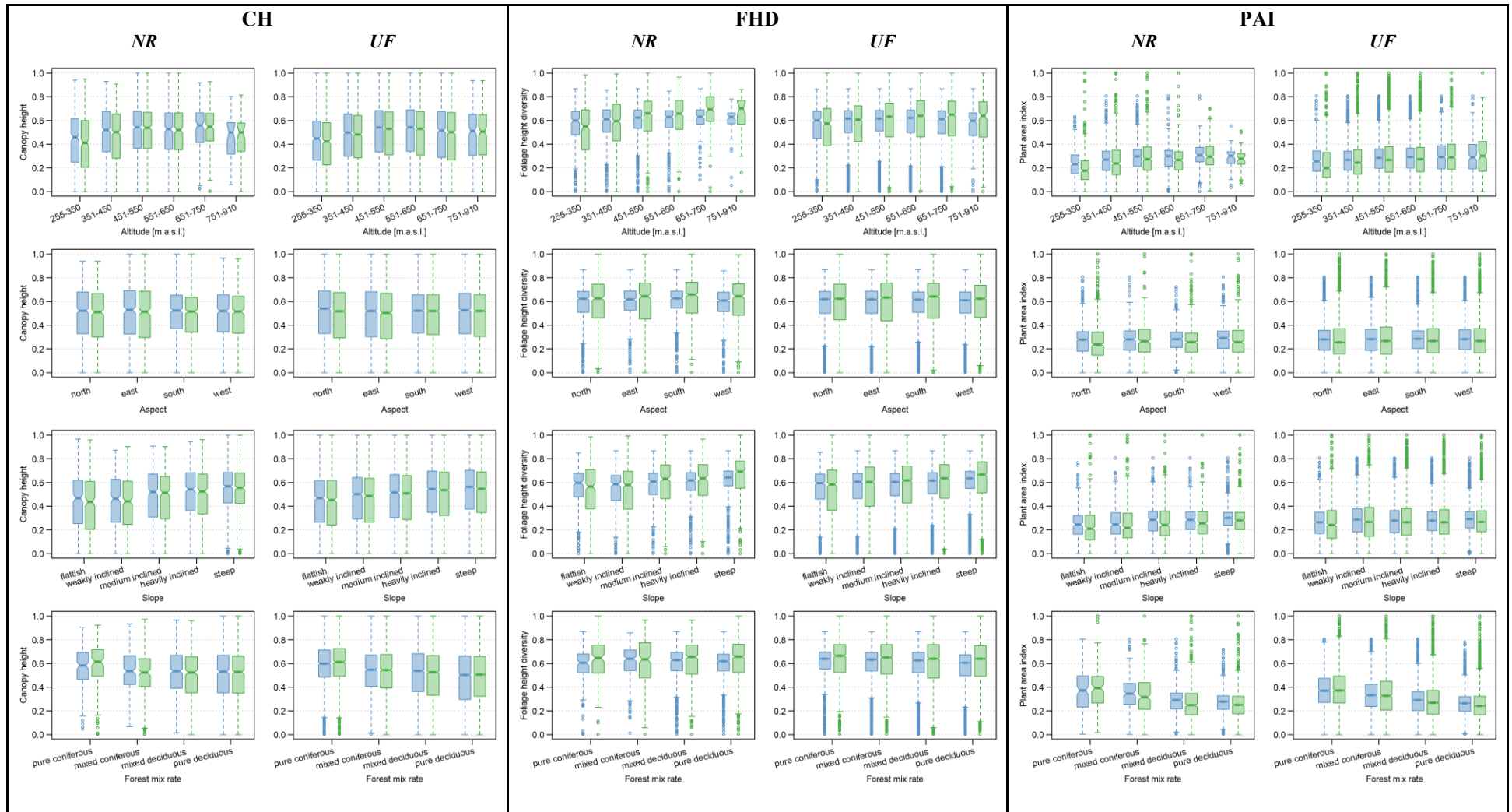
Figure 3.12: Trait boxplots of different topographic and forest classes.

In Figure 3.13, the changes (map 2019 – map 2014) are categorized and plotted using the same classes as before. Nature reserves and unprotected forest areas are plotted next to each other to provide insight into possible different behavior. The boxplots were generally very similar but observed differences are described in the following section. The interquartile range of canopy height differences in high altitudes was smaller in nature reserves than in unprotected forest areas. FHD increased more in higher altitudes. Also, there were fewer outliers in these altitudes in CH, FHD, and PAI. Furthermore, FHD seemed to increase more in steeper areas and forests with a higher fraction of deciduous trees. Below ~350 m.a.s.l., PAI decreased while the plant area index in unprotected forest areas showed almost no differences depending on height classes above this altitude. A very slight decrease in PAI was observable in nature reserves in higher regions. The traits did not show too many other clear patterns in other classes.
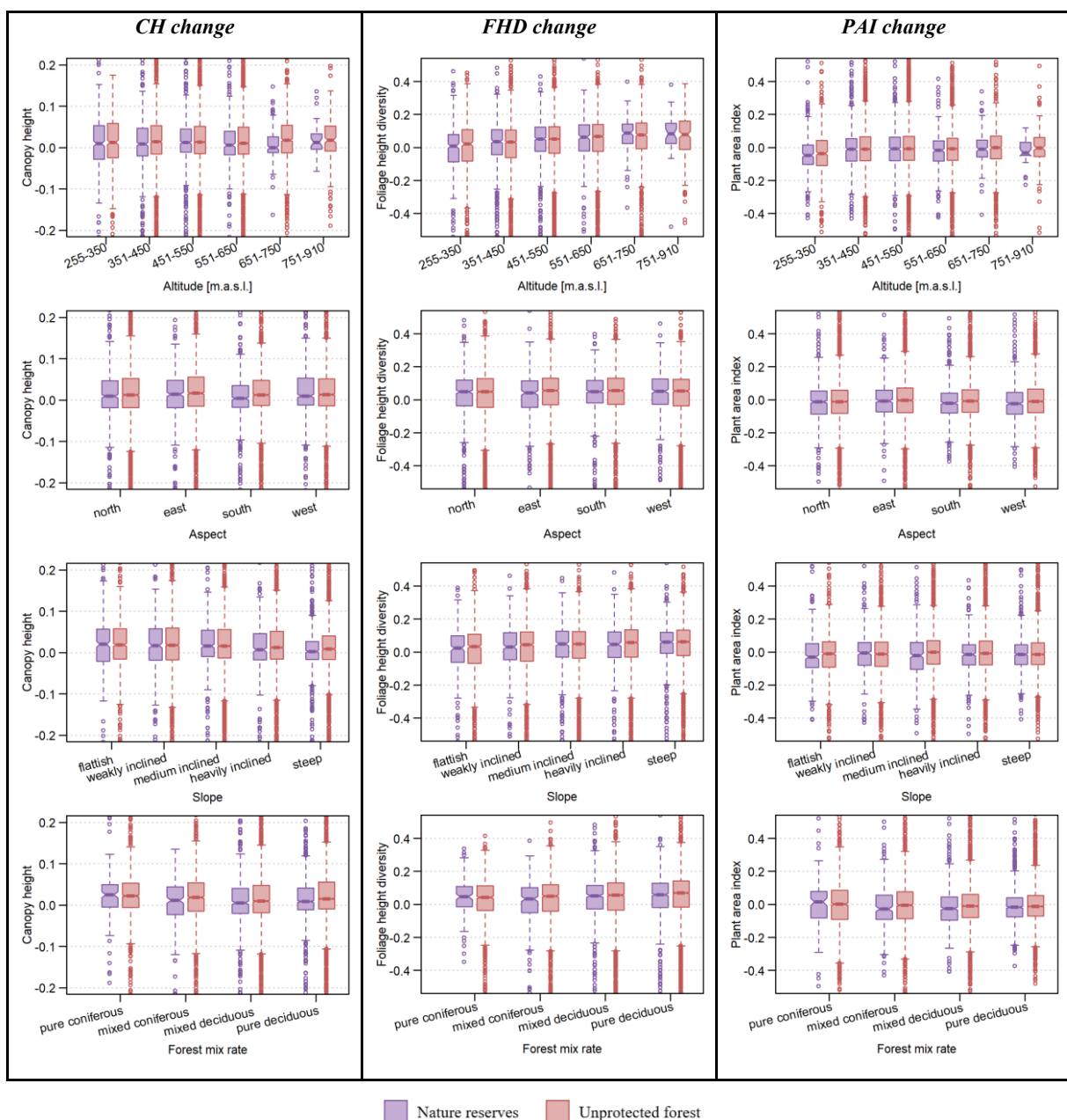
Figure 3.13: Trait change boxplots of different topographic and forest classes.

3.3.2 Functional diversity

Functional richness values of 2019 were much higher than in 2014, as already commented on in chapter 3.2. Interquartile ranges between the two years did not overlap. Nevertheless, there were some trends visible: In nature reserves, richness values were highest between ~ 350-550 m.a.s.l. It was not as clear in unprotected areas, but pixels lying below 350 m.a.s.l. showed a lower median in both years. Unprotected forests showed much higher richness than protected forests in higher altitude regions (>450 m.a.s.l.). In unprotected regions, richness stayed relatively constant with increasing altitude while the estimated values decreased substantially in nature reserves. This trend was visible in both recording years. Richness medians of all forest areas were highest on east-facing slopes and lowest on south-facing slopes. Furthermore, weakly to medium inclined surfaces showed the highest richness while flat areas had lower values. Steep slopes were observed to have the lowest values. In deciduous forests, functional richness was relatively low, while coniferous forests presented high richness values. These trends were similar in both years and protected and unprotected areas, respectively.

Unprotected forest areas showed a larger increase in richness in all classes than in nature reserves. Apart from this general observation, the largest increase was visible above ~350 m.a.s.l. where it was almost constant at 0.1. Richness in nature reserves increased most between ~350 – 550 m.a.s.l. Southern slopes had the smallest increase in protected areas, while unprotected forest showed a similar increase in all orientations. No trend was visible depending on the slope classes, but FRic increase was larger with an increase of coniferous trees.

Functional divergence did not vary as much as richness in the different classes. Protected areas seemed to be much more sensitive at higher altitudes. Especially in 2019, divergence decreased in altitudes above ~650 m.a.s.l. Apart from that, divergence appeared to have slightly higher medians and interquartile ranges in 2019 in all classes except pure deciduous forests.

Change in divergence was much less pronounced than in richness. FDiv increased more in lower altitudes. In nature reserves, FDiv decreased above ~550 m.a.s.l. and it increased generally more in flat areas and coniferous forests. Differences between protected and unprotected areas were minor.

Generally, all traits showed the least increase or even the most decrease in low-altitude areas. Furthermore, they were sensitive to steep slopes, especially CH and FHD.
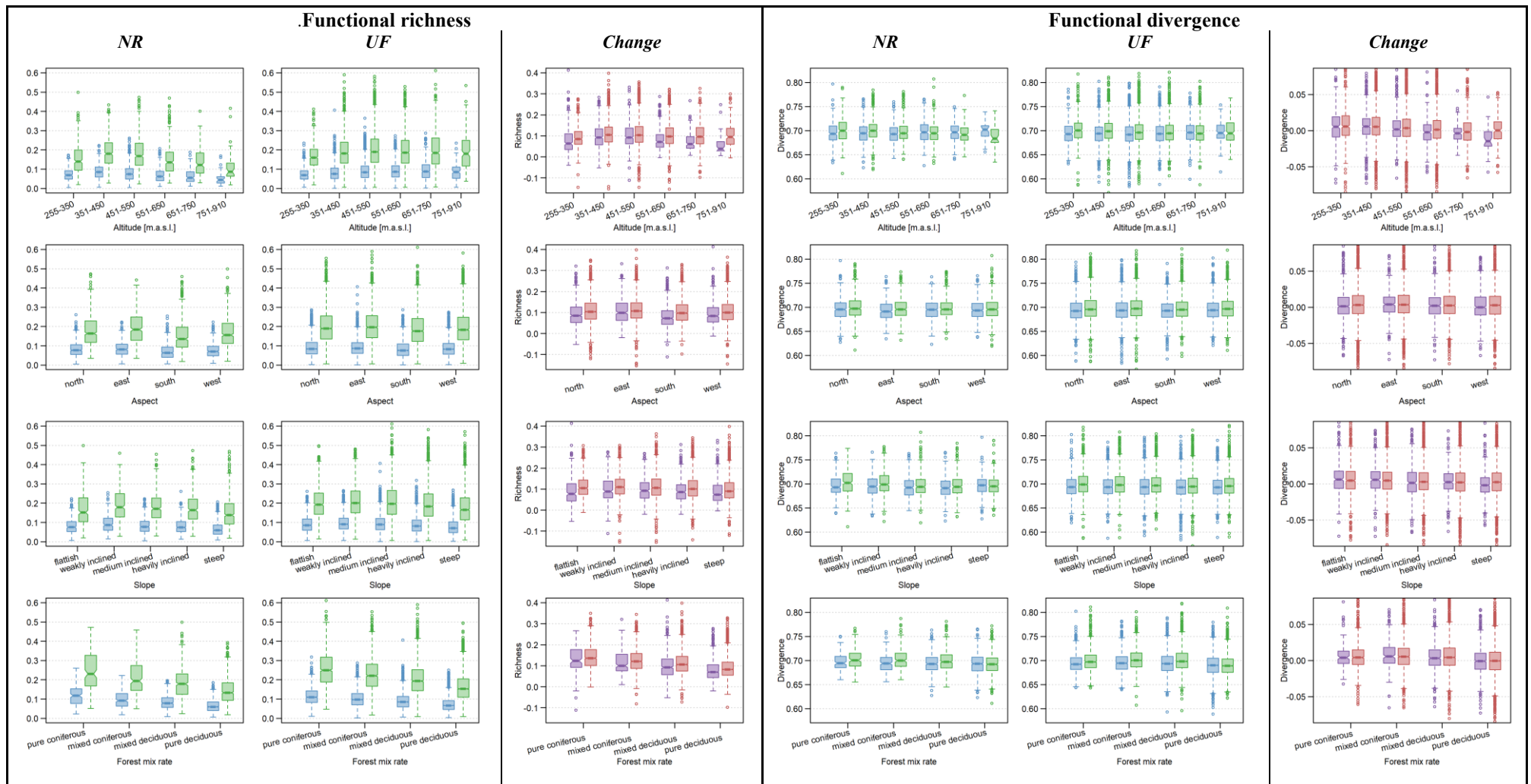
Figure 3.14: Functional richness (left) and divergence (right) boxplots of different topographic and forest classes. Corresponding change boxplots are found next to the diversity boxplots of the individual years and are colored in purple and red hues.

3.4 Occlusion mapping

We mapped the fraction of canopy volume occluded from the sensor to address possible changes caused by not seeing parts of the canopy using the approach by Kükenbrink et al. (2017). First, a ray-tracing of all laser pulses using the Voxel Traversal Algorithm by Amanatides and Woo (1987) was conducted. The output consisted of a 3D voxel grid containing the classification information (observed, empty, unobserved, occluded voxels). To match the 2D grid of the trait and functional diversity maps, the fraction of occluded canopy volume on a ground area of 2 x 2 m was computed. In Figure 3.15, the resulting occlusion maps are depicted.
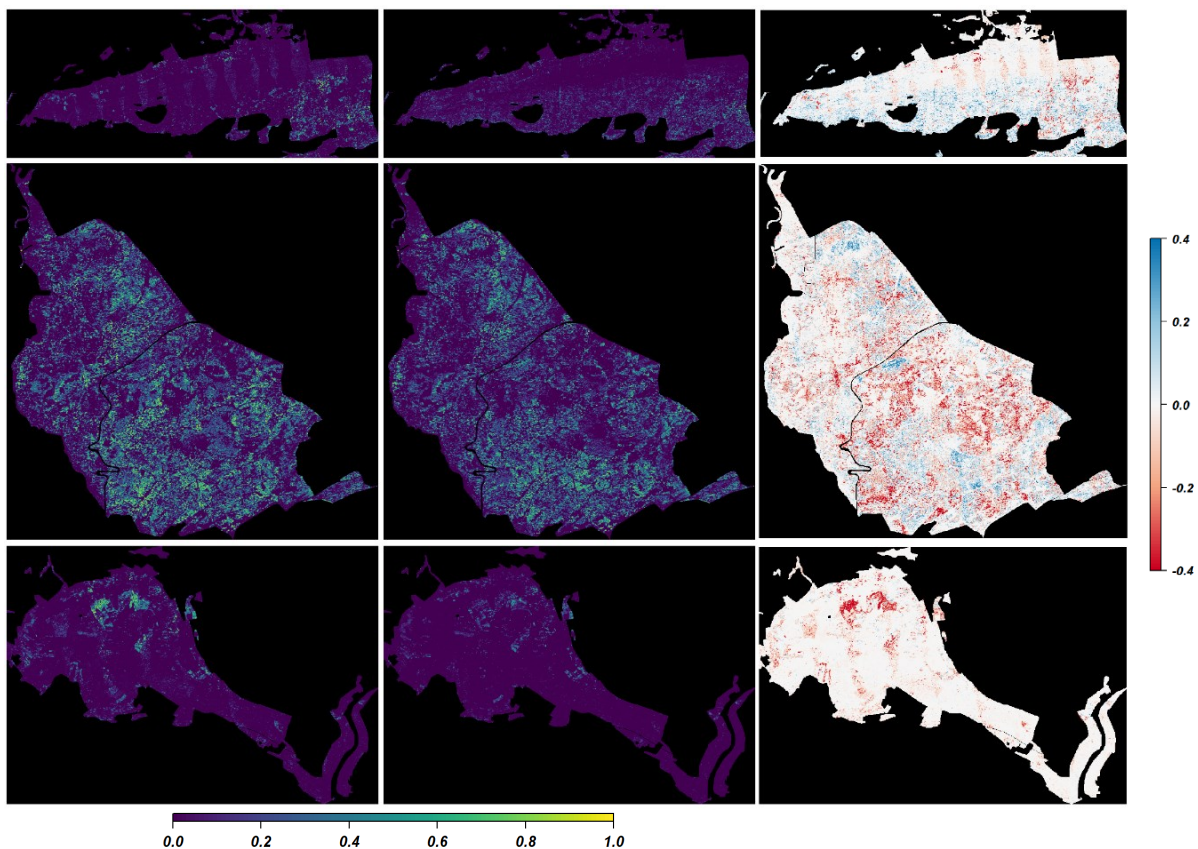
Figure 3.15: Occlusion maps of Laegern (top), Unterwald (middle) and Frickberg (bottom). The maps of the two recording years are in the left (2014) and middle (2019) columns. The values describe the fraction of occluded canopy volume on a 2 x 2 m pixel. 0 means that no canopy volume is occluded, 1 means that the total canopy volume is occluded. In the right column, the difference maps of all areas are depicted.

At Laegern in 2014, visible flight strips were located especially on the northern slopes. There, higher occlusion values were observed. Other high occlusion values were located on the southern slope, mostly where more coniferous trees growed. These two observations were apparent in the difference map of Laegern. Where no flight strip overlap existed in 2014, occlusion decreased, while more occlusion was observed along the southern slope in 2019.
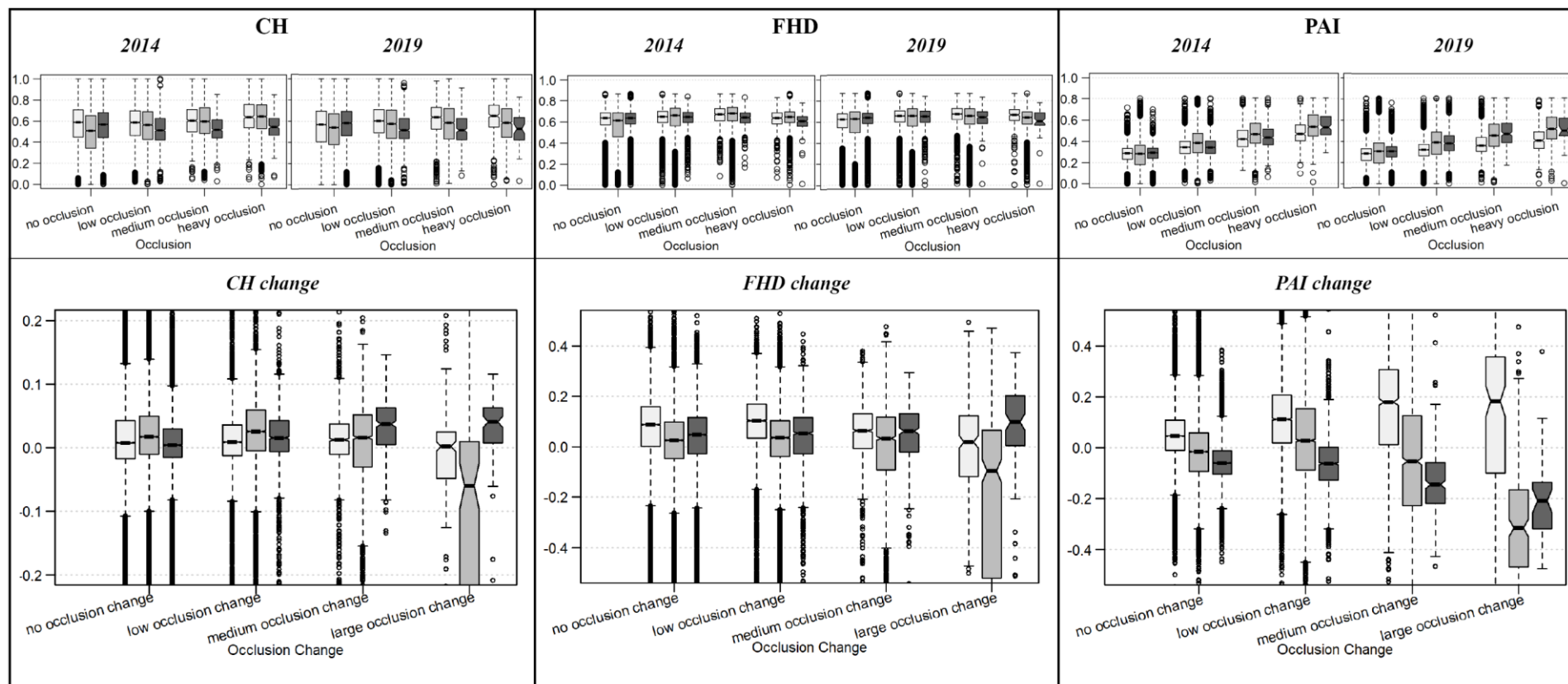
Figure 3.16: CH (left), FHD (middle) and PAI (right) boxplots of the three subregions Laegern, Unterwald and Frickberg. On top, boxplots show the trait values in the occlusion classes for 2014 and 2019. On the bottom, the change map boxplots show the behavior of the traits in different occlusion change classes.

In Unterwald, a decrease in occlusion was occurring at a similar scale as an increase. Unterwald being dominated by coniferous trees did not show as clear patterns as Laegern, but a slight striping of decreasing occlusion was observed. Frickberg also displayed heavy occlusion in areas with more conifers being present. Occlusion mostly decreased in 2019 compared to 2014.

Generally, occlusion mostly decreased between 2014 and 2019, except for larger patches in Unterwald and the southern slope of Laegern.

In Figure 3.16, the boxplots of the trait values are shown. CH median values increased slightly with higher occlusion at Laegern and Unterwald. In Frickberg, this trend was not visible. FHD boxplots did not show different characteristics that could indicate a trend depending on larger occlusion. The boxplots of all subregions varied slightly, but no obvious connection to occlusion was observable. For PAI values, the boxplots showed a clear trend with increasing occlusion. In all three subregions, PAI medians and interquartile ranges increased substantially with a larger fraction of the canopy being occluded.

Determining occlusion changes, i.e. difference in occlusion in 2014 and 2019 at the same place is necessary to detect areas that might contain a greater uncertainty in the observation. For example, in places where the occlusion had changed considerably, it can be assumed that part of the lower canopy was recorded very differently in the two years, either due to the viewing geometry variation or due to physical changes in the forest. For example, a large occlusion change means that in 2014, occlusion was high and in 2019, occlusion was low or vice-versa.

At Frickberg, the change in canopy height increased with increasing occlusion change. In the other subregions, the medians decreased with larger occlusion change. FHD showed the same trends, but PAI displayed a median increase with heavier occlusion change at Laegern and a decrease of PAI medians at Unterwald and Frickberg. At Laegern and Unterwald, the interquartile ranges increased considerably with heavier occlusion change. This was seen in Frickberg, too, but the trend was not as pronounced.
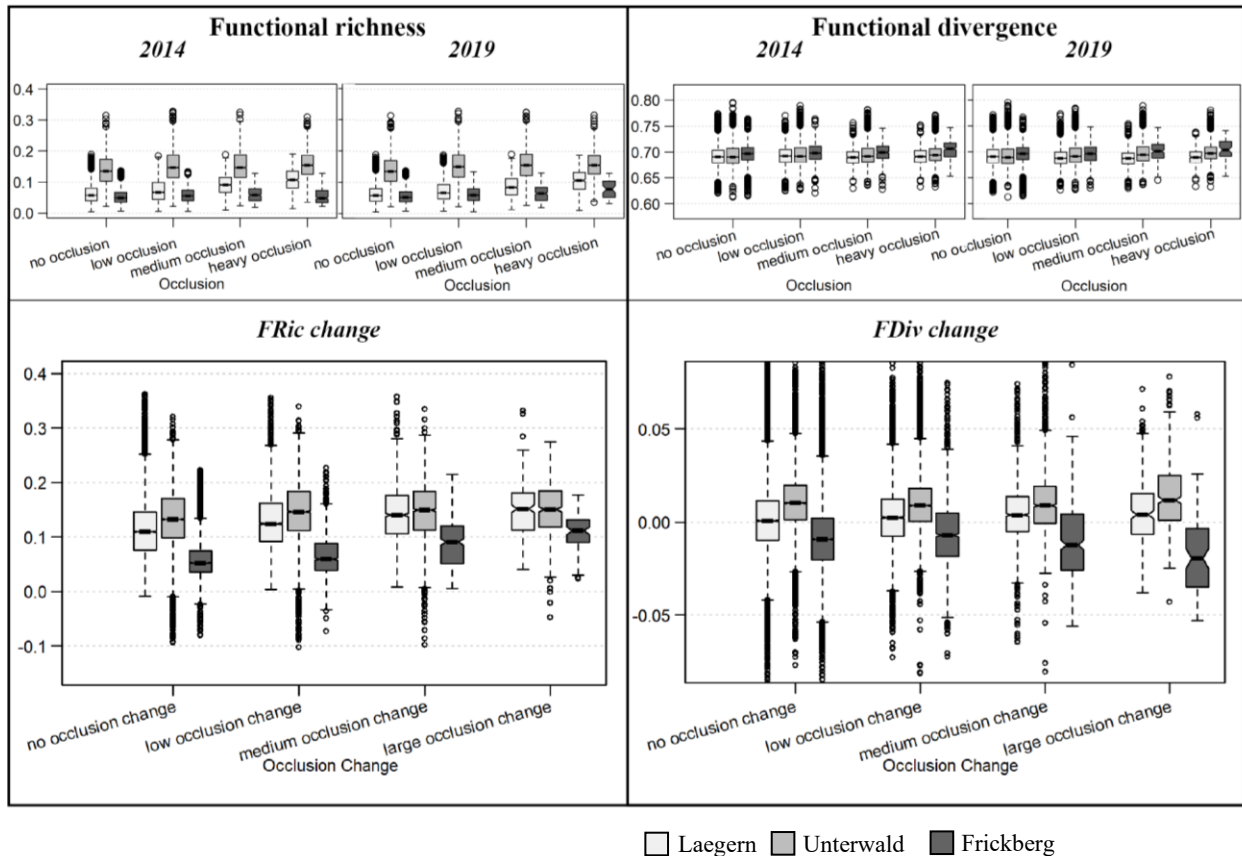
Figure 3.17: Functional richness (left) and diversity (right) boxplots of the three subregions Laegern, Unterwald, and Frickberg. On top, boxplots are plotted occlusion classes for 2014 and 2019. On the bottom, the change map boxplots show the behavior of the traits in different occlusion classes.

Richness increased very slightly with increasing occlusion at Laegern and Unterwald in both years. Frickberg did not show the same trend, it displayed almost constant richness values in all occlusion classes. This was different when examining the FRic change map: When a larger occlusion change was present, richness increased more in Frickberg. The same trend was true for Laegern and Unterwald.

Functional divergence did not react as strongly as richness to occlusion. The values stayed much more constant, even in heavily occluded areas. But there was still a slight increase in FDiv medians observable when occlusion got heavier in Unterwald.

At Laegern and Unterwald, divergence increased more in areas where the amount of occlusion changed strongly. This trend was the opposite at Frickberg. But all subregions showed an increase in their interquartile ranges with increasing occlusion change.

Summarizing, occlusion maps showed a dependency on point density. In 2014, where no flight strips overlapped, higher occlusion values were detected in certain regions. All functional traits seemed to be sensitive to occlusion, especially PAI which increased considerably in heavily occluded areas. Furthermore, the change maps showed that the traits became less

reliable with increasing occlusion, since the interquartile ranges increased strongly and the trait differences, i.e. the increases and decreases, differed vigorously depending on the subregion at high occlusion change. Functional diversity metrics seemed not to be as sensitive to occlusion. For richness and diversity values, only a moderate increase was noticeable. Also, diversity metrics changed only slightly depending on the occlusion change class, except for Frickberg, where larger changes were observable.

3.5   Statistical analysis of the computed metrics

We conducted an analysis of variance with a type-I sum of squares to see if the above-explored effects of the topographic, forest, and occlusion variables were significantly influencing functional traits and diversity metrics. The amount of variance explained by these variables is depicted in Figure 3.18. The detailed ANOVA type-I results of all subregions can be found in Appendix Table A.2 to Table A.4.

3.5.1   Functional traits

Canopy height

For CH, Altitude was significant for Laegern and Frickberg based on the generalized model and ANOVA of both years and explained 3-4% of the variance in Laegern and 1-1.5% in Frickberg. All exact values can be seen in Table 3.3, where significance is highlighted in bold font. Aspect was only found significant in Laegern for both years but explained less than 1% of the variance. Slope was significant in Laegern for 2014 and 2019, and in Unterwald only in 2019, explaining 2-2.5% of the variance. Forest mix rate was significant in Unterwald. Occlusion was significant for CH in 2019 in Laegern and Unterwald but explained only <0.5% and <2% of the variance in these two subregions. Point density was significant for Laegern and Frickberg in 2014, where it explained <2%, and all subregions in 2019, explaining 17-27% of the variance. The r^2 for 2014 of the generalized linear model was 0.03-0.07 and for 2019 0.24-0.34 for the different subregions.

When looking at the variables that could explain the change of CH between 2014 and 2019, changing occlusion was not significant for canopy height change and point density change was only significant in Unterwald (3.8% of the variance explained). The r^2 for the CH change model was very low (*Laegern:* 0.0002, *Unterwald:* 0.03, *Frickberg:* 0.002).

Table 3.3: Percentages of explained variances by the ANOVA of all tested models in the three subregions. Significant variable values are printed in bold, and non-significant values are grayed out.

Dependent variable	Independent variables	Laegern 2014	Laegern 2019	Unterwald 2014	Unterwald 2019	Frickberg 2014	Frickberg 2019
CH	Altitude	**3.37**	**0.89**	1.40	2.89	**1.15**	**0.71**
	Slope	**2.05**	**0.02**	1.73	**3.96**	0.36	0.38
	Aspect	**0.36**	**0.01**	0.02	1.31	0.00	0.34
	Forest mix	0.05	0.01	**2.24**	**2.62**	0.02	0.07
	Occlusion	0.00	**0.27**	0.66	**4.50**	0.02	0.42
	Point density	**1.20**	**14.20**	0.76	**22.16**	**1.68**	**12.12**
	Residual	*92.96*	*84.61*	*93.18*	*62.56*	*96.76*	*85.94*
CH change	Occlusion difference	0.18		1.32		0.57	
	Point density difference	0.03		**3.77**		0.07	
	Residual	*99.78*		*94.91*		*99.35*	
FHD	Altitude	**2.93**	**3.95**	**0.55**	1.08	**0.12**	**1.51**
	Slope	3.39	2.19	**14.65**	**2.07**	5.17	**0.22**
	Aspect	0.06	0.55	**1.32**	**0.09**	1.03	0.02
	Forest mix	6.21	**0.01**	**13.41**	**1.93**	14.62	0.07
	Occlusion	18.49	**8.90**	**19.45**	**1.61**	13.61	0.00
	Point density	**19.61**	**18.63**	**7.52**	**17.02**	**14.20**	**26.92**
	Residual	*49.31*	*65.77*	*43.11*	*76.20*	*51.24*	*71.26*
FHD change	Occlusion difference	**0.60**		0.00		0.14	
	Point density difference	**32.66**		**34.77**		**22.87**	
	Residual	*66.74*		*65.22*		*76.99*	
PAI	Altitude	**1.09**	**0.34**	0.12	**1.01**	0.82	0.00
	Slope	**0.00**	**2.33**	**9.53**	**0.69**	**2.77**	**5.22**
	Aspect	0.10	**3.39**	**1.65**	**0.87**	**0.01**	0.14
	Forest mix	**0.63**	**0.34**	**1.09**	**23.19**	**0.32**	**24.30**
	Occlusion	**4.83**	**52.61**	**7.84**	**38.66**	**0.19**	**19.12**
	Point density	**37.13**	**9.01**	**26.97**	**5.90**	**37.65**	**15.40**
	Residual	*56.22*	*31.98*	*52.80*	*29.67*	*58.26*	*35.83*
PAI change	Occlusion difference	**43.89**		1.48		**0.94**	
	Point density difference	**12.95**		**13.54**		**4.66**	
	Residual	*43.16*		*84.99*		*94.40*	
FRic	Altitude	0.29	**0.68**	0.03	**0.35**	0.27	**0.96**
	Slope	0.01	0.42	0.17	0.50	**1.08**	0.05
	Aspect	0.01	0.04	0.57	0.06	0.26	0.45
	Forest mix	**0.50**	**2.02**	1.48	**2.30**	0.02	**0.07**
	Occlusion	0.27	**0.77**	0.02	0.01	**2.23**	**0.82**
	Point density	0.13	0.73	0.28	0.00	**2.04**	**0.42**
	Residual	*98.78*	*95.34*	*97.45*	*96.78*	*94.11*	*97.23*
FRic change	CH difference	**11.70**		**13.75**		**11.74**	
	FHD difference	**0.77**		0.09		0.64	
	PAI difference	**9.62**		**4.88**		**3.73**	
	Occlusion difference	**0.29**		**2.46**		**2.14**	
	Point density difference	0.22		0.10		0.15	
	Residual	*77.39*		*78.72*		*81.59*	
FDiv	Altitude	**6.67**	0.29	2.42	0.03	**2.08**	0.27
	Slope	0.01	0.01	0.23	0.17	0.19	**1.08**
	Aspect	0.21	0.01	1.38	0.57	0.01	0.26
	Forest mix	**1.18**	**0.50**	**4.21**	1.48	5.30	0.02
	Occlusion	**6.30**	0.27	0.63	0.02	**4.40**	**2.23**
	Point density	**0.29**	0.13	0.28	0.28	1.45	**2.04**
	Residual	*85.35*	*98.78*	*90.84*	*97.45*	*86.56*	*94.11*
FDiv change	CH difference	0.00		**2.07**		0.10	
	FHD difference	0.07		1.22		0.20	
	PAI difference	**3.08**		0.71		0.46	
	Occlusion difference	**0.92**		0.40		0.24	
	Point density difference	0.00		**2.49**		**1.45**	
	Residual	*95.93*		*93.11*		*97.56*	

Foliage height diversity

For FHD, altitude was significant for all years and subregions except for Unterwald in 2019 and explained ~1% of the variance in Laegern, <3% in Unterwald, and <1% in Frickberg. Slope and aspect were significant only in Unterwald. Slope explained ~4% and ~9.5% of the variance in 2014 and 2019, respectively, and aspect ~1.3% in both study years in Unterwald. Forest mix was significant in Laegern only in 2019 explaining ~1% of the variance, but it was also significant for both study years in Unterwald and explained ~2 %. Point density was significant for all subregions and years and explained 12-37% of the variance, but occlusion only for Unterwald in both study years (4.5 and 7.8% explained) and Laegern 2019 explaining 4.8%. The r^2 for 2014 were 0.15, 0.37 and 0.14 for Laegern, Unterwald and Frickberg. In 2019, they were higher with 0.44, 0.47, and 0.42 in the respective subregions. Examining the analysis of the difference map, occlusion change was significant only for FHD change in Laegern with <1 %, while point density change was significant in all subregions with 22-34% explained variance. The change model had r^2 of 0.33, 0.34 and 0.23 in Laegern, Unterwald and Frickberg.

Plant area index

Altitude was significant for PAI in Laegern in both study years and in Unterwald only in 2019. In Laegern, it explained 2.9 and 0.3% of the variance in 2014 and 2019, respectively, while it explained in Unterwald ~1% in 2019. Slope and forest mix rate were significant in all subregions and years. Slope explained in Laegern 2-3.5%, in Unterwald 14.7 and 0.7% in 2014 and 2019, and ~5.2% of the variance in Frickberg in both years. Forest mix rate explained most variance in Unterwald and Frickberg in 2019 with 23.2 and 24.3%, respectively. In 2014, it explained 13.4% and 14.6% of the variance in Unterwald and Frickberg while it explained in Laegern only 0.3% and 6.2% in 2014 and 2019. Aspect was significant in Laegern in 2019 explaining ~3.5%, in Unterwald in both years explaining 0.5-1.5% and in Frickberg in 2014 explaining ~1% of the variance. Occlusion and point density were significant for 2014 and 2019 in all subregions. Occlusion explained 13-19% in 2014, and 19-50% in 2019 while point density explained 7-19% of the variance in 2014 and 5.9-15% in 2019. In 2014, the r^2 of Laegern, Unterwald, and Frickberg were 0.51, 0.57, and 0.49 and for 2019 they were 0.68, 0.70, and 0.64, in the respective subregions. For the PAI change between the study years, occlusion change was significant for the different PAI values in Laegern and Frickberg and point density change was significant in all subregions. Occlusion and point density change explained 0.9 and 4.7%, respectively, of the PAI change variance. The r^2 of the PAI change model of Laegern, Unterwald and Frickberg were 0.57, 0.14 and 0.05, respectively.
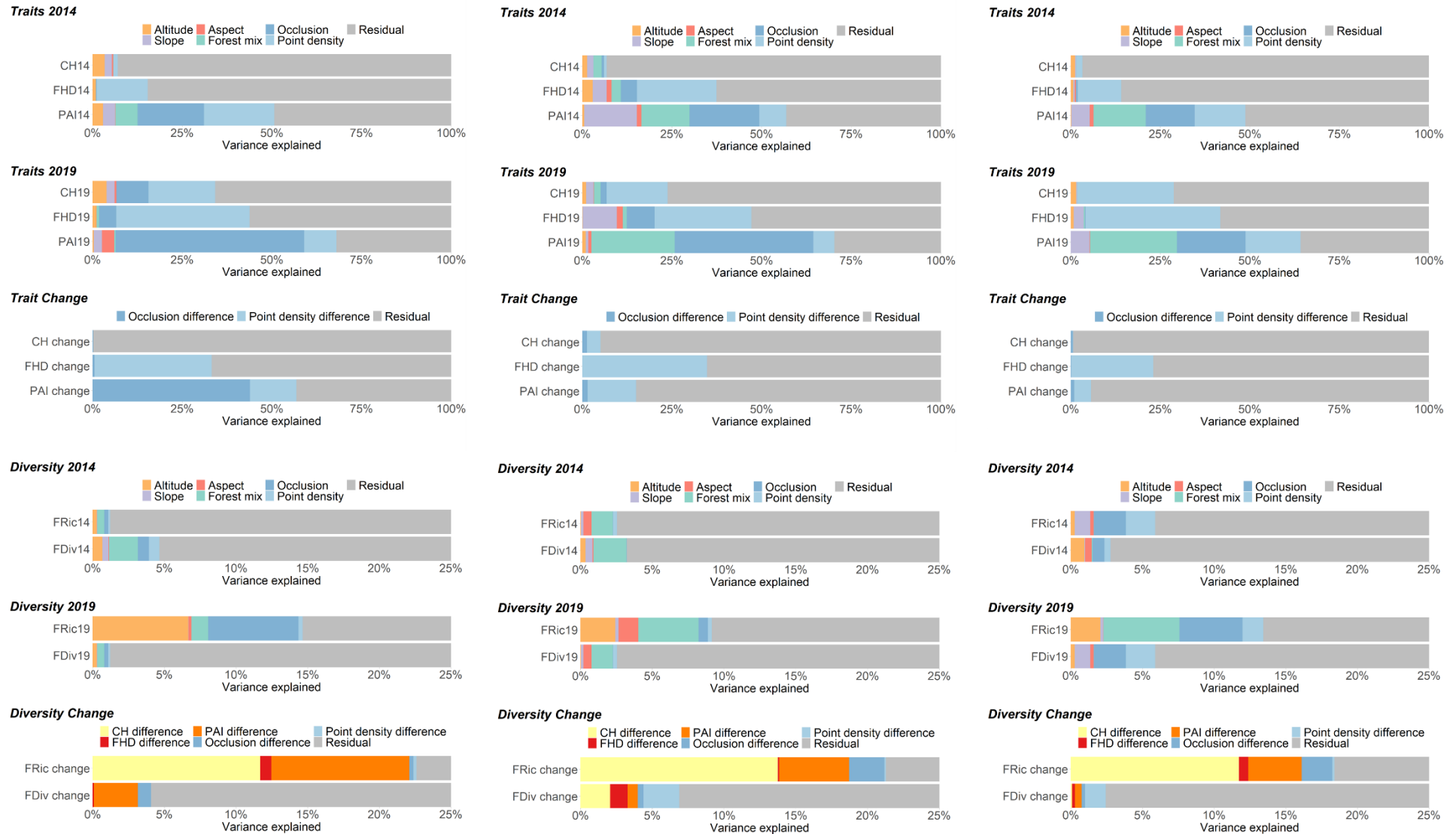
Figure 3.18: Variance explained by the different topographic, forest, occlusion, and flight setting variables. Not all models use all variables. For example, the topographic and forest variables cannot be used in the explanation of the trait and diversity change. See Table 2.11.

3.5.2 Functional diversity

Richness

For FRic, altitude was significant in all subregions in 2019 and explains 2-7% of the variance. Slope was only significant in Frickberg in 2014 explaining ~1%, while aspect was never found significant. Forest mix rate was significant in Laegern in 2014 and in all subregions in 2019 and explained ~1%, 4.2%, and 5.3% of the variance in Laegern, Unterwald, and Frickberg, respectively. Occlusion was significant in Frickberg in 2014 and 2019 (explained 2-45% of the variance) and Laegern in 2019 (6.3% explained), while point density was significant in Frickberg in both study years explaining ~1.5-2% of the observed variance. The r^2 of the generalized 2014 linear models were 0.01, 0.03, and 0.06 and in 2019 they were 0.15, 0.09, and 0.13 in Laegern, Unterwald, and Frickberg. For the change in richness between 2014 and 2019, occlusion change was significant in all subregions (0.3-2.5% explained), while point density was not. The changes in CH and PAI differences were significant for all subregions, but FHD change was only significant in Laegern. CH change explained most of the variance of richness change (11.7-13.8%), PAI change explained 3.7-9.6% and FHD explained 0.8%. The r^2 of the change models in Laegern, Unterwald and Frickberg were 0.23, 0.21, and 0.18.

Divergence

Altitude was significant for FDiv in Laegern and Frickberg in 2014 and explained <1% in both subregions. Slope was significant in Laegern 2014 and Frickberg 2019 and explained <0.5% in both subregions. Aspect was not significant for FDiv. Forest mix rate was significant in Laegern and Unterwald in 2014 explaining 2% -2.5% and Laegern in 2019 where only 0.5% of the variance was explained. Occlusion was significant in Frickberg in both years (0.8 and 2.2% of variance explained) and in Laegern in 2014 (0.8% explained). Point density was significant in Laegern in 2014 and also in Frickberg in 2019 explaining 0.7 and 2% of the variance, respectively. The models of 2014 showed r^2 values of 0.05, 0.03 0.03 and in 2019 0.01, 0.03, 0.06 for Laegern, Unterwald and Frickberg. The model for the FDiv change showed that occlusion change was only significant in Laegern (explained variance: 0.9%) while point density change was significant for Unterwald and Frickberg, explaining 2.5% and 1.5% of the variance. Only PAI difference in Laegern and CH difference in Unterwald were significant for FDiv change, explaining 3.1% and 2.1% of the variance. In the subregions Laegern, Unterwald, and Frickberg, the change models had r^2 of 0.01, 0.07, and 0.02, respectively.

4 Discussion

In this thesis, we evaluate the possibilities and limitations of applying morphological diversity mapping to a large area in a multitemporal analysis. First, we will discuss general implications of different sensors and flight settings and the available leaf-off data on change detection using functional diversity mapping. Also, the potential of the used methods is examined (Chapter 4.1). Second, the detected patterns and changes in the study area are going to be discussed and linked to the general effects examined before. (Chapter 4.2). Last, the possibilities of occlusion mapping in such a multitemporal analysis will be explored (Chapter 4.3).

4.1 Functional diversity mapping in a multitemporal analysis

4.1.1 General sensor and flight setting effects on trait estimation methods

In this thesis, we compared trait and diversity estimations using ALS data of two different sensors with varying flight parameters. A commercial laser sensor has a relatively short typical life cycle of fewer than 4 years which leads to subsequent ALS data inventories usually recorded with different instruments (Ørka et al., 2010). It has been shown in numerous studies how differences in sensors and flight settings such as flying altitude, beam divergence, scan angle, pulse repetition frequency, and footprint size influence derived height and density parameters (Morsdorf et al., 2008; Næsset, 2009; Ørka et al., 2010; Solberg et al., 2009).

Higher flying altitude has been related to a reduction of the peak pulse power concentration where the laser pulse hits the surface. This leads to decreased backscatter intensities which have implications for the datasets (Hopkinson, 2007). The high flying altitude (1250 m) in 2019 compared to 2014 (600 m) can partially be compensated for with the smaller beam divergence (0.25 mrad in 2019 compared to 0.5 mrad in 2014) but it still results in lower backscatter intensities. Therefore, some intermediate echoes have probably not been recorded due to their backscatter intensity being below the noise level (Korpela et al., 2012). A reduction in the peak pulse power concentration is also expected in the 2019 ALS dataset due to the higher pulse repetition frequency (1000 kHz compared to 300 kHz in 2014). This intensity reduction is associated with increased canopy penetration because the reduced power of the laser pulse needs to travel further into the canopy until the backscatter intensity is high enough for the sensor to record a first return. The effect has been recognized especially for tall vegetation with

canopy gaps (Hopkinson, 2007). We analyzed leaf-off datasets, meaning that the observed canopy is mostly open because the Aargau forest is dominated by mixed and deciduous trees (Kanton Aargau: Departement Bau Verkehr und Umwelt, 2018). A normalization of the ALS data, especially for the intensities could improve the accuracy of the derived traits and diversity metrics (Hopkinson, 2007).

The effects of sensor and flight parameters on the individual methods are discussed in the following subsections.

4.1.2 Methods for functional trait retrieval

When conducting a multitemporal analysis, it is crucial to choose appropriate traits and to use robust methods for the determination of them. In this thesis, we chose canopy height to represent the first structural axis and foliage height diversity and plant area index as representatives of the second and third structural axes, namely vertical layering and openness of the three primary components of variation in canopy space (Fahey et al., 2019). Different functional traits could be representative of the three axes and may thus be used for diversity mapping. The thesis aimed to use the approach introduced by Schneider et al. (2017), which is why we chose CH, FHD, and PAI. They have been used and validated in Schneider et al. (2017) and show high relevancy for plant ecosystem function.

Canopy height is the most robust of the three chosen traits (Coops et al., 2016). FHD and PAI are much more sensitive to sensor and flight settings. Furthermore, PAI estimates are hard to validate due to a lack of accurate reference values, as ground-based estimates also carry uncertainty (Arnqvist et al., 2020). Various algorithms for PAI estimation were developed in the past years, but out of the three that were tested in this thesis, only one was suitable for our data. All the other methods require datasets with either scan angles close to nadir or first return only data. These conditions can oftentimes not be met using ALS data of forest inventory, as small scan angles would need an immense effort when large areas are recorded. Therefore, increasing flying altitude and swath width helps with cost reduction because a larger area can be covered by one flight line (Næsset, 2009). Considering only first returns would have led to gaps in our dataset, especially on steeper hills where flight strip overlap is low or even non-existent. The used method circumvents these problems, but it showed some rectangular patterns in 2014 when the algorithm was first used (see Appendix Figure A.16). We tried numerous approaches to remove these artifacts, like filtering points, thinning the point cloud (homogenization of the dataset), and investigating the various parameters that could explain

them. After investigating the problem, it was solved by swapping the *number of returns* with the *return number* variable in the algorithm. It is possible that an error happened during the preprocessing step of the ALS data. Unfortunately, it is not possible to track down the source of this permutation. We validated the resulting PAI values on the Star of Laufenburg (see Appendix Figure A.15) Therefore, we continued with the PAI values that have no artifacts anymore.

The determination of the parameters used in the method is also a possible cause for uncertainty. The used SR method is sensitive to grid size in heterogeneous forests (Arnqvist et al., 2020). Therefore, the used 2 x 2 m grid might not have been appropriate in all areas of the canton and might have led to uncertainties. Unfortunately, it was not possible to give exact numbers for such uncertainties.

There are visible differences between 2014 and 2019 that entail the need to normalize PAI between the two study years. The reasons for the differences are complex and cannot be explained conclusively. One possible cause might be that the approach is associated with being sensitive to ground albedo (Arnqvist et al., 2020). Having leaf-off datasets, more ground is visible and could therefore contribute to a certain deviation in PAI values between the two recording years. Furthermore, PAI is a complex metric that is sensitive to different point densities, flight altitudes, scan angles, and other parameters (Morsdorf et al., 2008, 2006). Although scan angle is accounted for, there are still other parameters that can influence the result.

For example, the determination of the scaling factor (see Eq. (6)) using the summed-up intensity values of each pulse could pose some problems. In ALS datasets, losses due to below-the-noise-level backscattering have been observed to decrease the recorded intensities up to 10-15% in understory vegetation (Korpela et al., 2012). For our scaling factor estimation, this means that not the entire backscattering intensities are used to assign the weights. Due to the leaf-off conditions, weak intensity backscatter can be expected, especially for intermediate returns. This could contribute to uncertainties in PAI results. Although the 2019 dataset might seem to be more reliable due to higher and more continuous point densities, PAI estimates may not be accurate because of the decreased peak pulse power concentration discussed above. Such uncertainties in the methods could also be a possible cause of the larger correlation between the trait and diversity metrics observed in 2019 (see Figure 3.2).

Differences between FHD maps in 2014 and 2019 are much less pronounced than for PAI values, indicating that the FHD algorithm is less sensitive to different sensor and flight

configurations. As with PAI, FHD needs some input parameter definition. We chose a 1 m binning width and excluded the lowest 3 m to distinguish between understory and canopy vegetation. When absolute FHD values are needed, i.e. if no temporal comparison is performed, the binning width would have to be chosen carefully and deliberately. However, our sensitivity analysis of FHD binning width has shown that change can always be mapped at smaller as well as larger bin widths (see Appendix Figure A.1). The magnitude of the change decreases with increasing bin width without differing the description of the vertical structure significantly (Leiterer et al., 2015).

We chose a simple mean normalization to account for the differences in FHD and PAI values between 2014 and 2019. Thus, a global constancy of the traits across the entire study region was assumed resulting in only locally observable change, which is a drawback to our approach. Therefore, caution must be exercised when interpreting the change maps of FHD and PAI values. It can be observed that there was a change, but the exact zero point, i.e. the exact values where there was no change between the two study years, is difficult to determine. A better way would have been to use ground-measured data to adapt FHD and PAI estimations. Unfortunately, there was no ground truth data available for the two recording dates. But, especially for PAI estimations, ground-based methods are also related to uncertainties, which have often been raised in the discussion sections of previous work: Sky exposure level and difficulties regarding the reproduction of the footprint can influence ground-measured PAI values (de Almeida et al., 2019; Morsdorf et al., 2006; Solberg et al., 2009; Vincent et al., 2017).

A large study region like ours has very diverse inherent characteristics that might influence the results. The chosen parameters might be suited for a certain region of our study area, but may not be appropriate in a different one that might show a different kind of vegetation community. Like McElhinny et al. (2005) discussed structural complexity metrics to be a relative concept, depending on the characteristics of the study site.

4.1.3 Considerations about the seasonal influence

To conduct a multitemporal analysis, data acquired at a similar time of the year is needed to have all datasets either under leaf-on or leaf-off conditions. Unfortunately, leaf-on data was only available for the year 2014, not 2019. Canton Aargau being dominated by broadleaved tree species implied that we were only able to analyze woody material in a large part of the study area. Therefore, short-term changes in leave composition due to disturbances before the ALS acquisitions are not influencing the analysis. Additionally, density and layering of the

lower canopy can be observed better, which would have been occluded in a summer ALS dataset. It has been recognized that leaf-off datasets are the next best alternative after combined leaf-on and leaf-off data for such analyses because it enables a detailed characterization of the lower canopy layers (Davison et al., 2020).

FHD and PAI measurements are generally expected to be lower in winter than in summer in broadleaved dominated forests. Arnqvist et al. (2020) found in their study larger differences between estimated leaf-off PAI values and ground-measured PAI compared to leaf-on PAI estimations. In this thesis, no absolute values of the functional traits were analyzed. Therefore, the observed differences between leaf-off PAI estimated by the SR method and in the study of Arnqvist et al. (2020) do not impair this thesis, apart from the possible inaccuracy of the measured PAI values already discussed.

It is important to note that in 2014, the recording dates are in February/March, and in 2019, the ALS recording took place in March/April. Out of the 164 recorded flight lines of 2019, 57 were recorded between 19. and 21. April 2019. Forests started to green from mid-April and by the end of the month, green birch leaves appeared up to altitudes of 1000 m.a.s.l. (MeteoSchweiz, 2020a). In 2014, the data acquisition took place before the greening of the forests, which was in mid-April, too (MeteoSchweiz, 2015). Thus, a certain influence can be expected, for example, higher PAI values in low-altitude regions. But such an effect is not visible in the boxplots (see Figure 3.12). A moderate increase in trait values is observable in the change boxplots in most topographic and forest classes which could be explained partially by greener forests (see Figure 3.13). But there must be also other reasons because the effect of greener forests in 2019 would most certainly be visible in the forest mix classes, which is not the case in our data. PAI values, which we would expect to react the most to greener forests, were not increasing in low-altitude areas. On the contrary, the values even decreased below 350 m.a.s.l.. A possible reason for that could be the discussed sensitivity of PAI to flight and sensor parameters or the conducted temporal normalization not being appropriate in these regions.

The effect of occlusion is supposed to be lower than under leaf-on conditions. At Laegern, Kükenbrink et al. (2017) found that only 1.5% of the total canopy volume was occluded under leaf-off conditions, while under leaf-on conditions, 25% of the canopy volume was occluded. To account for the decreased occlusion volume, we decided to use voxels with a side length of 0.5 m and aggregated the results into a 2 x 2 m grid. This allowed us to estimate even small occlusion volumes that would have been missed with a voxel side length of 2 m.

4.2 Change detection in the forests of the canton Aargau

In the following subsections, the observed patterns and changes that are trait and diversity metric specific will be discussed in detail. We have shown that we can map changes in functional trait values using ALS data. The observed differences between 2014 and 2019 vary by trait. Generally, the most distinctive change is visible as a strong decrease in all traits and diversity metrics in small areas. These are regions that were probably either logged or damaged by a storm. Unfortunately, the canton Aargau does not provide GIS data containing forest management interference, thus we cannot conclusively answer if the observed disturbances originate from anthropogenic or natural causes.

4.2.1 Patterns and changes in trait estimations

To see smaller scaled variations of the functional trait composition, having a closer look into the morphological trait distribution in the three subregions is important (see Figure 4.1). Blueish-green regions show high PAI values, low to medium vertical layering, and low to medium canopy height. They are most prominent on the flat areas on top of Frickberg, in the eastern part of Unterwald, and the west and on the ridge of Laegern where the steep slope leads towards the distinctive ridge. There, the tree height decreases to a shrub-type forest (Schneider et al., 2017). Conifer trees are oftentimes present in these areas at Frickberg and Unterwald.
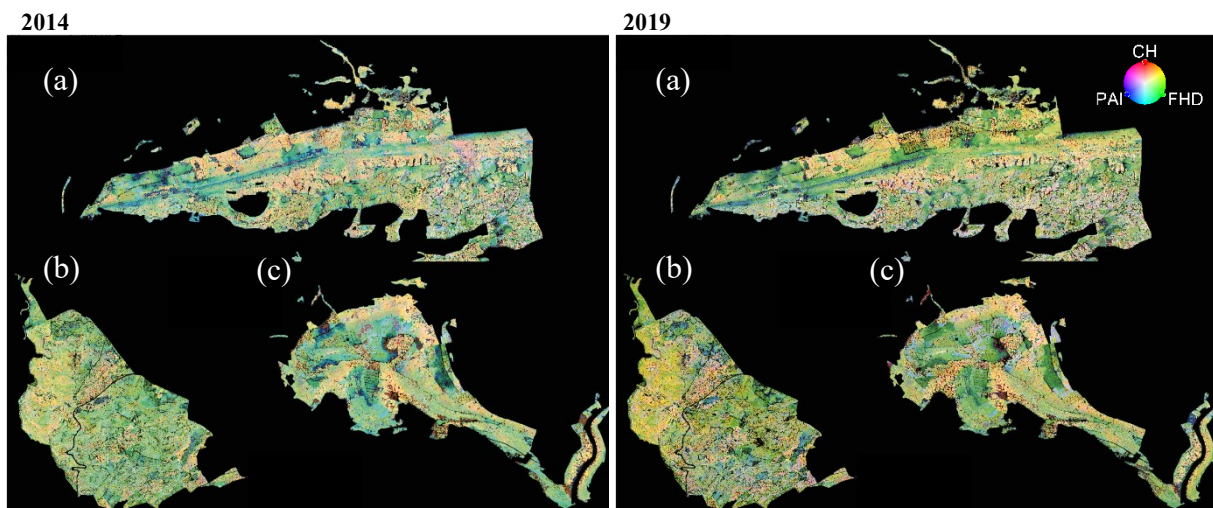
Figure 4.1: RGB composite of the morphological traits of 2014 (left) and 2019 (right) in the three subregions Laegern (a), Unterwald (b), and Frickberg (c).

Pink hues can be found close to these areas, especially on top of Frickberg and on the southern slope of Laegern. Such regions are characterized by high canopy height, little canopy layering, and medium to high canopy density. These areas are found where coniferous trees are most prominent. Having a leaf-off condition, evergreen conifers show high PAI values because

they did not shed their foliage. Yellow patches appear mainly at the steeper slopes of Laegern and Frickberg facing in a northern or north-western direction. In these regions, high trees that also have high vertical layering but low density are mostly beech trees according to community data.

The observed shift from more blueish to greener hues in 2019 can be explained by the broader dispersion of FHD values and the lower peak of PAI values that year (see histograms in Figure 3.1). Therefore, the change might be mostly due to a slightly different distribution in the trait estimates and not because of a real change in forest structure. Canopy height displays similar distribution and values in both recording years, meaning that it does not influence the trait composition as much as FHD and PAI which are much more sensitive traits.

4.2.1.1 Canopy height

Very high and low CH values were observed in the entire study region, which means that all over the canton, patches of large and small trees were observed. CH generally shows relatively small local changes, except for many small patches with a strong decrease that were probably caused by trees being cut down by management or damaged by a storm. This is reasonable because in Switzerland, large clear-cuttings are generally avoided (Oehri, 2018).

A slight increase in canopy height all over the canton and subregions can be explained by the natural growth of the trees. This increase is visible in the change maps (Figure 3.5 - Figure 3.8) and boxplots (Figure 3.12) but not in the overall mean change (see Appendix Table A.1) which means that the effect cancels itself out over the entire study area. CH increase with steeper slopes visible in Figure 3.12 could come from problems concerning the derivation of canopy height out of the ALS point clouds. Slope has also been found to be significant in half of the models. In the height normalization process of the point cloud, before the estimation of tree height, a bias will occur in steep areas. Due to this normalization, a systematic overestimation of tree height is expected (Khosravipour et al., 2015).

The topographic variables used in the models for the ANOVA are not found to be significant in all subregions. The models all have relatively low r^2 values, indicating that the models do not describe CH and CH change sufficiently. Therefore, we can assume that the studied independent variables have only a small influence on CH.

The decrease in CH in low altitudes is harder to explain. There might be more impact of wind causing more trees to fall in storms. This hypothesis is hard to verify because local windthrows are not mapped. Only maps showing damage from bigger storms like Vivian (1990)

or Lothar (1999) are available today. In unprotected forest areas, this decrease could be explained by management cuttings. Low altitude areas are easy to access and it would thus be more probable that management disturbances were higher in such regions. There is less CH increase in high-altitude protected forest areas than in unprotected forests. There, many nature reserves are located in more remote and inaccessible regions, i.e. on steep or cliffy slopes. Especially older forest reserves were located in such remote areas so that the more productive regions did not need to be excluded from management. Such decisions are caused by the requirement to protect a defined fraction of the forested area. In these inaccessible forest areas, soil depth, water availability, and other factors may be not as beneficial for tree growth, which could explain the smaller CH increase in nature reserves.

4.2.1.2   *Foliage height diversity*

Foliage height diversity shows relatively homogenous values all across the canton, especially in 2014. The 2019 values have a wider value dispersion and also show some more pronounced features. We do not expect this change in dispersion to be caused solely by topographic or other natural factors and thus being real morphological change, but also coming from different viewing geometries, point densities, and scan angles, meaning it to be sensor-related change. FHD is a much more sensitive trait than CH that could respond to such sensor and flight settings, thus it cannot be excluded that they have an impact on FHD results. The higher point density in 2019 might lead to a better differentiation in FHD values as more data points are available. Also, because the recording dates were generally later in spring than 2014, there might have been already some greening in the forest which could also explain the differences in distribution. Because we stratified in 1 m vertical slabs, 2014 point density may be on the lower end of suitable point densities to capture vertical layering. Especially in areas with no flight strip overlap, point density might be too low resulting in an increase in random undersampling of the vertical structure (Leiterer et al., 2015). At Laegern, there is a very slight striping effect visible. This increase corresponds to low-density areas caused by no overlapping flight strips. This may indicate that low point densities lead to an underestimation of FHD values at the Laegern. FHD changes with altitude and slope steepness, maybe because of similar normalization problems discussed above in Chapter 4.2.1.1. This observation is supported by the significant influence of altitude in five out of the six studied models and of slope in half of the models. The change in FHD values seems to be similar in protected and unprotected forest areas across all studied topographic and forest classes.

4.2.1.3 *Plant area index*

PAI values show a slight increase in the southern part of the canton and generally decreasing values in the northern part of the Jura.

Especially in 2019, many gaps (*NaN*-values) can be observed in the maps. The reason is that the algorithm needs at least one ground classified point in a raster cell to be able to compute the PAI. In dense forest areas with high PAI, the ground is oftentimes occluded and no ground point is available. In such cases, the algorithm assigns *NaN* to this raster cell. This has implications for our results. First, pixel gaps in our dataset are almost always at high-density areas indicating that the highest values in our study area were not estimated. Therefore, we can expect a systematic underestimation of PAI values. This in turn has implications for the temporal normalization process. Since the mean value is probably not quite correct, because especially high values are not present, the normalization factor is also not precise and the assumption that there was no global change can thus not be fully fulfilled. However, as has already been discussed, this is a somewhat tricky assumption anyway, since it is entirely possible that there was a global increase or decrease over the 5 years.

Slope and forest mix rate have been found to be significant for PAI in all models of the subregions. We did not find different PAI values depending on slope by the examination of the boxplots. This could either be due to the aggregation process of the boxplots or that the three subregions do not fully represent the behavior of the PAI values across the entire canton. High PAI values in coniferous forests are reasonable because of our leaf-off condition in the used winter ALS dataset. Evergreen trees have naturally a higher density than leafless trees (Davison et al., 2020).

The decrease of PAI in low altitudes is consistent with the observed low values of CH and FHD at the same altitudes. Because nature reserves show the same behavior, it cannot be solely due to management. It is possible that in unprotected areas the decrease may come from loggings. The exact causes would need to be examined further. Increasing PAI values could be caused by higher point densities in 2019 and higher flying altitudes resulting in lower accuracy in the weighting process of the intensities, as discussed above (see Chapter 4.1.2).

Most differences between protected and unprotected areas are minor and we thus cannot conclude that PAI values differ significantly depending on protection. The only difference between these two forest area groups is that except for pure coniferous forests, PAI values decreased slightly more in nature forest reserves than in unprotected forests.

4.2.2 Temporal differences in functional diversity metrics

It is very unlikely that the large increase in richness of almost 123% can be entirely attributed to the natural diversification of the Aargau forests. The observed period spans only 5 years and since we can only observe woody material except for needles, the size change in richness is most certainly not too large. It is very probable that besides biotic and abiotic factors also factors concerning the methods led to this increase.

Although the mean has increased sharply, the same patterns can be seen in both years. It can therefore be assumed that this metric is reliable but needs some kind of normalization, which would be subject to further research. The trait values were much more dispersed in 2019 (see Figure 3.1) that could cause FRic, being highly susceptible to outliers, to show these high values in 2019. The classification of the change map corrects for this large difference because the mean ± one standard deviation is used as the "no-change" pixels. Of course, this visualization has to be interpreted with care, because it may well be that a global change to the positive or negative has taken place during this period. But it still enables the reader to find certain patterns that can be interpreted.

The impact of different radii used for the computation of diversity metrics has been investigated and discussed in prior work (Helfenstein et al., 2022; Schneider et al., 2017). The very small local patterns of divergence values in our study area might be caused by the radius used for the computation of the diversity metric. We chose a neighborhood of 30 m to be included in the diversity metric (richness and divergence) estimation due to computational effort. When using a larger neighborhood, divergence is expected to show bigger areas of changing values (Schneider et al., 2017).

High diversity values in southern Aargau can be explained by the higher occurrence of evergreen coniferous needle trees due to the absence of foliage in deciduous trees. It would be interesting to explore if the diversity difference between southern and north-western Aargau was smaller under leaf-on conditions, which would be subject to further studies. Low diversity, especially richness values at high, steep, and/or southern facing slopes can be explained by unfavorable soil and topographic conditions that only allow certain plants to exist. These stress factors can lower water availability and soil depth and thus limit resource availability which limits the range of the biotope space (Schneider et al., 2017). A less pronounced increase or even a decrease in the diversity metrics observed in these areas can also be attributed to the factors mentioned above. A more restricted community niche can lead to a less stable system that could respond even more to abiotic stress factors like water scarcity.

2015, 2017, and 2018 were among the five warmest years since measurement start in 1864 (MeteoSchweiz, 2020b; Sturm et al., 2022). Looking at the aridity indices (*ETa/ETp*) published by BAFU (Bundesamt für Umwelt) from the years before the 2014 data acquisitions, most years provided enough water for the plants. The period between both recording dates is characterized by the very hot and dry years 2015 and 2018. The aridity index displays the rate of actual evapotranspiration (*ETa*) divided by the potential evapotranspiration (*ETp*) during the growing season (April-August). In 2015, 2017, and 2018, especially in the chalky soils of Jura, water availability was severely limited. This puts trees under a lot of stress. If the *ETa/ETp*-rate is too low, which was the case in these years and regions, plants close their stomata for parts of the day leading to a decrease in photosynthesis and gas exchange that results in weakened plants and resilience (Remund and Augustin, 2015). This extreme drought stress could cause a low increase or even decrease in functional richness and divergence values in Jura.

Unprotected forests show generally higher diversity values. This is particularly pronounced in functional richness, but also divergence tends to behave in this way. These forests display much higher richness in higher altitudes than nature reserves which might also be due to the chosen forest areas that got protected (see Chapter 4.2.1.1). Diversity has been linked to management and forest development (Schneider et al., 2017). Therefore, higher diversity values in unprotected forest areas may be due to management rejuvenating forest patches and thus increasing the community niche extent. This can be small-scale variability of the morphological traits which did not necessarily show in the boxplots of the individual traits due to the aggregation process involved in boxplot creation. Because richness and divergence compute the total community niche extent and density, this small-scale variability of the traits may be depicted in the diversity metric values.

Although we have found decreases or simply smaller increases in the protected areas compared to the unprotected areas, one has to be careful with conclusions. It cannot be decisively stated that the computed higher structural diversity leads to higher species diversity, as this has been proven and disproven in many studies (Tanabe et al., 2001). It is possible that the chosen diversity metrics do not fully portray species richness or species diversity in our study region. But still, the observed tendencies could give indications that the discussed areas might be under more stress leading to the noted changes.

4.2.3 Comparison with other functional diversity mapping results

Our used approach introduced was first tested on the Laegern by Schneider et al. (2017). Therefore, we can compare our results with theirs. They did not map diversity metrics at a 30 m radius, which is why our resulting maps (radius 30 m) are compared to theirs with a radius of 60 m. Only a small part of our Laegern subregion overlaps with theirs and the comparison is visible in Figure A.17. There, the RGB composites, FRic, and FDiv maps are depicted.

The means and standard deviations of CH and FHD were very similar, only PAI had a much higher mean than in our study, which makes sense because we estimated PAI under leaf-off conditions. Furthermore, the already discussed difficulties of PAI estimations can lead to deviations. Correlations between the traits are different, but this may be because we examined the entire canton and Schneider et al. (2017) only looked at Laegern.

The spatial patterns of the RGB composites do match, especially with our 2014 dataset. Most obvious are the higher fraction of blue hues in the results of Schneider et al. (2017), which represent areas with high density and comparable low CH and vertical diversity. Again, this is reasonable because they examined Laegern in the foliated state while we looked at data under defoliated conditions.

The found functional richness and divergence patterns are also similar but are harder to compare due to the different radii in the two studies. Especially the local changes in divergence can hardly be compared between the two studies. But still, in both studies, it is found that richness changes with topography. For example, areas around the ridge showed lower diversity values.

Schneider et al. (2017) conducted the same ANOVA but used slightly different models. They additionally used curvature, soil type, soil depth, soil rocks, and radiation as independent variables. But they did not use the forest mix rate, occlusion, and point density as independent variables. Therefore, the results are different but general observations can be compared. For example, the general magnitude of the CH variance explained by altitude has a similar range (<5% in both studies). The largest difference can be observed in the variance explained by diversity metrics. The large impact found by Schneider et al. (2017) of altitude has not been found in our Laegern dataset. In their study, they found that altitude and slope explained together more than 15% of the variance of functional richness, but in our study, these variables explained only <10% of the respective variance. Possible reasons might be the different radii or the designed models.

Concluding, the results are comparable but not the same, which was expected due to the different recording dates (different years and foliage states), different computation methods of PAI estimates, and different radii used for the diversity metrics.

4.3   Occlusion mapping

Lastly, we will discuss the influence of occlusion on our results. We used the approach by Kükenbrink et al. (2017) to map occlusion occurring in the ALS acquisitions of 2014 and 2019. Due to the computational expense and problems using the ScienceCluster, only the three subregions Laegern, Unterwald, and Frickberg have been mapped.

All regions without flight strip overlap are visible as striping in a mostly north-south direction in the occlusion maps (see Figure 3.15). Especially at Laegern, the areas without flight strip overlap show increased occlusion values. They occur mostly around the ridge where the increase in altitude is large. The flight direction of the airplane was almost north-south or vice-versa. The 2014 ALS data was particularly vulnerable because the flight strip overlap was smaller than in 2019, resulting in more areas only being covered by one flight strip. In 2014, most of the canton was covered by two flight strips, while in 2019 most of the area was recorded by three or even four flight strips (see Figure 4.2). Kükenbrink et al. (2017) found that the fraction of observed canopy volume increases significantly when more flight strips cover the ground. Furthermore, a higher point density is favorable for a better observation of the canopy fraction, which we also see in our study (Kükenbrink et al., 2017). In 2019, the mean point density in the three subregions Laegern, Unterwald, and Frickberg is 67% higher than in 2014. Therefore in 2019, point density and the number of flight strips covering the study area are advantageous for a higher fraction of observed canopy volume and thus lead to less occlusion. This corresponds with the findings of Kükenbrink et al. (2017).
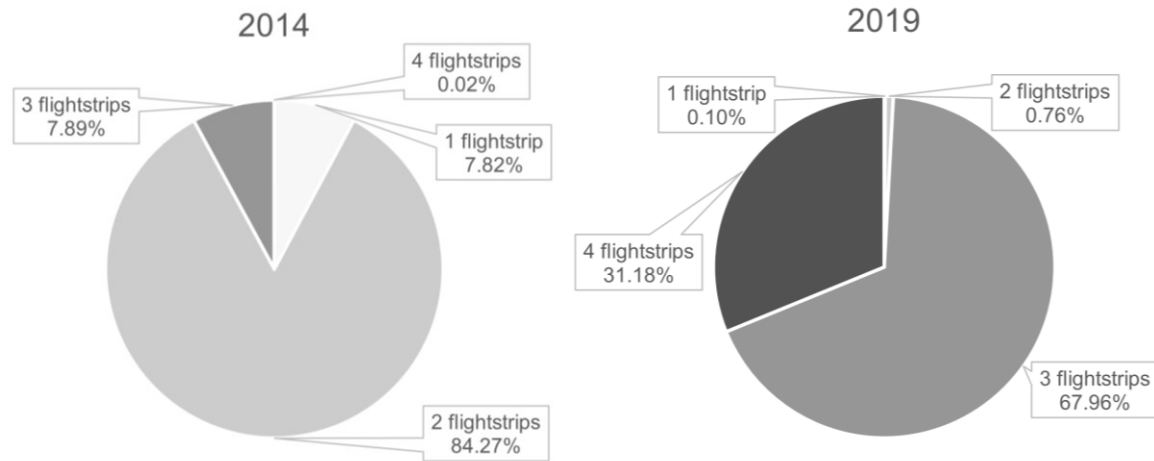
Figure 4.2: Fraction of the amount of flight strip overlap in the canton Aargau during both ALS campaigns. In 2014 (left), more than 4/5 of the study area was recorded by two flight strips, in 2019 (right), more than 2/3 of the area was recorded by 3 flight strips.

High occlusion value patterns mostly coincide with higher fractions of evergreen conifers present that occlude more of the lower canopy volume than leafless broadleaf trees. This has also been found by Kükenbrink et al. (2017). Appendix Figure A.18 shows an example of this occluding effect of evergreen conifer trees in the Frickberg region.

The observed decrease in occlusion is either due to higher point density in the areas of 2019 or different viewing angles in both campaigns. In Unterwald, decreasing and increasing pixels are oftentimes mixed and do not form a somewhat connected change patch, as can be observed in other subregions (for example northern Laegern). This could indicate change caused by different flight paths and thus different viewing geometries.

Canopy height and FHD derivations do not seem to be very sensitive to occlusion. Even in Unterwald, where the highest occlusion is observed of all subregions, CH and FHD values are relatively robust. The only effect visible, mostly in Unterwald and Laegern, is a slightly decreasing CH with less occlusion. Generally, more noise is inherent to canopy height estimations under leaf-off conditions compared to leaf-on conditions (Davison et al., 2020). Thus, very open parts of the canopy might cause first returns not to record the absolute top of the trees because small branches could cause backscatter intensities below the noise level. This could lead to a minimal underestimation of trees with a very open crown that might explain part of the lower CH values in low occluded areas (Davison et al., 2020). In the ANOVA, occlusion is not found to be significant for CH estimates. But as the model has such a low r^2, the parametrization seems not to be representative and therefore has to be interpreted with care.

We expected FHD to be sensitive to occlusion because bottom canopy layers would not have been recorded where heavy occlusion is present. In such areas, the vertical structure would not

be known and FHD estimates would be unreliable. The ANOVA results support this hypothesis, as occlusion is significant Unterwald in both years and even explains ~20% of the variance in 2019. Furthermore, point density is also found significant, which is linked to occlusion. Areas with low point densities are also more prone to higher occlusion (Kükenbrink et al., 2017). In the boxplots, FHD does not display a dependence on occlusion. A possible explanation might be that due to the aggregation process inherent to boxplots, the effect was absorbed and thus small-scale variability might not be shown in the boxplots.

Out of the three traits, PAI values show the largest differences with increasing occlusion. High PAI values in heavily occluded areas make sense as the leaf and branch density in such areas must be very high to cause large parts of the canopy to be occluded. This finding is supported by the results of the ANOVA, where occlusion and point density explained together 27 to 38% of the PAI variance in 2014. In 2019, the effect is even stronger. Occlusion and point density explained in Frickberg 35%, in Unterwald 45%, and in Laegern 62% of the variance. The models of 2019 showed also relatively high r^2, indicating a good fit of the model variables. This influence can also be seen in the models explaining PAI change: Point density and occlusion change explained together 57% of the variance, which is also visible in our change maps. In Unterwald for example, the areas with increasing PAI values match the regions with increasing occlusion (see Figure 3.7 and Figure 3.15). Therefore, PAI is extremely sensitive to scene parameters like point density and occlusion.

Occlusion influences also the diversity metrics, richness, and divergence, but much less than it influences PAI. This is visible in the results of the ANOVA, where <10% of the richness variance was explained by the variable and the r^2 of the models were low (*2014: r^2 < 0.06, 2019: r^2 < 0.15*). For the change of functional richness, occlusion change was found to be significant, but only explained less than 2.5 % of the variance, while the model also had a low r^2 of less than 0.23. For the diversity change, it was even lower (r^2 < 0.07). A possible reason could be, that the neighborhood of 30 m which was used for the computation of richness and divergence, decreased the occlusion and point density influence which lead to the diversity metrics being much more robust. But there is still uncertainty in these two metrics because they were calculated out of the traits that are sometimes highly susceptible to occlusion.

4.3.1 Geographically weighted regression

Because our ANOVA analysis showed that only very little of the variance of FRic and FDiv had been explained and the r^2 were very low, we also tested if a geographically weighted regression (GWR) could better describe the changes in the diversity metrics. The methodology is described in Appendix B, because this method is only an outlook. We only tested it for Frickberg with two models:

1. FRic_diff ~ occlusion_diff + point density_diff
2. FDiv_diff ~ occlusion_diff + point density_diff

The model outputs can be found in Appendix Figure B.1 and Figure B.2Figure A.13. The FRic model had an r^2 of 0.92 the FDiv model had a slightly lower r^2 of 0.80. This also hints at a very large influence of occlusion and point density in richness and divergence change between 2014 and 2019 more than what we found in our generalized linear regression and ANOVA. It would be needed to examine the GWR results more closely and run much more models with different neighborhoods to have robust results, which could be subject to further studies. But these preliminary results show how GWR might be more fitting to describe the relationship between the diversity metrics and our studied independent variables.

The large computational effort is one of the key limitations of the occlusion mapping method when researching a large study area. There are possibilities to speed up the occlusion mapping algorithm. Especially the process of reading the ALS data in and the preparation of the grids used later for ray-tracing can be optimized. This would have to be researched in further studies and would enable occlusion mapping to be used as a tool to know uncertainties in datasets used for multitemporal analyses. For example, heavily occluded areas could either be excluded from further analyses or at least treated with great caution.

5 Conclusion

In this Master's thesis, we have shown that it is possible to map functional diversity using ALS data in large areas. A comparison between two points in time is possible, but certain constraints arise in the analysis. As ALS datasets from different years are often recorded with different sensors and flight settings, the influence of these parameters must be taken into account. It is possible to map the functional traits and derive changes from them, but depending on which traits are chosen, the influence of sensor and flight parameters must be expected to vary in quantity. We could show that simple and robust traits like canopy height form a good base for such a comparison. The more complex the derivation of a morphological trait, the more sensitive it reacts to external influences. Thus, if sensor differences are too large, one has to be careful in the subsequent use of such estimates. Concluding, we were able to map changes in trait and diversity metrics, but it is not possible to quantify the differences exactly, as uncertainties in the calculation of traits and diversity metrics between the two intake years, such as temporal normalization, lead to inaccuracies in the results. Nevertheless, patterns and general statements on change can be analyzed. In further research, it would be interesting to try to classify the influences into real and sensor-based changes and to quantify maximal sensor and flight attributes, such as minimal point density, that still allow accurate trait and diversity mapping.

We have shown that it is very difficult to disentangle the effects of real morphological change and sensor-related change. We have observed that all three traits, CH, FHD, and PAI slightly increased in the topographic and forest classes between 2014 and 2019. We have observed the strongest decrease or less pronounced increase (in FRic) of diversity in high-altitude regions, steep and southern-facing slopes. Forests in such areas seem to respond even more to abiotic stress factors, such as drought and heat, due to a more restricted community niche that supports the findings of Schneider et al. (2017). The Jura region is particularly affected by this, where diversity metrics showed a decrease between both study years.

Forest nature reserves showed generally lower values in trait and diversity metrics, increased less, or respectively displayed a bigger decrease during the 5 years. It cannot be conclusively said that higher species diversity can be found in areas where higher structural diversity was computed. Therefore, we cannot state that natural forest reserves are generally performing poorer in diversity than unprotected areas. It might be that our estimated metrics do not fully represent species richness in our study area which might be equal to or even higher in protected regions, which should be subject to further studies.

It has been shown that occlusion has a significant effect on trait estimations. Especially PAI values were highly influenced by the amount of occlusion. Therefore, it is very important to consider occlusion effects in multitemporal analyses of ALS datasets. The major drawback of the used approach is the immense computational effort it requires to map a large region. The computational expenses must be lowered significantly to enable the integration of occlusion in change detection.

It will be possible to perform accurate change detection with ALS using functional diversity mapping in the future, but the goal must be to include as many sensor and flight parameters in the calculation of the metrics as possible. Therefore, it is important to work very carefully in the campaigns and to put a lot of effort into the collection of these parameters. With such improvements, high-quality multitemporal analyses using ALS data can be conducted and help in monitoring diversity or biodiversity parameters continuously over large areas.

Bibliography

AGIS, 2019. Waldareale.

Ahmed, D.A., van Bodegom, P.M., Tukker, A., 2018. Evaluation and selection of functional diversity metrics with recommendations for their use in life cycle assessments. Int. J. Life Cycle Assess. 24, 485–500. https://doi.org/10.1007/s11367-018-1470-8

Amanatides, J., Woo, A., 1987. A Fast Voxel Traversal Algorithm for Ray-tracing. Eurographics 87, 3–10.

Arnqvist, J., Freier, J., Dellwik, E., 2020. Robust processing of airborne laser scans to plant area density profiles. Biogeosciences 17, 5939–5952. https://doi.org/10.5194/bg-17-5939-2020

Bienert, A., Queck, R., Schmidt, A., Bernhofer, C., Maas, H.-G., 2010. Voxel Space Analysis of Terrestrial Laser Scans in Forests for. Int. Arch. Photogramm. Remote Sens. Spat. Inf. Sci. 38, 92–97.

Bivand, R., Piras, G., 2015. Comparing Implementations of Estimation Methods for Spatial Econometrics, JSS Journal of Statistical Software.

Bojinski, S., Verstraete, M., Peterson, T.C., Richter, C., Simmons, A., Zemp, M., 2014. The concept of essential climate variables in support of climate research, applications, and policy. Bull. Am. Meteorol. Soc. 95, 1431–1443. https://doi.org/10.1175/BAMS-D-13-00047.1

Bornand, A., 2020. Large-scale individual tree classification using airborne laser scanning in temperate mixed forests.

Brändli, U.-B., Abegg, M., Allgaier Leuch, B., 2020. Schweizerisches Landesforstinventar. Ergebnisse der vierten Erhebung 2009–2017.

Bundesamt für Landestopografie swisstopo, 2022a. swissBOUNDARIES3D.

Bundesamt für Landestopografie swisstopo, 2022b. SWISSIMAGE.

Carmona, C.P., de Bello, F., Mason, N.W.H., Lepš, J., 2016. Traits Without Borders: Integrating Functional Diversity Across Scales. Trends Ecol. Evol. 31, 382–394. https://doi.org/10.1016/j.tree.2016.02.003

Chen, J.M., Black, T.A., Adams, R.S., 1991. Evaluation of hemispherical photography for determining plant area index and geometry of a forest stand. Agric. For. Meteorol. 56, 129–143. https://doi.org/10.1016/0168-1923(91)90108-3

Chun, Y., Griffith, D., 2013. Spatial statistics and geostatistics: theory and applications for geographic information science and technology. SAGE Publications Ltd. https://doi.org/10.1007/978-3-319-23519-6_1650-1

Comber, A., Brunsdon, C., Charlton, M., Dong, G., Harris, R., Lu, B., Yihe, L., Murakami, D., Nakaya, T., Wang, Y., Harris, P., 2022. A Route Map for Successful Applications of Geographically Weighted Regression. Geogr. Anal. 1–24. https://doi.org/10.1111/gean.12316

Coops, N.C., Tompaski, P., Nijland, W., Rickbeil, G.J.M., Nielsen, S.E., Bater, C.W., Stadt, J.J., 2016. A forest structure habitat index based on airborne laser scanning data. Ecol. Indic. 67, 346–357. https://doi.org/10.1016/j.ecolind.2016.02.057

Davison, S., Donoghue, D.N.M., Galiatsatos, N., 2020. The effect of leaf-on and leaf-off forest

canopy conditions on LiDAR derived estimations of forest structural diversity. Int. J. Appl. Earth Obs. Geoinf. 92, 102160. https://doi.org/10.1016/j.jag.2020.102160

de Almeida, D.R.A., Stark, S.C., Shao, G., Schietti, J., Nelson, B.W., Silva, C.A., Gorgens, E.B., Valbuena, R., Papa, D. de A., Brancalion, P.H.S., 2019. Optimizing the remote detection of tropical rainforest structure with airborne lidar: Leaf area profile sensitivity to pulse density and spatial sampling. Remote Sens. 11. https://doi.org/10.3390/rs11010092

de Almeida, D.R.A., Stark, S.C., Silva, C.A., Hamamura, C., Valbuena, R., 2022. leafR: Calculates the Leaf Area Index (LAD) and Other Related Functions.

Fahey, R.T., Atkins, J.W., Gough, C.M., Hardiman, B.S., Nave, L.E., Tallant, J.M., Nadehoffer, K.J., Vogel, C., Scheuermann, C.M., Stuart-Haëntjens, E., Haber, L.T., Fotis, A.T., Ricart, R., Curtis, P.S., 2019. Defining a spectrum of integrative trait-based vegetation canopy structural types. Ecol. Lett. 22, 2049–2059. https://doi.org/10.1111/ele.13388

Geiger, W., Göttin, T., Guignet, E.M., Hofmann, C., Wild, F., 2012. Strategie Biodiversität Schweiz.

Helfenstein, I.S., Schneider, F.D., Schaepman, M.E., Morsdorf, F., 2022. Assessing biodiversity from space: Impact of spatial and spectral resolution on trait-based functional diversity. Remote Sens. Environ. 275, 113024. https://doi.org/10.1016/j.rse.2022.113024

Hijmans, R.J., 2022. terra: Spatial Data Analysis.

Homolová, L., Malenovský, Z., Clevers, J.G.P.W., García-Santos, G., Schaepman, M.E., 2013. Review of optical-based remote sensing for plant trait mapping. Ecol. Complex. 15, 1–16. https://doi.org/10.1016/j.ecocom.2013.06.003

Hopkinson, C., 2007. The influence of flying altitude, beam divergence, and pulse repetition frequency on laser pulse return intensity and canopy frequency distribution. Can. J. Remote Sens. 33, 312–324. https://doi.org/10.5589/m07-029

Hopkinson, C., Chasmer, L., 2009. Testing LiDAR models of fractional cover across multiple forest ecozones. Remote Sens. Environ. 113, 275–288. https://doi.org/10.1016/j.rse.2008.09.012

Horn, B.K.P., 1981. Hill Shading and the Reflectance Map. Proc. IEEE 69, 14–47. https://doi.org/10.1109/PROC.1981.11918

Isenburg, M., 2021. LAStools - efficient LiDAR processing software.

Ishii, H.T., Tanabe, S.I., Hiura, T., 2004. Exploring the relationships among canopy structure, stand productivity, and biodiversity of temperate forest ecosystems. For. Sci. 50, 342–355.

Kanton Aargau: Departement Bau Verkehr und Umwelt, 2021. Aargauer Naturwaldreservate [WWW Document]. Kant. Aargau. URL https://www.ag.ch/de/bvu/wald/naturschutz_im_wald/waldreservate_im_aargau/waldres ervate_im_aargau.jsp

Kanton Aargau: Departement Bau Verkehr und Umwelt, 2018. Zustand und Entwicklung des Aargauer Waldes: Ergebnisse der 2. Aargauer Waldinventur 2016.

Khosravipour, A., Skidmore, A.K., Wang, T., Isenburg, M., Khoshelham, K., 2015. Effect of slope on treetop detection using a LiDAR Canopy Height Model. ISPRS J. Photogramm. Remote Sens. 104, 44–52. https://doi.org/10.1016/j.isprsjprs.2015.02.013

Korpela, I., Hovi, A., Morsdorf, F., 2012. Understory trees in airborne LiDAR data - Selective mapping due to transmission losses and echo-triggering mechanisms. Remote Sens. Environ. 119, 92–104. https://doi.org/10.1016/j.rse.2011.12.011

Kükenbrink, D., Leiterer, R., Schneider, F.D., Morsdorf, F., 2015. Mapping Occluded volume and voxel based Plant Area Index from Airborne Laser Scanning using ray-tracing, in: Proceedings of SilviLaser 2015. pp. 232–234.

Kükenbrink, D., Schneider, F.D., Leiterer, R., Schaepman, M.E., Morsdorf, F., 2017. Quantification of hidden canopy volume of airborne laser scanning data using a voxel traversal algorithm. Remote Sens. Environ. 194, 424–436. https://doi.org/10.1016/j.rse.2016.10.023

Leiterer, R., Furrer, R., Schaepman, M.E., Morsdorf, F., 2015. Forest canopy-structure characterization: A data-driven approach. For. Ecol. Manage. 358, 48–61. https://doi.org/10.1016/j.foreco.2015.09.003

Liu, J., Li, L., Akerblom, M., Wang, T., Skidmore, A., Zhu, X., Heurich, M., 2021. Comparative evaluation of algorithms for leaf area index estimation from digital hemispherical photography through virtual forests. Remote Sens. 13, 1–25. https://doi.org/10.3390/rs13163325

MacArthur, R.H., MacArthur, J.W., 1961. On Bird Species Diversity. Ecology 42, 594–598.

MATLAB, 2021. version 9.10.0.1739362 (R2021a) Update 5. The MathWorks Inc., Natick, Massachusetts.

McElhinny, C., Gibbons, P., Brack, C., Bauhus, J., 2005. Forest and woodland stand structural complexity: Its definition and measurement. For. Ecol. Manage. 218, 1–24. https://doi.org/10.1016/j.foreco.2005.08.034

MeteoSchweiz, 2020a. Klimareport 2019. Zürich.

MeteoSchweiz, 2020b. Klimabulletin Jahr 2019. Zürich.

MeteoSchweiz, 2015. Klimareport 2014. Zürich.

Milan Geoservice, 2020. Projektdokumentation Abschlussbericht: LiDAR-Datensatz Kanton Aargau 2019.

Milan Geoservice, 2014. Projektdokumentation: LiDAR-Befliegung Kanton Aargau unbelaubt März/April 2014.

Moles, A.T., Warton, D.I., Warman, L., Swenson, N.G., Laffan, S.W., Zanne, A.E., Pitman, A., Hemmings, F.A., Leishman, M.R., 2009. Global patterns in plant height. J. Ecol. 97, 923–932. https://doi.org/10.1111/j.1365-2745.2009.01526.x

Morsdorf, F., Frey, O., Meier, E., Itten, K.I., Allgöwer, B., 2008. Assessment of the influence of flying altitude and scan angle on biophysical vegetation products derived from airborne laser scanning. Int. J. Remote Sens. 29, 1387–1406. https://doi.org/10.1080/01431160701736349

Morsdorf, F., Kötz, B., Meier, E., Itten, K.I., Allgöwer, B., 2006. Estimation of LAI and fractional cover from small footprint airborne laser scanning data based on gap fraction. Remote Sens. Environ. 104, 50–61. https://doi.org/10.1016/j.rse.2006.04.019

Næsset, E., 2009. Effects of different sensors, flying altitudes,ulse repetition frequencies on forest canopy metrics and biophysical stand properties derived from small-footprint airborne laser data. Remote Sens. Environ. 113, 148–159. https://doi.org/10.1016/j.rse.2008.09.001

Noss, R.F., 1990. Indicators for Monitoring Biodiversity: A Hierarchical Approach. Conserv. Biol. 4, 355–364. https://doi.org/10.1111/j.1523-1739.1990.tb00309.x

Oehri, J., 2018. Biodiversity and Ecosystem Functioning across Scales in Real-World Landscapes. Universität Zürich. https://doi.org/10.5167/uzh-172199

Ørka, H.O., Næsset, E., Bollandsås, O.M., 2010. Effects of different sensors and leaf-on and leaf-off canopy conditions on echo distributions and individual tree properties derived from airborne laser scanning. Remote Sens. Environ. 114, 1445–1461. https://doi.org/10.1016/j.rse.2010.01.024

Python Software Foundation, 2021. Python Language Reference, version 3.9.7.

QGIS.org, 2022. QGIS Geographic Information System.

R Core Team, 2022. R: A Language and Environment for Statistical Computing.

Remund, J., Augustin, S., 2015. Zustand und Entwicklung der Trockenheit in Schweizer Wäldern. Schweizerische Zeitschrift fur Forstwes. 166, 352–360. https://doi.org/10.3188/szf.2015.0352

Schleuter, D., Daufresne, M., Massol, F., Argillier, C., 2010. A user's guide to functional diversity indices. Ecol. Monogr. 80, 469–484. https://doi.org/10.1890/08-2225.1

Schneider, F.D., Leiterer, R., Morsdorf, F., Gastellu-Etchegorry, J.P., Lauret, N., Pfeifer, N., Schaepman, M.E., 2014. Simulating imaging spectrometer data: 3D forest modeling based on LiDAR and in situ data. Remote Sens. Environ. 152, 235–250. https://doi.org/10.1016/j.rse.2014.06.015

Schneider, F.D., Morsdorf, F., Schmid, B., Petchey, O.L., Hueni, A., Schimel, D.S., Schaepman, M.E., 2017. Mapping functional diversity from remotely sensed morphological and physiological forest traits. Nat. Commun. 8, 1–12. https://doi.org/10.1038/s41467-017-01530-3

Seidel, D., Ehbrecht, M., Puettmann, K., 2016. Assessing different components of three-dimensional forest structure with single-scan terrestrial laser scanning: A case study. For. Ecol. Manage. 381, 196–208. https://doi.org/10.1016/j.foreco.2016.09.036

Skidmore, A.K., Pettorelli, N., Coops, N.C., Geller, G.N., Hansen, M., Lucas, R., Mücher, C.A., O'Connor, B., Paganini, M., Pereira, H.M., Schaepman, M.E., Turner, W., Wang, T., Wegmann, M., 2015. Environmental science: Agree on biodiversity metrics to track from space. Nature 523, 403–405. https://doi.org/10.1038/523403a

Solberg, S., Brunner, A., Hanssen, K.H., Lange, H., Næsset, E., Rautiainen, M., Stenberg, P., 2009. Mapping LAI in a Norway spruce forest using airborne laser scanning. Remote Sens. Environ. 113, 2317–2327. https://doi.org/10.1016/j.rse.2009.06.010

Sponagel, H., 2005. Bodenkundliche Kartieranleitung, 5., verbes. ed. Schweizerbart, Stuttgart.

Stahl, U., Reu, B., Wirth, C., 2014. Predicting species' range limits from functional traits for the tree flora of North America. Proc. Natl. Acad. Sci. U. S. A. 111, 13739–13744. https://doi.org/10.1073/pnas.1300673111

Sturm, J., Santos, M.J., Schmid, B., Damm, A., 2022. Satellite data reveal differential responses of Swiss forests to unprecedented 2018 drought. Glob. Chang. Biol. 28, 2956–2978. https://doi.org/10.1111/gcb.16136

Tanabe, S.I., Toda, M.J., Vinokurova, A. V., 2001. Tree shape, forest structure and diversity of drosophilid community: Comparison between boreal and temperate birch forests. Ecol. Res. 16, 369–385. https://doi.org/10.1046/j.1440-1703.2001.00402.x

Villéger, S., Mason, N.W.H., Mouillot, D., 2008. New multidimensional functional diversity indices for a multifaceted framework in functional ecology. Ecology 89, 2290–2301.

https://doi.org/10.1890/07-1206.1

Vincent, G., Antin, C., Laurans, M., Heurtebize, J., Durrieu, S., Lavalley, C., Dauzat, J., 2017. Mapping plant area index of tropical evergreen forest by airborne laser scanning. A cross-validation study using LAI2200 optical sensor. Remote Sens. Environ. 198, 254–266. https://doi.org/10.1016/j.rse.2017.05.034

Waser, L., Ginzler, C., 2021. Forest Type NFI. https://doi.org/10.16904/1000001.3

Wittwer, R., 2016. 20 Jahre Naturschutzprogramm Wald. Umwelt Aargau 45–48.

Zheng, Z., Zeng, Y., Schneider, F.D., Zhao, Y., Zhao, D., Schmid, B., Schaepman, M.E., Morsdorf, F., 2021. Mapping functional diversity using individual tree-based morphological and physiological traits in a subtropical forest. Remote Sens. Environ. 252. https://doi.org/10.1016/j.rse.2020.112170

A Appendix – Additional figures and tables
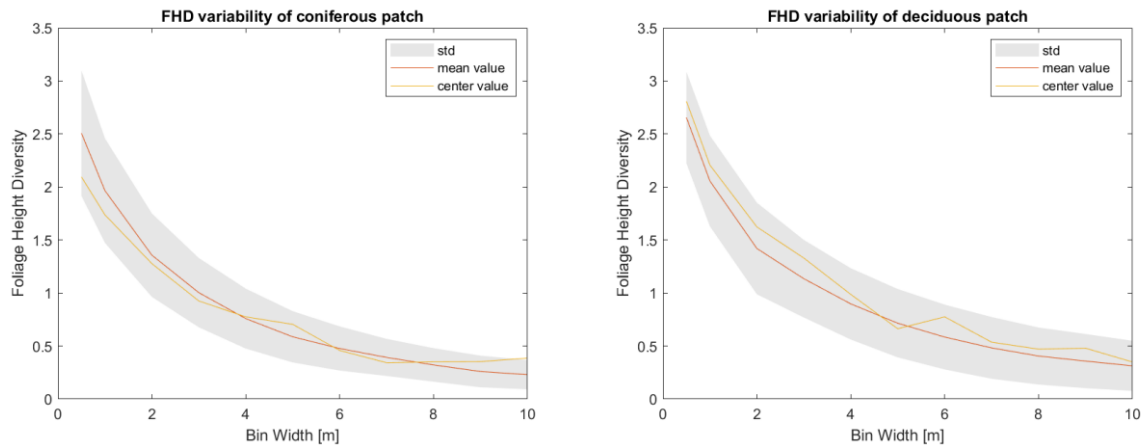
Figure A.1: Behavior of FHD values depending on vertical binning resolution. Results for a 150 x 150 m coniferous forest patch (left) and deciduous forest patch (right) with center coordinates in CH1903+/LV95 of [2'639'572.0, 1'260'354.0] and [2'639'666.0, 1'260'114.0], respectively. Vertical binning widths of 1 – 10 m were computed and the value of the center pixel of the forest patch (center value), the mean of the patch (mean value) and the respective standard deviation (std) are plotted.

Table A.1: Global statistics of the traits of the entire canton before normalization.

		min	mean±std	max	mean change [%]
CH	*2014*	0.21	20.93±9.86	42.35	-1.96
	2019	0.04	20.52±10.50	43.2	
FHD	*2014*	0	1.85±0.61	2.85	-4.68
	2019	0	1.76±0.80	3.13	
PAI	*2014*	0.02	2.39±1.23	6.88	-6.69
	2019	0.01	2.23±1.39	7.99	
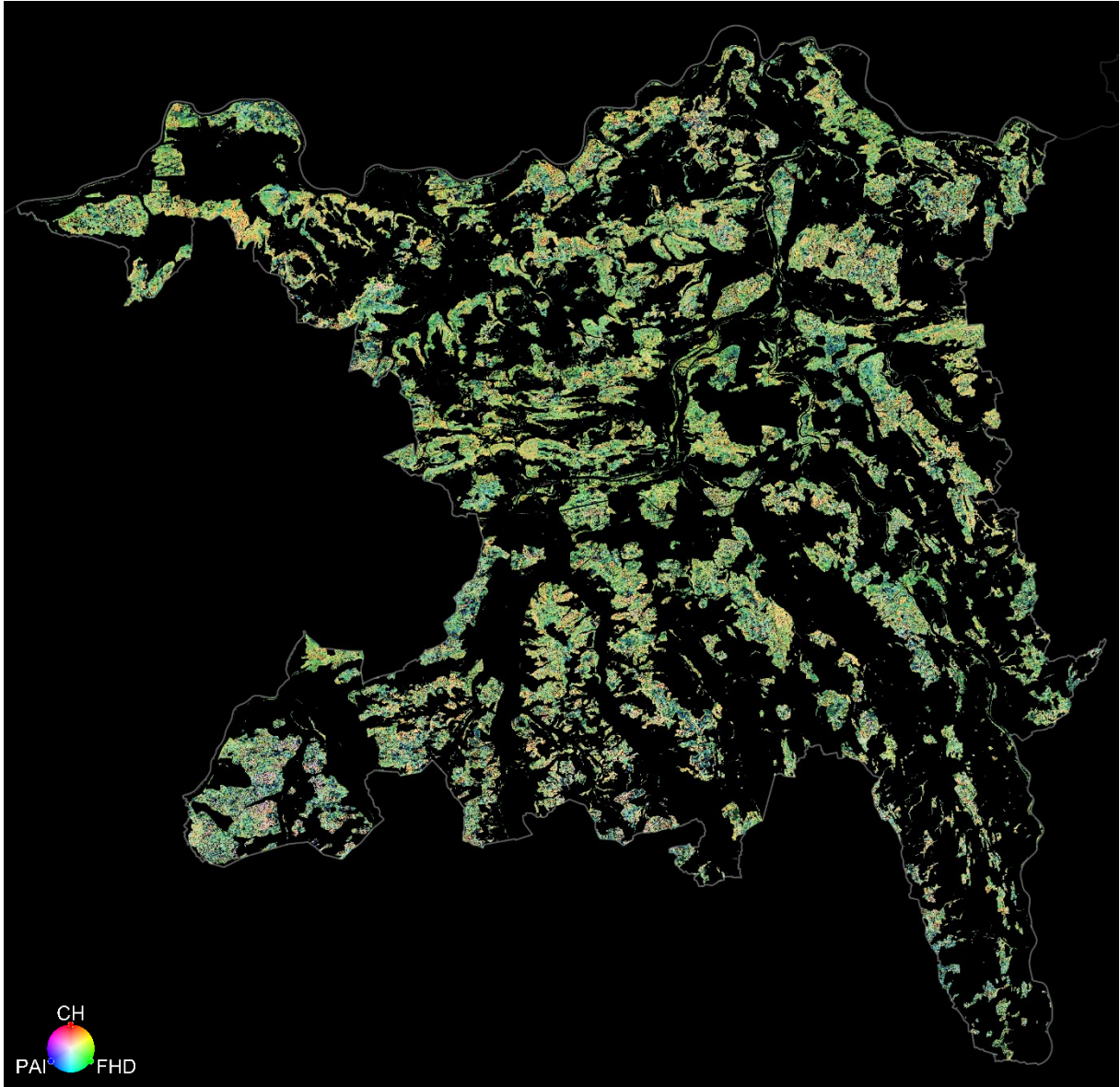
Figure A.2: Higher resolution RGB Composite of the functional traits 2014.
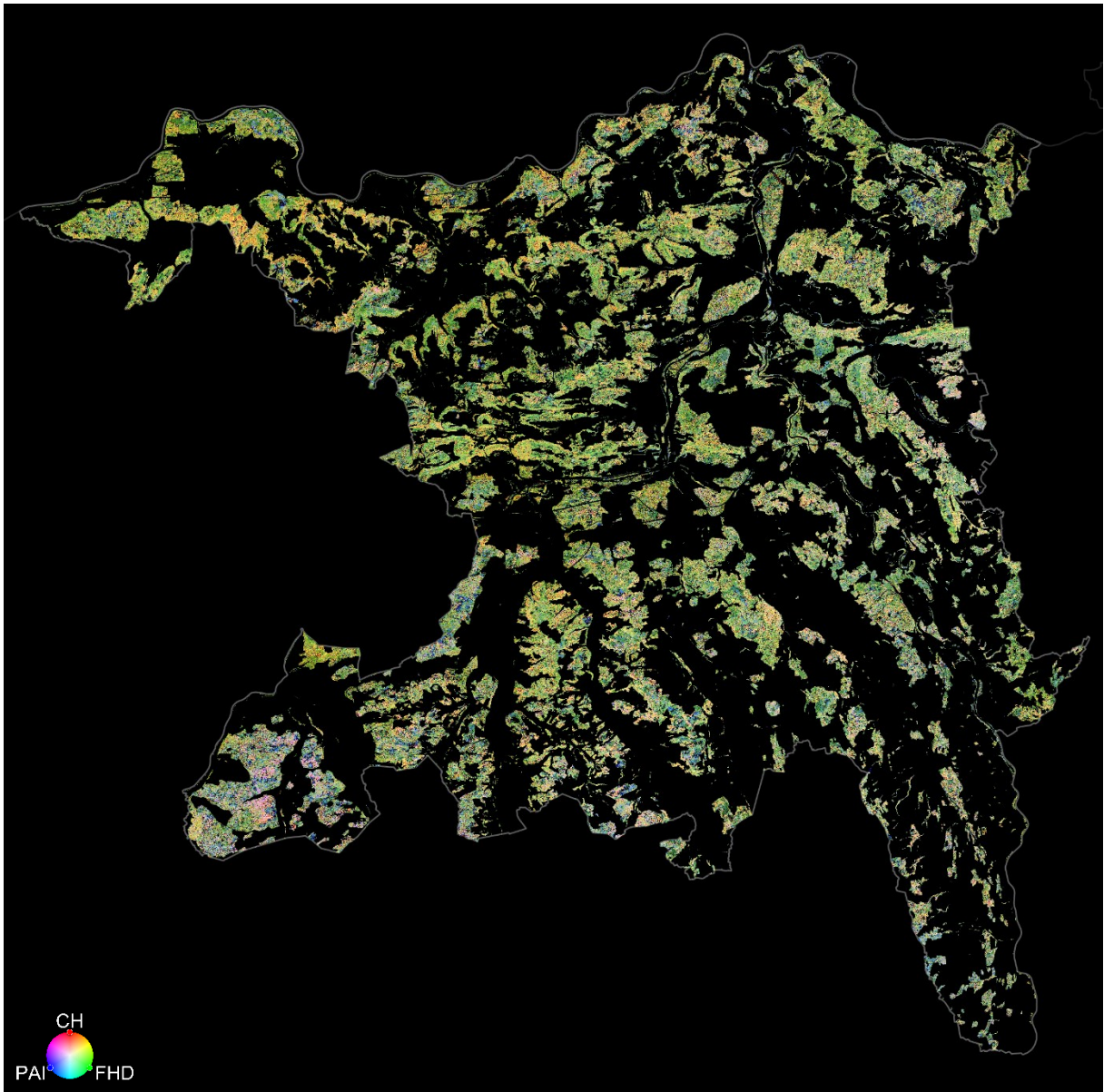
Figure A.3: Higher resolution RGB Composite of the functional traits 2019.
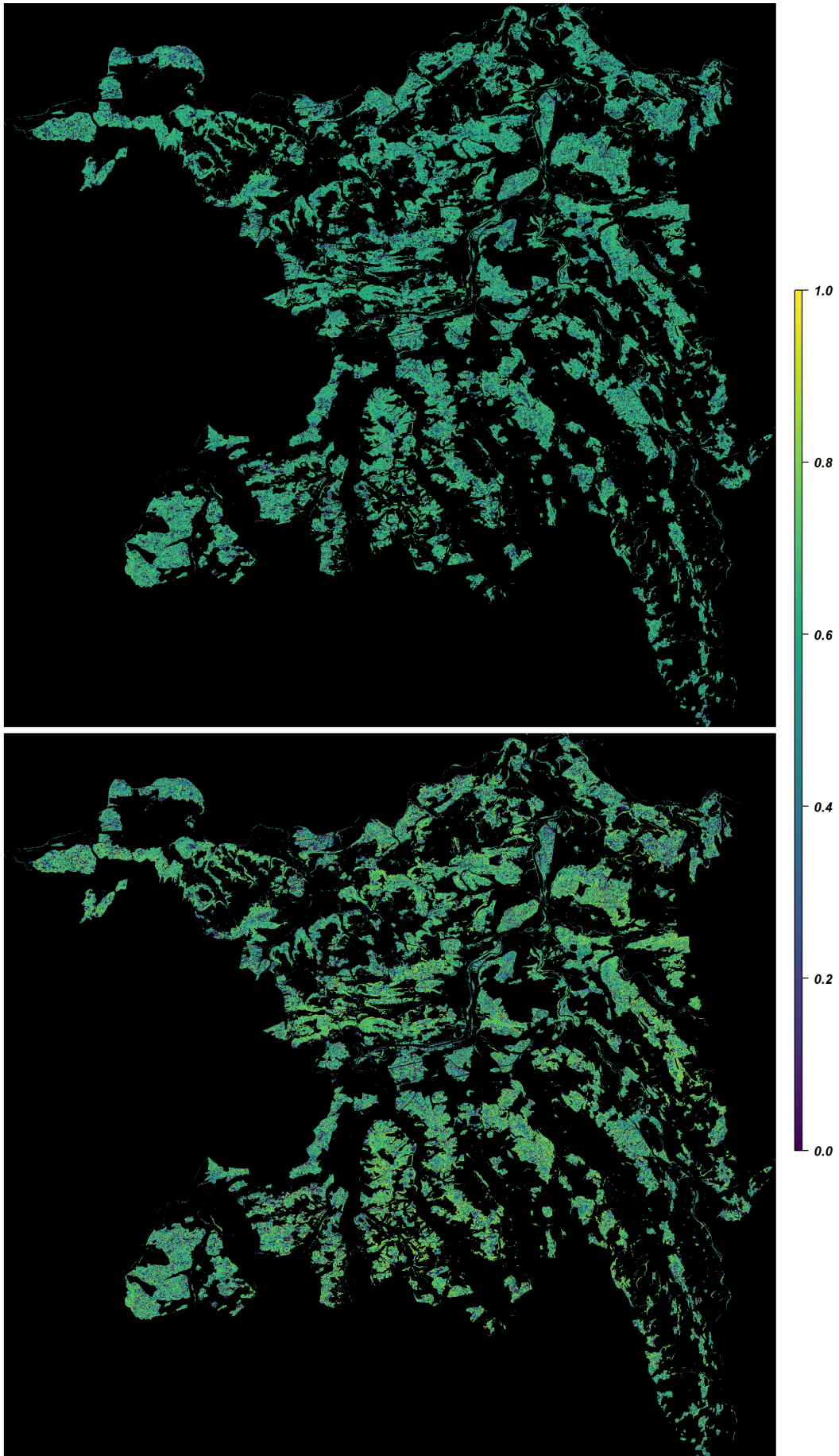
Figure A.4: Foliage height diversity maps of the canton Aargau of 2014 (top) and 2019 (bottom).

Figure A.5: Difference map of foliage height diversity between the years 2014 and 2019. Red pixels indicate higher values in 2014, blue pixels show higher values in 2019.
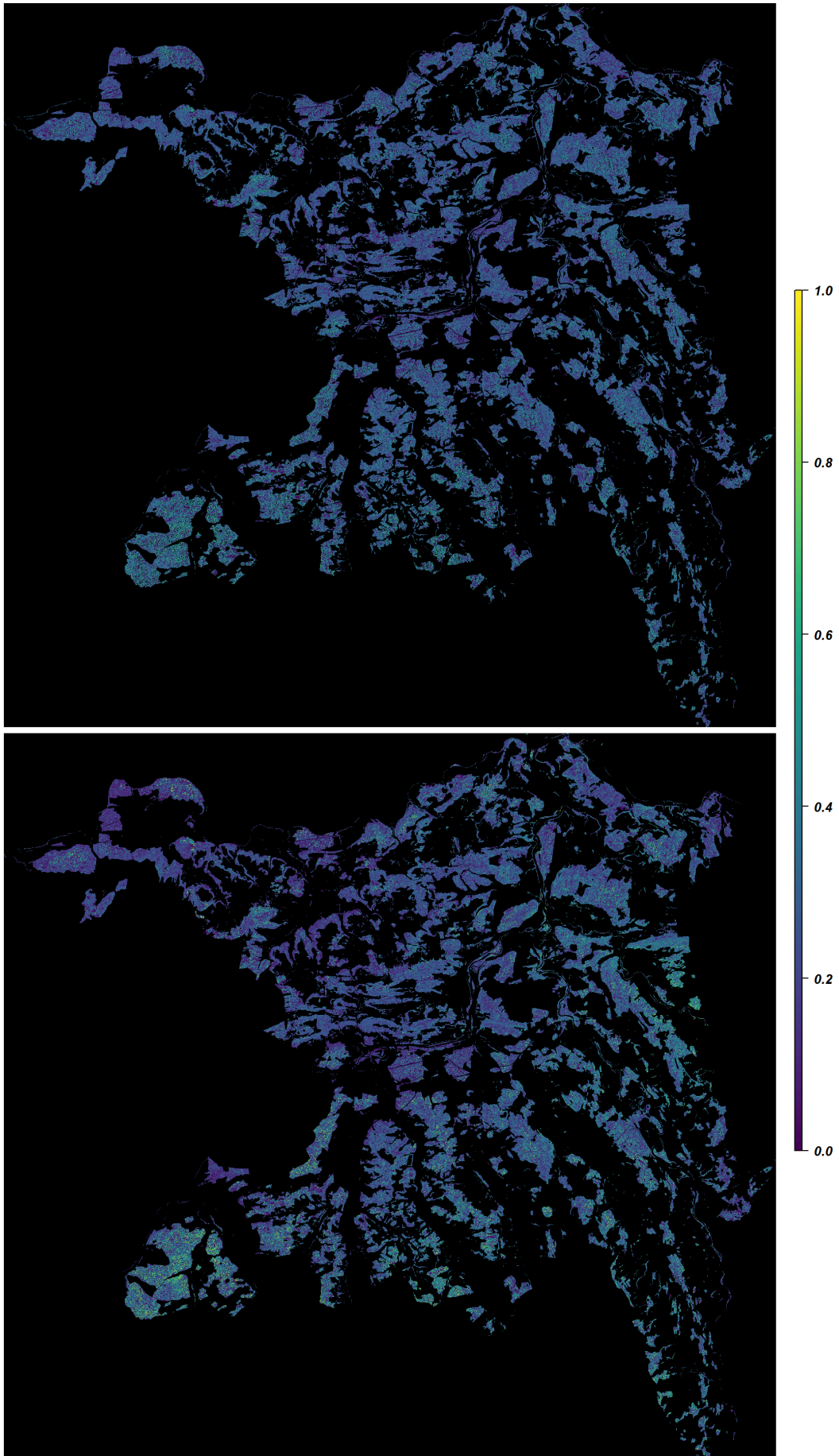
Figure A.6: Plant area index maps of the canton Aargau of 2014 (top) and 2019 (bottom).
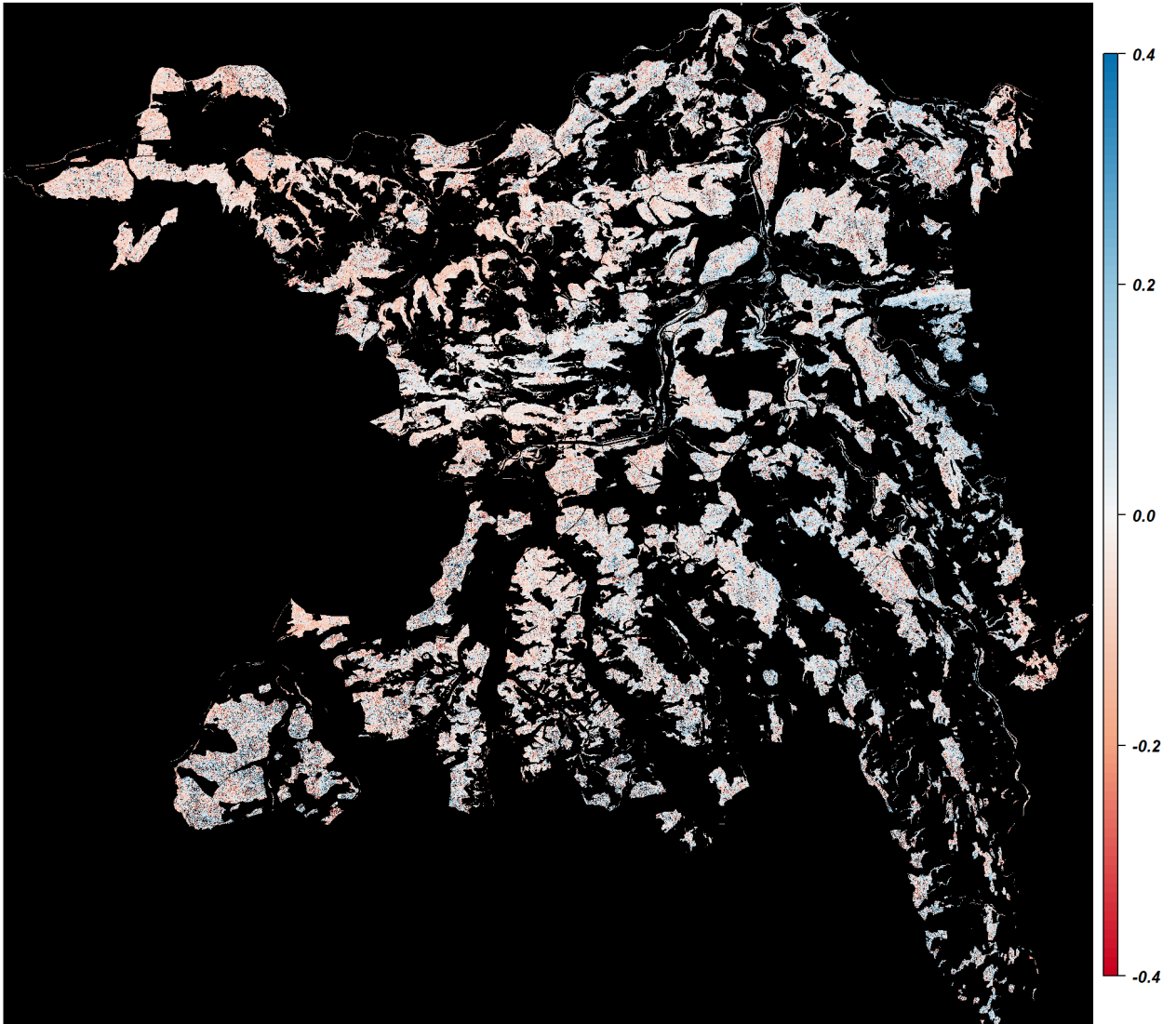
Figure A.7: Difference map of plant area index between the years 2014 and 2019. Red pixels indicate higher values in 2014, blue pixels show higher values in 2019.
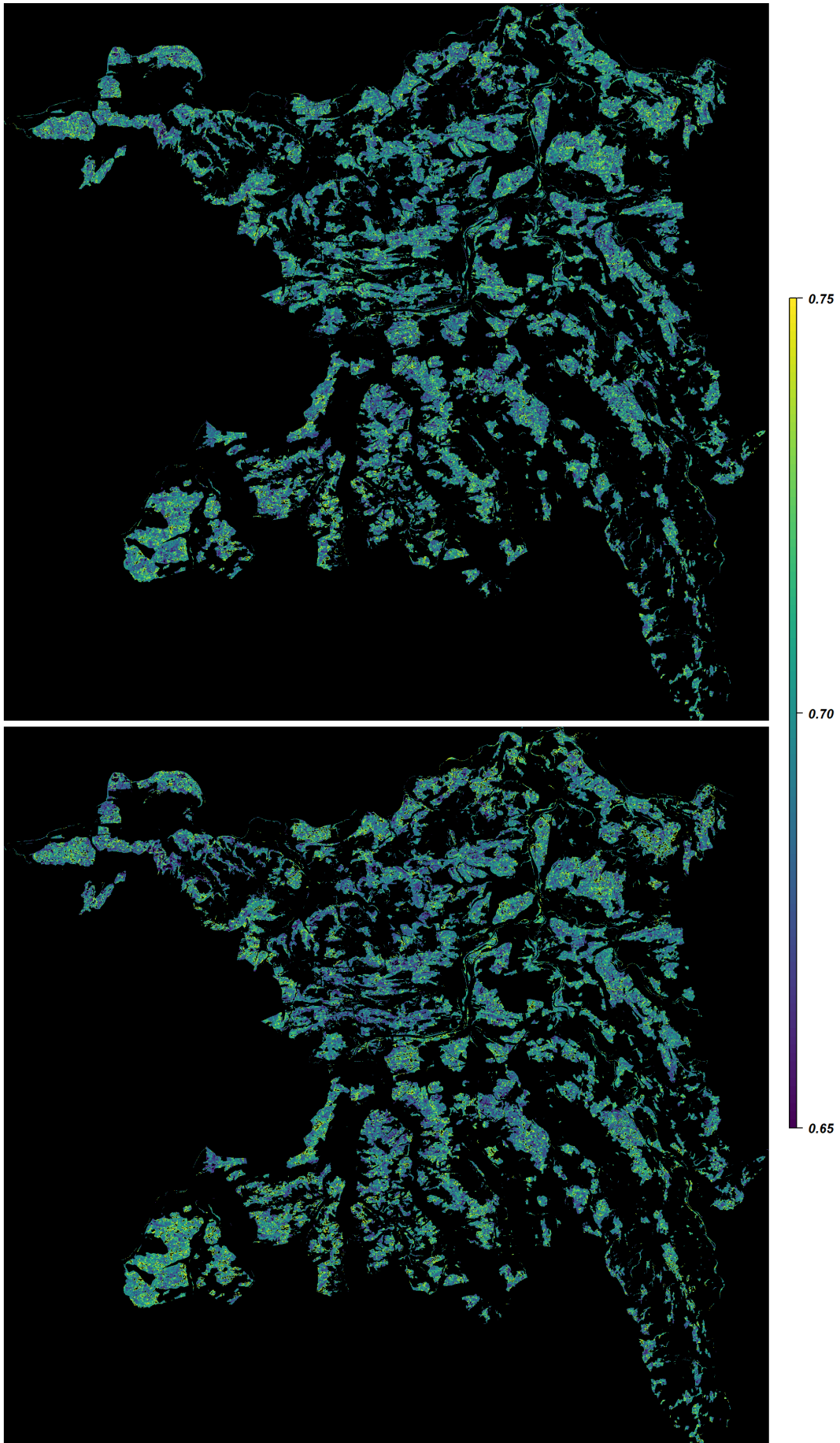
Figure A.8: Functional divergence maps of the canton Aargau of 2014 (top) and 2019 (bottom).

Figure A.9: Classified difference map of functional divergence. It is classified using its mean (μ_{FDiv} = 0.017). Values within one standard deviation of the observed change in occlusion are beige, within two standard deviations are light red/blue up to four which are dark red/blue. Red pixels indicate higher values in 2014, blue pixels show higher values in 2019 compared to the mean.

Forest mix rate
[% of deciduous trees]

■ <10
■ 50
■ 90
■ >90

Aspect
■ North
■ East
■ South
■ West
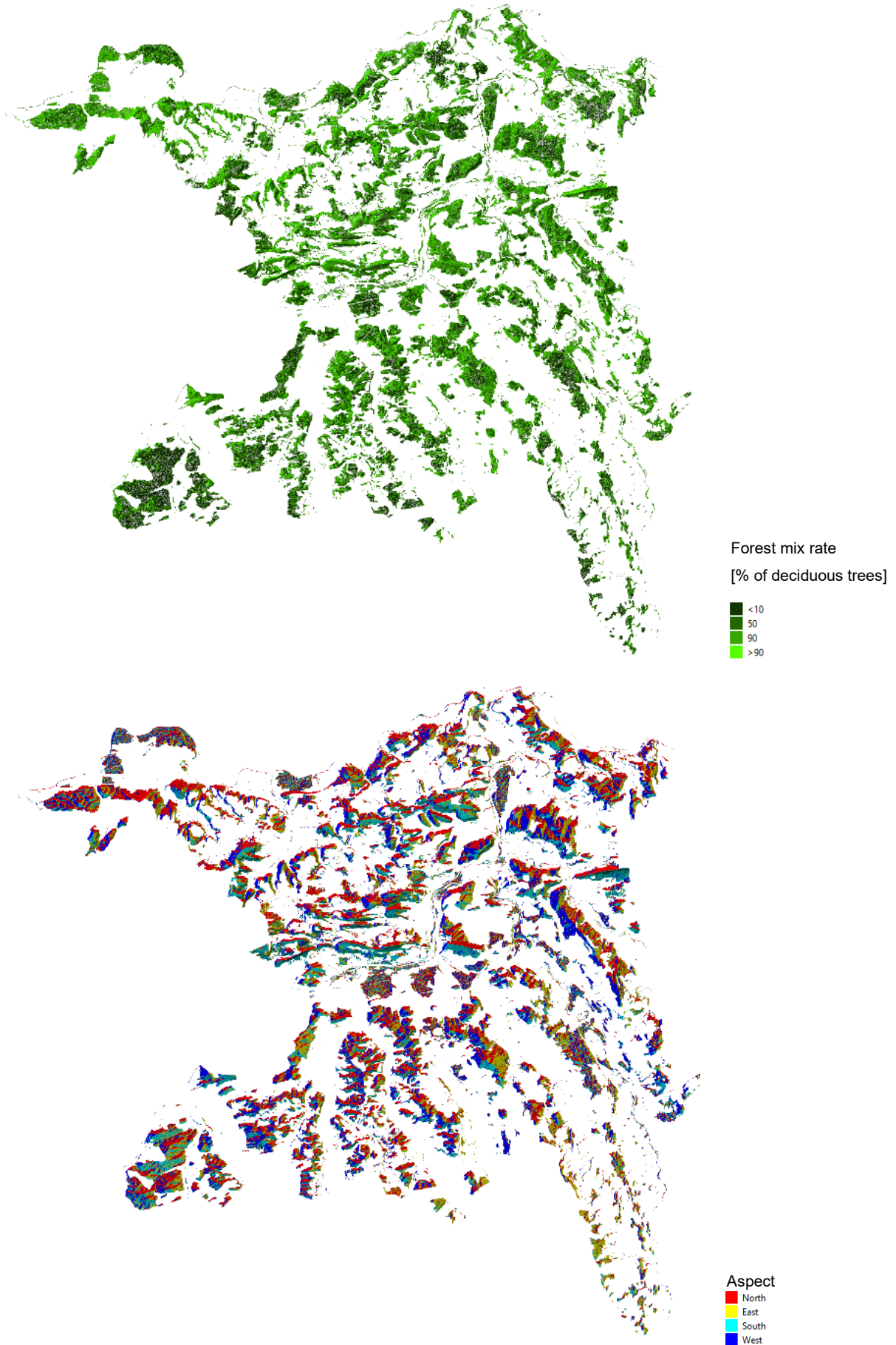
Figure A.10: Explanatory variables forest mix rate and aspect classified under Chapter 2.5.1.

Altitude [m.a.s.l.]
- <255
- 350
- 450
- 550
- 650
- 750
- >750

Slope
- Flat to very gently inclined
- Slightly inclined
- Medium inclined
- Strong to very strong incline
- Steep
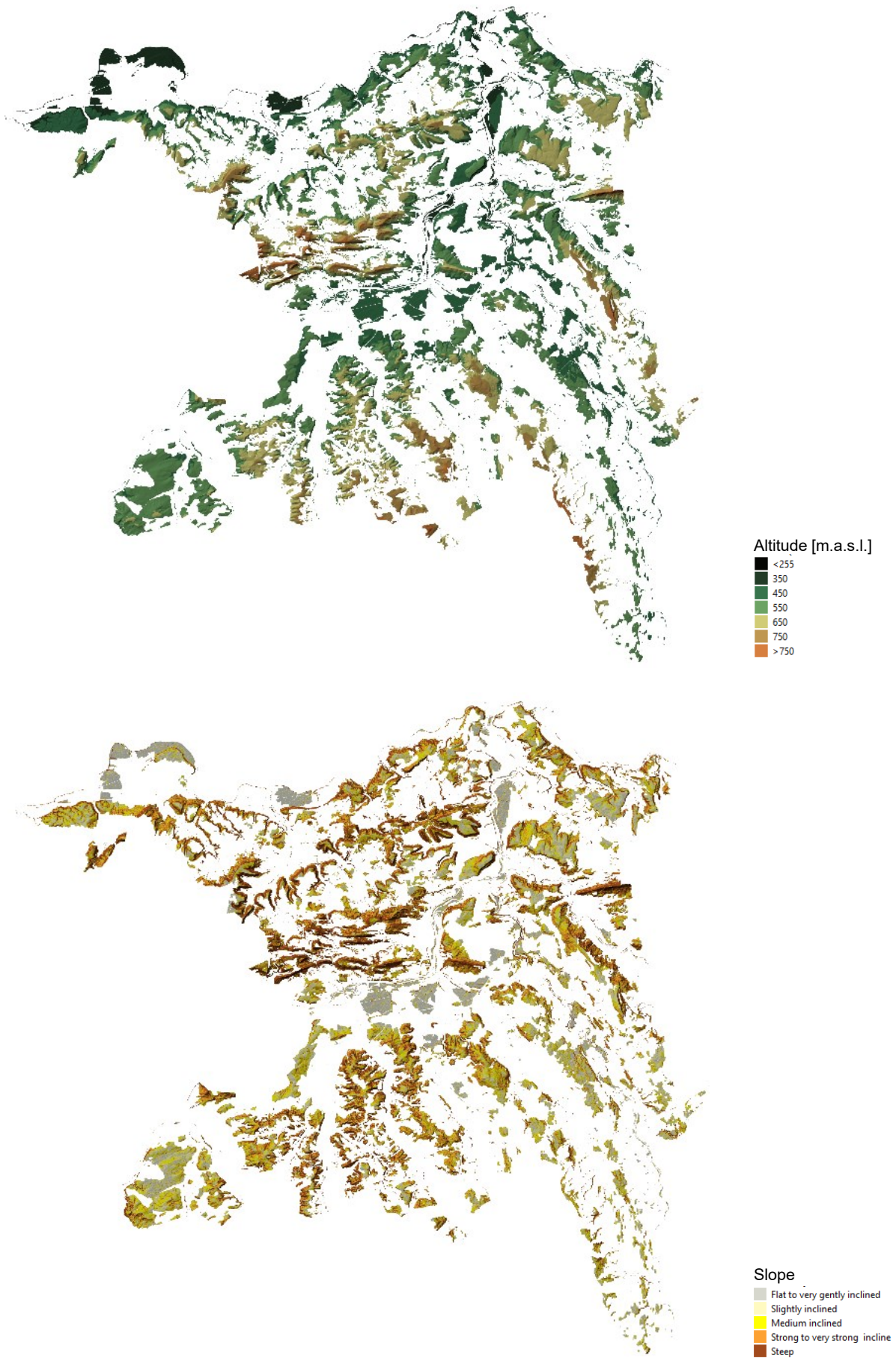
Figure A.11: Explanatory variables altitude and slope classified under Chapter 2.5.1.

ANOVA results in Laegern

*Table A.2: ANOVA type I results in Laegern for traits and diversity metrics explained by topographic, forest, and sensor variables. Stars indicate significance levels ***0.001, **0.01 and *0.05.*

Dependent variable	Variable	SumSq	DF	MeanSq	F	pValue	r²
CH14	Altitude	0.364	1	0.364	37.726	***0.000	0.070
	Slope	0.222	1	0.222	22.937	***0.000	
	Aspect	0.039	1	0.039	4.008	*0.046	
	Forest mix	0.006	1	0.006	0.611	0.435	
	Occlusion	0.000	1	0.000	0.001	0.976	
	Point density	0.130	1	0.130	13.481	***0.000	
	Residual	10.048	1040	0.010			
FHD14	Altitude	0.014	1	0.014	10.920	**0.001	0.154
	Slope	0.000	1	0.000	0.239	0.625	
	Aspect	0.000	1	0.000	0.124	0.725	
	Forest mix	0.000	1	0.000	0.074	0.786	
	Occlusion	0.004	1	0.004	3.286	0.070	
	Point density	0.228	1	0.228	174.508	***0.000	
	Residual	1.356	1040	0.001	0.154	-	
PAI14	Altitude	0.020	1	0.020	61.854	***0.000	0.507
	Slope	0.023	1	0.023	71.480	***0.000	
	Aspect	0.000	1	0.000	1.256	0.263	
	Forest mix	0.041	1	0.041	131.032	***0.000	
	Occlusion	0.123	1	0.123	389.926	***0.000	
	Point density	0.131	1	0.131	413.637	***0.000	
	Residual	0.329	1040	0.000		-	
CH19	Altitude	0.343	1	0.343	62.511	***0.000	0.342
	Slope	0.190	1	0.190	34.584	***0.000	
	Aspect	0.048	1	0.048	8.771	**0.003	
	Forest mix	0.000	1	0.000	0.081	0.776	
	Occlusion	0.772	1	0.772	140.754	***0.000	
	Point density	1.616	1	1.616	294.513	***0.000	
	Residual	5.707	1040	0.005		-	
FHD19	Altitude	0.027	1	0.027	20.141	***0.000	0.438
	Slope	0.000	1	0.000	0.001	0.977	
	Aspect	0.002	1	0.002	1.761	0.185	
	Forest mix	0.015	1	0.015	11.631	**0.001	
	Occlusion	0.118	1	0.118	89.441	***0.000	
	Point density	0.906	1	0.906	686.948	***0.000	
	Residual	1.371	1040	0.001		-	
PAI19	Altitude	0.005	1	0.005	11.192	**0.001	0.680
	Slope	0.037	1	0.037	75.822	***0.000	
	Aspect	0.054	1	0.054	110.312	***0.000	
	Forest mix	0.005	1	0.005	11.116	**0.001	
	Occlusion	0.831	1	0.831	1711.021	***0.000	
	Point density	0.142	1	0.142	292.991	***0.000	
	Residual	0.505	1040	0.000		-	
FRic14	Altitude	0.000	1	0.000	3.067	0.080	0.012
	Slope	0.000	1	0.000	0.100	0.751	
	Aspect	0.000	1	0.000	0.153	0.696	
	Forest mix	0.001	1	0.001	5.235	*0.022	
	Occlusion	0.000	1	0.000	2.893	0.089	
	Point density	0.000	1	0.000	1.351	0.245	
	Residual	0.143	1040	0.000		-	
FDiv14	Altitude	0.001	1	0.001	7.442	**0.006	0.047
	Slope	0.001	1	0.001	4.591	*0.032	
	Aspect	0.000	1	0.000	0.391	0.532	
	Forest mix	0.004	1	0.004	22.008	***0.000	
	Occlusion	0.002	1	0.002	8.396	**0.004	
	Point density	0.001	1	0.001	7.996	**0.005	
	Residual	0.191	1040	0.000		-	

FRic19	Altitude	0.055	1	0.055	81.278	***0.000	0.147
	Slope	0.000	1	0.000	0.148	0.701	
	Aspect	0.002	1	0.002	2.552	0.110	
	Forest mix	0.010	1	0.010	14.333	***0.000	
	Occlusion	0.052	1	0.052	76.759	***0.000	
	Point density	0.002	1	0.002	3.477	0.063	
	Residual	0.706	1040	0.001		-	
FDiv19	Altitude	0.000	1	0.000	3.067	0.080	0.012
	Slope	0.000	1	0.000	0.100	0.751	
	Aspect	0.000	1	0.000	0.153	0.696	
	Forest mix	0.001	1	0.001	5.235	*0.022	
	Occlusion	0.000	1	0.000	2.893	0.089	
	Point density	0.000	1	0.000	1.351	0.245	
	Residual	0.143	1040	0.000		-	
FRic change	CH difference	0.059	1	0.059	157.390	***0.000	0.226
	FHD difference	0.004	1	0.004	10.410	**0.001	
	PAI difference	0.048	1	0.048	129.429	***0.000	
	Occlusion difference	0.001	1	0.001	3.933	*0.048	
	Point density difference	0.001	1	0.001	2.955	0.086	
	Residual	0.388	1041	0.000		-	
FDiv change	CH difference	0.000	1	0.000	0.023	0.878	0.010
	FHD difference	0.000	1	0.000	0.787	0.375	
	PAI difference	0.004	1	0.004	33.417	***0.000	
	Occlusion difference	0.001	1	0.001	9.935	**0.002	
	Point density difference	0.000	1	0.000		0.919	
	Residual	0.113	1041	0.000	0.041	-	
CH change	Occlusion difference	0.001	1	0.001	1.931	0.165	0.0002385
	Point density difference	0.000	1	0.000	0.319	0.572	
	Residual	0.631	1044	0.001			
FHD change	Occlusion difference	0.008	1	0.008	9.369	**0.002	0.331
	Point density difference	0.412	1	0.412	510.913	***0.000	
	Residual	0.842	1044	0.001			
PAI change	Occlusion difference	0.690	1	0.690	1061.816	***0.000	0.568
	Point density difference	0.204	1	0.204	313.273	***0.000	
	Residual	0.678	1044	0.001			

ANOVA results in Unterwald

*Table A.3: ANOVA type I results in Unterwald for traits and diversity metrics explained by topographic, forest, and sensor variables. Stars indicate significance levels ***0.001, **0.01 and *0.05.*

Dependent variable	Variable	SumSq	DF	MeanSq	F	pValue	r²
CH14	Altitude	0.020	1	0.020	2.942	0.088	0.068
	Slope	0.025	1	0.025	3.649	0.058	
	Aspect	0.000	1	0.000	0.034	0.853	
	Forest mix	0.032	1	0.032	4.718	*0.031	
	Occlusion	0.010	1	0.010	1.398	0.239	
	Point density	0.011	1	0.011	1.609	0.206	
	Residual	1.336	196	0.007		-	
FHD14	Altitude	0.007	1	0.007	9.065	**0.003	0.374
	Slope	0.009	1	0.009	12.401	**0.001	
	Aspect	0.003	1	0.003	4.097	*0.044	
	Forest mix	0.006	1	0.006	8.205	**0.005	
	Occlusion	0.010	1	0.010	14.093	***0.000	
	Point density	0.050	1	0.050	69.429	***0.000	
	Residual	0.142	196	0.001		-	
PAI14	Altitude	0.002	1	0.002	2.485	0.117	0.569
	Slope	0.052	1	0.052	66.617	***0.000	
	Aspect	0.005	1	0.005	5.993	*0.015	
	Forest mix	0.048	1	0.048	60.959	***0.000	
	Occlusion	0.069	1	0.069	88.433	***0.000	
	Point density	0.027	1	0.027	34.168	***0.000	
	Residual	0.154	196	0.001		-	
CH19	Altitude	0.012	1	0.012	2.774	0.097	0.238
	Slope	0.023	1	0.023	5.315	*0.022	
	Aspect	0.001	1	0.001	0.241	0.624	
	Forest mix	0.021	1	0.021	4.957	*0.027	
	Occlusion	0.018	1	0.018	4.136	*0.043	
	Point density	0.188	1	0.188	43.781	***0.000	
	Residual	0.844	196	0.004		-	
FHD19	Altitude	0.001	1	0.001	0.433	0.512	0.472
	Slope	0.045	1	0.045	35.371	***0.000	
	Aspect	0.008	1	0.008	6.132	*0.014	
	Forest mix	0.005	1	0.005	4.045	*0.046	
	Occlusion	0.037	1	0.037	29.107	***0.000	
	Point density	0.128	1	0.128	100.102	***0.000	
	Residual	0.251	196	0.001		-	
PAI19	Altitude	0.005	1	0.005	6.683	*0.010	0.703
	Slope	0.004	1	0.004	4.548	*0.034	
	Aspect	0.004	1	0.004	5.747	*0.017	
	Forest mix	0.118	1	0.118	153.194	***0.000	
	Occlusion	0.197	1	0.197	255.357	***0.000	
	Point density	0.030	1	0.030	39.002	***0.000	
	Residual	0.151	196	0.001		-	
FRic14	Altitude	0.000	1	0.000	0.053	0.817	0.025
	Slope	0.000	1	0.000	0.343	0.559	
	Aspect	0.000	1	0.000	1.149	0.285	
	Forest mix	0.000	1	0.000	2.983	0.086	
	Occlusion	0.000	1	0.000	0.042	0.838	
	Point density	0.000	1	0.000	0.556	0.457	
	Residual	0.027	196	0.000		-	
FDiv14	Altitude	0.000	1	0.000	0.701	0.404	0.032
	Slope	0.000	1	0.000	1.003	0.318	
	Aspect	0.000	1	0.000	0.121	0.728	
	Forest mix	0.001	1	0.001	4.667	*0.032	
	Occlusion	0.000	1	0.000	0.028	0.867	
	Point density	0.000	1	0.000	0.001	0.976	
	Residual	0.038	196	0.000		-	

FRic19	Altitude	0.008	1	0.008	5.231	*0.023	0.092
	Slope	0.001	1	0.001	0.503	0.479	
	Aspect	0.005	1	0.005	2.967	0.087	
	Forest mix	0.014	1	0.014	9.084	**0.003	
	Occlusion	0.002	1	0.002	1.364	0.244	
	Point density	0.001	1	0.001	0.604	0.438	
	Residual	0.298	196	0.002		-	
FDiv19	Altitude	0.000	1	0.000	0.053	0.817	0.025
	Slope	0.000	1	0.000	0.343	0.559	
	Aspect	0.000	1	0.000	1.149	0.285	
	Forest mix	0.000	1	0.000	2.983	0.086	
	Occlusion	0.000	1	0.000	0.042	0.838	
	Point density	0.000	1	0.000	0.556	0.457	
	Residual	0.027	196	0.000		-	
FRic change	CH difference	0.027	1	0.027	34.414	***0.000	0.213
	FHD difference	0.000	1	0.000	0.235	0.629	
	PAI difference	0.009	1	0.009	12.201	**0.001	
	Occlusion difference	0.005	1	0.005	6.164	*0.014	
	Point density difference	0.000	1	0.000	0.257	0.613	
	Residual	0.152	197	0.001		-	
FDiv change	CH difference	0.000	1	0.000	4.371	*0.038	0.069
	FHD difference	0.000	1	0.000	2.579	0.110	
	PAI difference	0.000	1	0.000	1.512	0.220	
	Occlusion difference	0.000	1	0.000	0.840	0.361	
	Point density difference	0.001	1	0.001	5.277	*0.023	
	Residual	0.020	197	0.000		-	
CH change	Occlusion difference	0.002	1	0.002	2.782	0.097	0.041
	Point density difference	0.004	1	0.004	7.937	**0.005	
	Residual	0.108	200	0.001			
FHD change	Occlusion difference	0.000	1	0.000	0.002	0.968	0.341
	Point density difference	0.090	1	0.090	106.630	***0.000	
	Residual	0.170	200	0.001			
PAI change	Occlusion difference	0.005	1	0.005	3.473	0.064	0.142
	Point density difference	0.043	1	0.043	31.856	***0.000	
	Residual	0.269	200	0.001			

ANOVA results in Frickberg

Table A.4: ANOVA type I results in Frickberg for traits and diversity metrics explained by topographic, forest, and sensor variables. Stars indicate significance levels ***0.001, **0.01 and *0.05.

Dependent variable	Variable	SumSq	DF	MeanSq	F	pValue	r^2
CH14	Altitude	0.047	1	0.047	5.591	*0.018	0.032
	Slope	0.015	1	0.015	1.737	0.188	
	Aspect	0.000	1	0.000	0.000	0.988	
	Forest mix	0.001	1	0.001	0.118	0.732	
	Occlusion	0.001	1	0.001	0.103	0.748	
	Point density	0.069	1	0.069	8.159	**0.004	
	Residual	3.947	469	0.008		-	
FHD14	Altitude	0.009	1	0.009	3.900	*0.049	0.141
	Slope	0.005	1	0.005	2.073	0.151	
	Aspect	0.004	1	0.004	1.868	0.172	
	Forest mix	0.001	1	0.001	0.408	0.523	
	Occlusion	0.005	1	0.005	2.316	0.129	
	Point density	0.146	1	0.146	66.150	***0.000	
	Residual	1.035	469	0.002		-	
PAI14	Altitude	0.000	1	0.000	1.132	0.288	0.488
	Slope	0.018	1	0.018	47.332	***0.000	
	Aspect	0.004	1	0.004	9.397	**0.002	
	Forest mix	0.052	1	0.052	133.821	***0.000	
	Occlusion	0.048	1	0.048	124.587	***0.000	
	Point density	0.050	1	0.050	129.973	***0.000	
	Residual	0.182	469	0.000		-	
CH19	Altitude	0.049	1	0.049	9.942	**0.002	0.287
	Slope	0.007	1	0.007	1.429	0.232	
	Aspect	0.001	1	0.001	0.110	0.740	
	Forest mix	0.002	1	0.002	0.488	0.485	
	Occlusion	0.000	1	0.000	0.020	0.888	
	Point density	0.875	1	0.875	177.177	***0.000	
	Residual	2.317	469	0.005		-	
FHD19	Altitude	0.008	1	0.008	6.608	**0.010	0.417
	Slope	0.028	1	0.028	22.268	***0.000	
	Aspect	0.000	1	0.000	0.043	0.836	
	Forest mix	0.003	1	0.003	2.566	0.110	
	Occlusion	0.002	1	0.002	1.502	0.221	
	Point density	0.381	1	0.381	303.085	***0.000	
	Residual	0.589	469	0.001		-	
PAI19	Altitude	0.000	1	0.000	0.006	0.941	0.642
	Slope	0.021	1	0.021	68.287	***0.000	
	Aspect	0.001	1	0.001	1.843	0.175	
	Forest mix	0.097	1	0.097	318.031	***0.000	
	Occlusion	0.077	1	0.077	250.209	***0.000	
	Point density	0.062	1	0.062	201.502	***0.000	
	Residual	0.144	469	0.000		-	
FRic14	Altitude	0.000	1	0.000	1.362	0.244	0.059
	Slope	0.001	1	0.001	5.368	*0.021	
	Aspect	0.000	1	0.000	1.273	0.260	
	Forest mix	0.000	1	0.000	0.081	0.777	
	Occlusion	0.001	1	0.001	11.095	**0.001	
	Point density	0.001	1	0.001	10.160	**0.002	
	Residual	0.063	469	0.000		-	
FDiv14	Altitude	0.001	1	0.001	4.633	*0.032	0.028
	Slope	0.000	1	0.000	0.248	0.619	
	Aspect	0.000	1	0.000	2.155	0.143	
	Forest mix	0.000	1	0.000	0.342	0.559	
	Occlusion	0.001	1	0.001	3.976	*0.047	
	Point density	0.000	1	0.000	2.004	0.158	
	Residual	0.086	469	0.000		-	

FRic19	Altitude	0.004	1	0.004	11.247	**0.001	0.134
	Slope	0.000	1	0.000	1.047	0.307	
	Aspect	0.000	1	0.000	0.061	0.805	
	Forest mix	0.010	1	0.010	28.736	***0.000	
	Occlusion	0.009	1	0.009	23.849	***0.000	
	Point density	0.003	1	0.003	7.856	***0.005	
	Residual	0.168	469	0.000		-	
FDiv19	Altitude	0.000	1	0.000	1.362	0.244	0.059
	Slope	0.001	1	0.001	5.368	*0.021	
	Aspect	0.000	1	0.000	1.273	0.260	
	Forest mix	0.000	1	0.000	0.081	0.777	
	Occlusion	0.001	1	0.001	11.095	**0.001	
	Point density	0.001	1	0.001	10.160	**0.002	
	Residual	0.063	469	0.000		-	
FRic change	CH difference	0.013	1	0.013	67.633	***0.000	0.184
	FHD difference	0.001	1	0.001	3.703	0.055	
	PAI difference	0.004	1	0.004	21.510	***0.000	
	Occlusion difference	0.002	1	0.002	12.339	***0.000	
	Point density difference	0.000	1	0.000	0.838	0.360	
	Residual	0.092	470	0.000		-	
FDiv change	CH difference	0.000	1	0.000	0.461	0.498	0.024
	FHD difference	0.000	1	0.000	0.963	0.327	
	PAI difference	0.000	1	0.000	2.216	0.137	
	Occlusion difference	0.000	1	0.000	1.133	0.288	
	Point density difference	0.001	1	0.001	6.991	**0.008	
	Residual	0.060	470	0.000		-	
CH change	Occlusion difference	0.001	1	0.001	2.733	0.099	0.002
	Point density difference	0.000	1	0.000	0.342	0.559	
	Residual	0.122	473	0.000			
FHD change	Occlusion difference	0.000	1	0.000	0.857	0.355	0.227
	Point density difference	0.081	1	0.081	140.489	***0.000	
	Residual	0.273	473	0.001			
PAI change	Occlusion difference	0.002	1	0.002	4.698	*0.031	0.052
	Point density difference	0.012	1	0.012	23.364	***0.000	
	Residual	0.240	473	0.001			
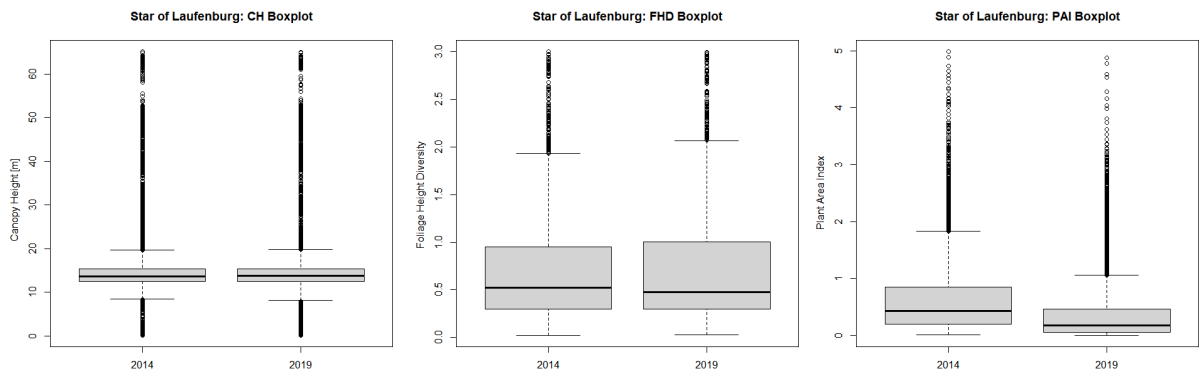
	CH		FHD		PAI	
	2014	*2019*	*2014*	*2019*	*2014*	*2019*
25th **percentile**	12.6	12.5	0.297	0.299	0.1983	0.0543
50th **percentile**	13.7	13.8	0.52	0.481	0.428	0.168
75th **percentile**	15.4	15.4	0.951	1.012	0.85	0.458

Figure A.12: Swissgrid switching substation known as Star of Laufenburg. Used as validation area of the traits because it has many masts, lines, etc. having a tree-like structure that were used as persistent scatterers. In the top row, the SWISSIMAGE Orthofotos (swisstopo, 2022) of 2014 (left) und 2019 (right) and in the bottom row, the boxplots of the three traits and their corresponding statistics are depicted before normalization.

Original code:　　　　　**Code *return number* swapped with *number of returns***
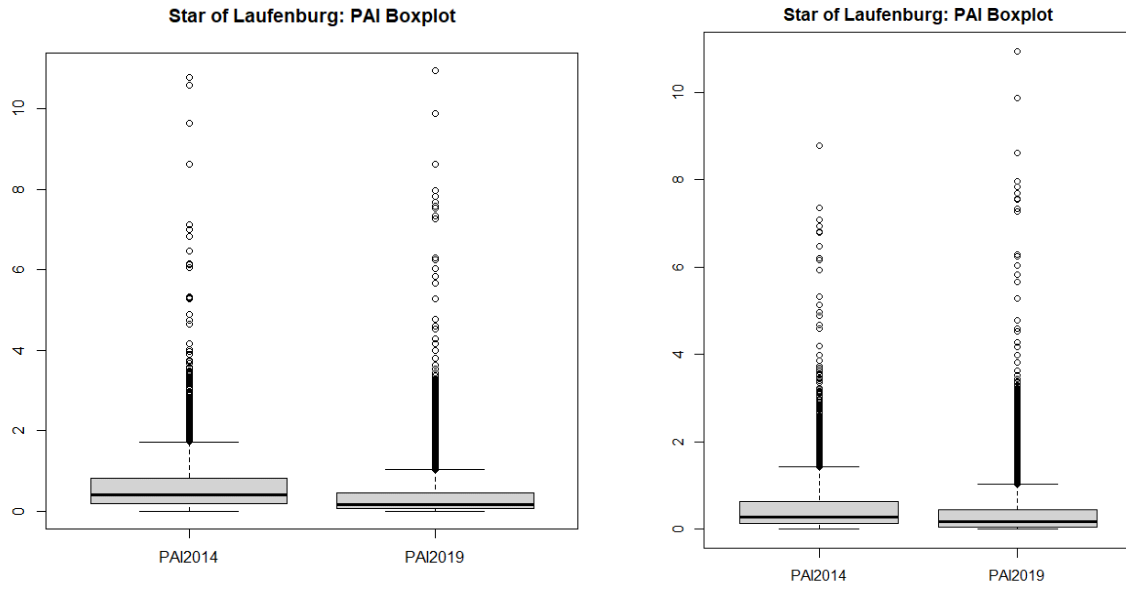
Figure A.13: PAI boxplots of the Star of Laufenburg area before the swap of return number and number of return parameters (left) and after (right).
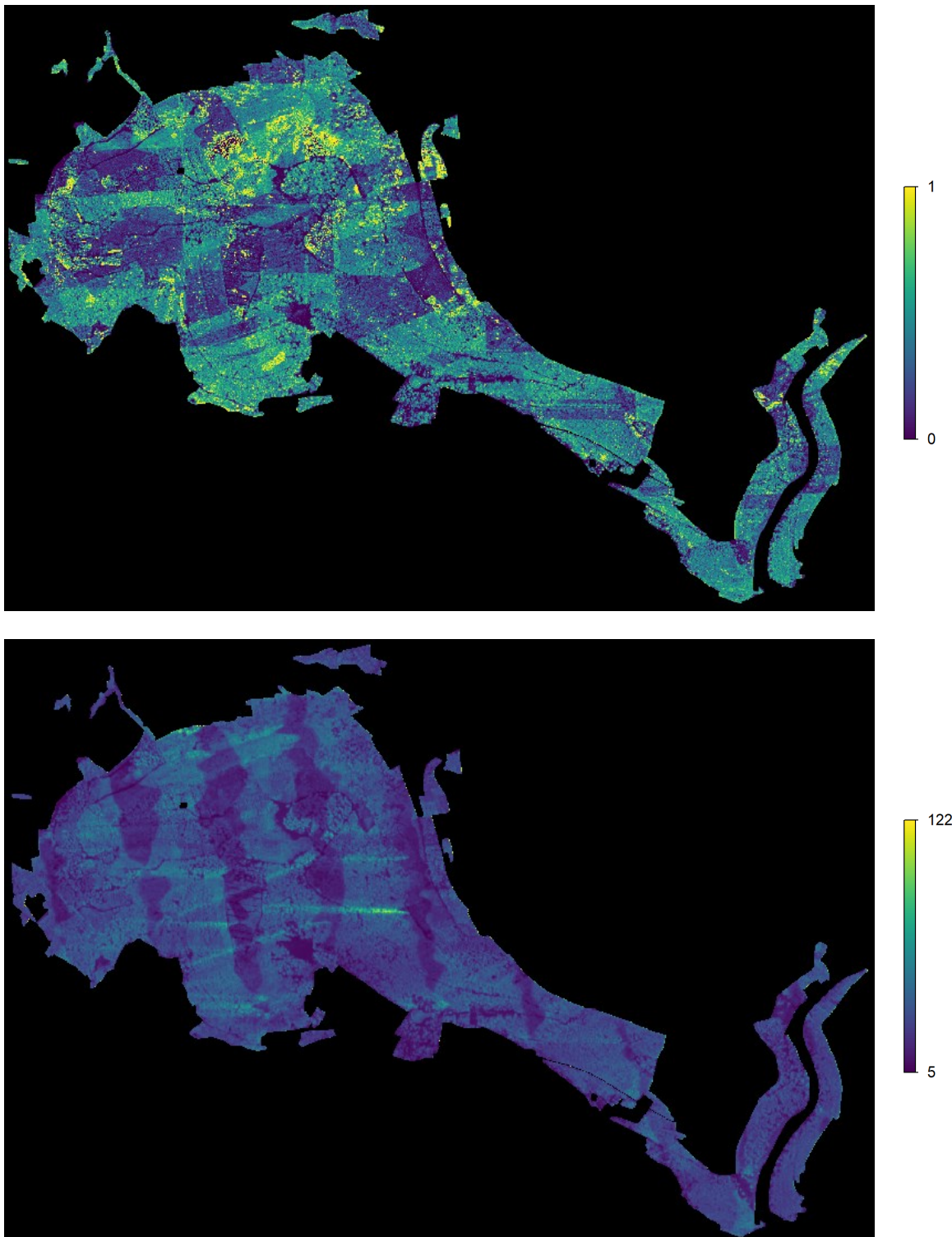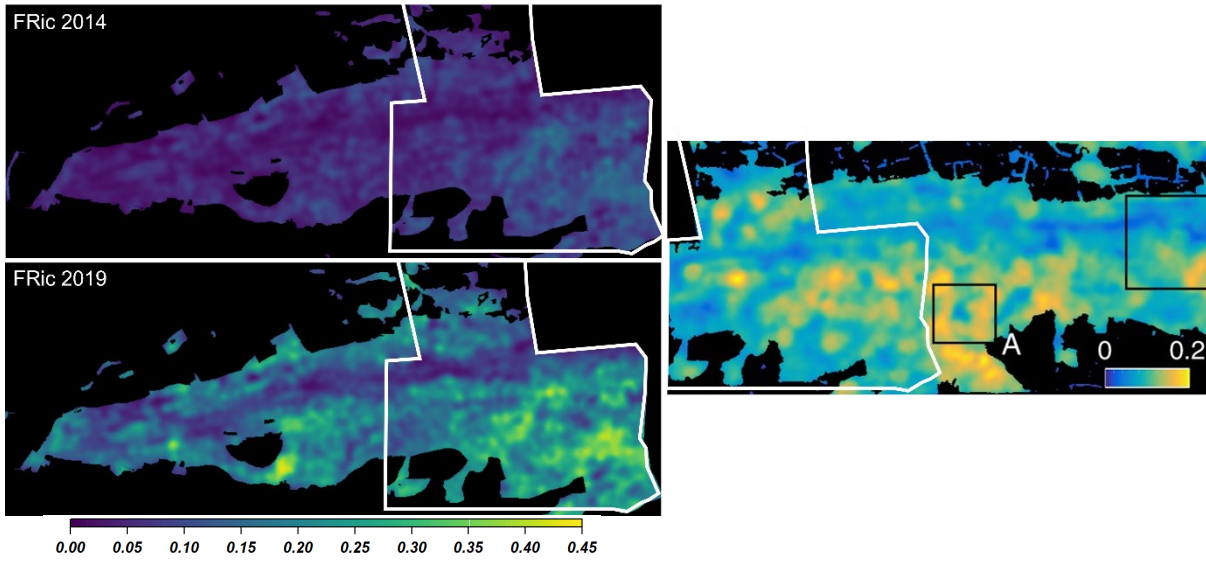
Figure A.14: Artifacts in PAI map (top) in Frickberg as an example before the parameter swap. The corresponding point density (number of points per 4 m^2) map is on the bottom.
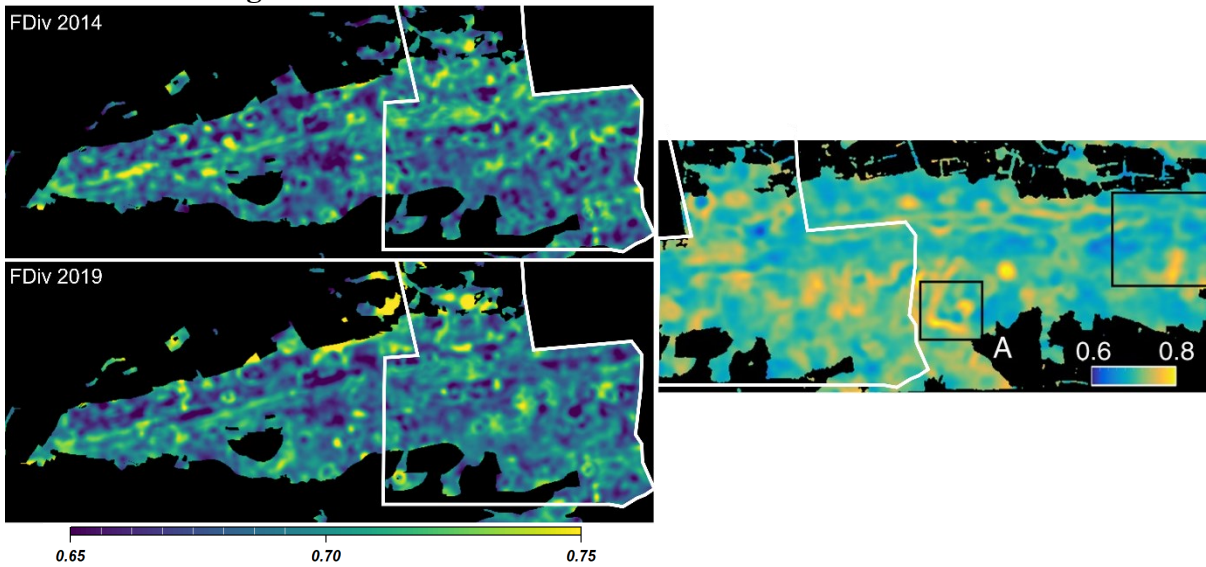
Figure A.15: Comparison of functional richness and divergence maps of the overlapping part of the two studies on Laegern. In the left column, the results of our study (30 m radius) are mapped and on the right column, the results of the study of Schneider et al. (2017) with a radius 60 m are reprinted. The area inside the white polygon marks the overlapping area of the thesis and the study by Schneider et al. (2017). The differences in the scale come mostly from the different radii (30 m vs. 60 m).
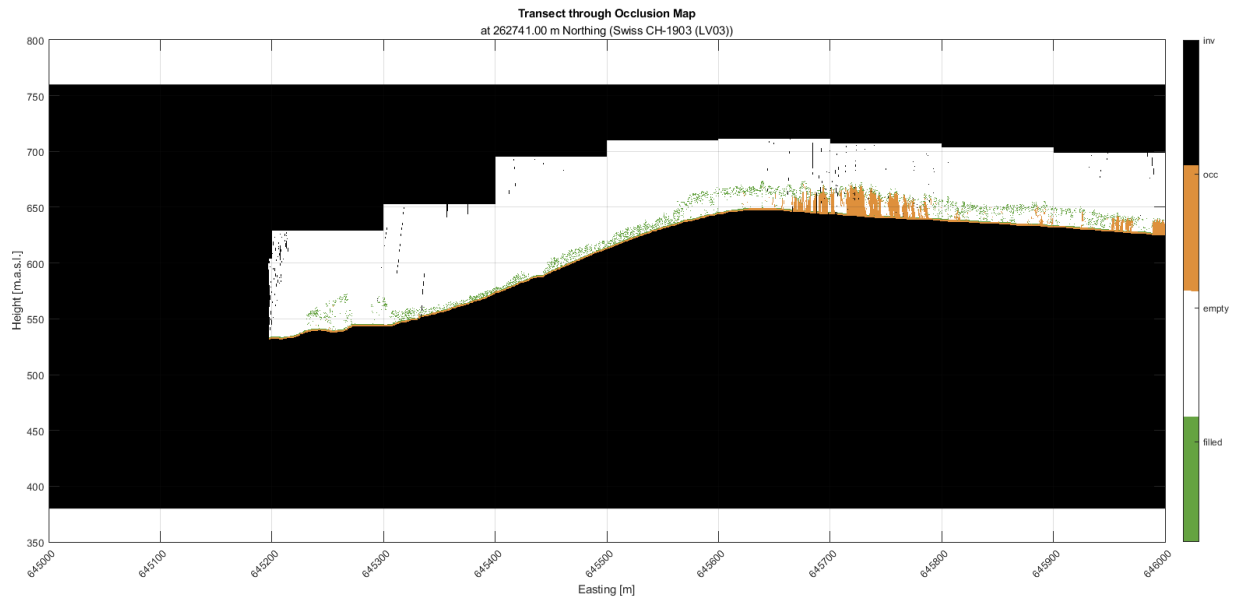
Figure A.16: Slice through the output of the occlusion mapping of a 1 km tile at Frickberg.

B Appendix – Geographically weighted regression analysis

As an outlook, we also conducted a GWR for the subregion Frickberg, additionally to the linear regression and ANOVA described above. It is a method first introduced by Brunsdon and Fotheringham that detects if and how response and predictor variables relate to each other spatially. The underlying assumption is that a global regression wrongly assumes the relationship of the variables to be identical no matter where in the study region it is investigated. GWR is a method to investigate geographical variation in data relationships and generates varying regression coefficients that are mappable. It has been a widely used method in various disciplines (Comber et al., 2022). A standard GWR builds upon a linear regression but at every predefined geographical location, data that is falling within a moving window or kernel is used to calibrate the regression model. It is a reflection of Tobler's first law of geography which observes that data in close proximity to each other oftentimes have similar characteristics. The standard GWR definition is as follows:

$$y_i = \beta_0(u_i, v_i) + \sum_{k=1}^{m} \beta_k(u_i, v_i) x_{ik} + e_i, \qquad (15)$$

where y_i is the response variable and x_{ik} the value of the predictor variable. The number of predictor variables is m. The spatial coordinates are defined as (u_i, v_i) of the observation i and the estimated coefficients at these locations is $\beta_k(u_i, v_i)$. $\beta_0(u_i, v_i)$ is the intercept term and e_i forms the error term.

Thus, GWR conducts a local regression to many different locations and estimates local coefficients while it uses the neighboring observations and weighs them according to their distance to the center of the moving window. This weight is defined by the bandwidth and a kernel-based distance decay function (Comber et al., 2022).

The use and determination of the bandwidth distincts different cases of GWR. The standard GWR uses a single bandwidth for all predictor variables assuming the relationship operates at the same scale for all predictor variables. In some cases, this might be unrealistic. To solve this problem, a multiscale GWR can be applied which estimates the bandwidth for every predictor variable separately (Comber et al., 2022).

Because the GWR approach is only an outlook, we did not test many different models, which is usually done in a GWR analysis. This could be done in further research.
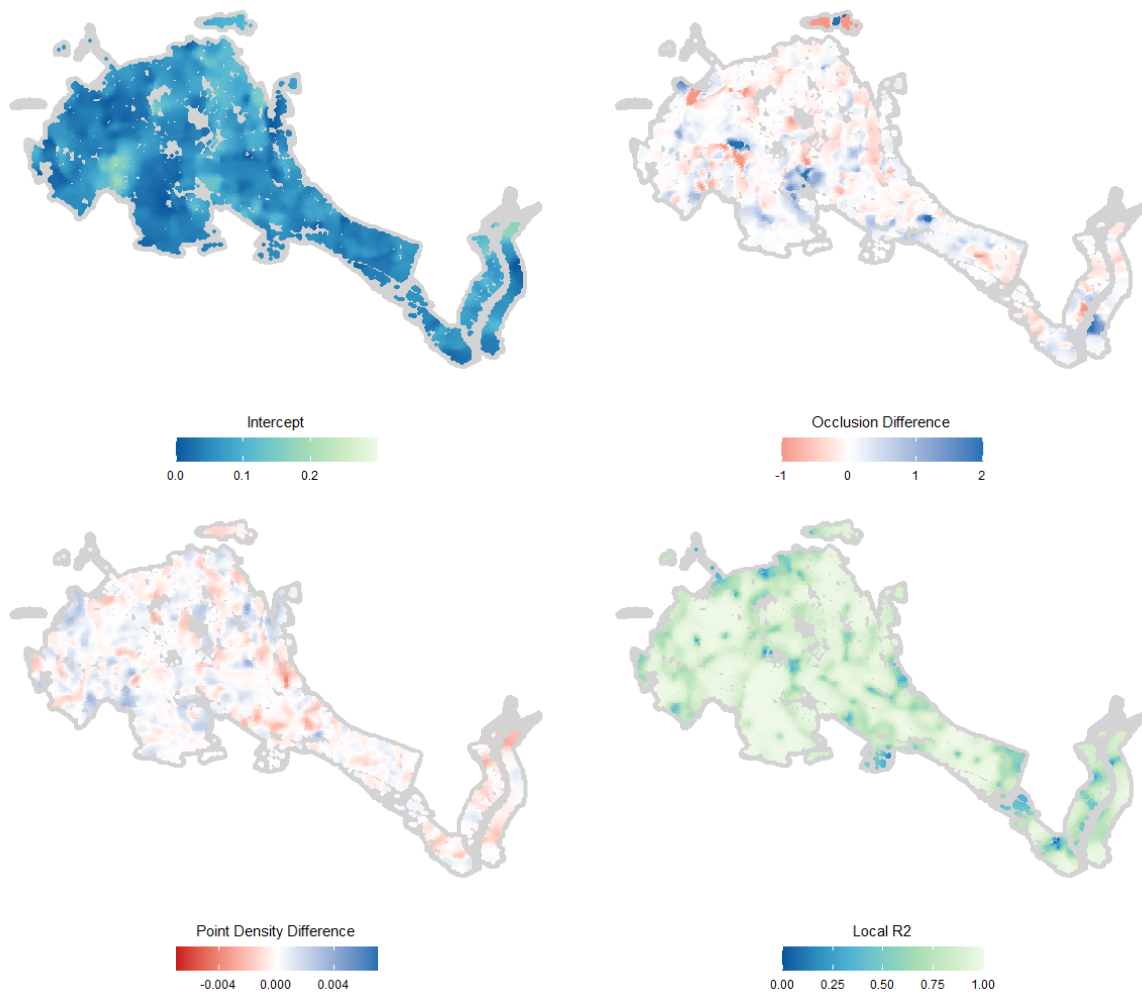
GWR Output of the FRic Model in Frickberg

Figure B.1: Spatial variation of the local coefficient estimates from the GWR FRic model in Frickberg.

```
***********************************************************************
*                       Package   GWmodel                            *
***********************************************************************
Program starts at: 2022-07-27 09:49:52
Call:
gwr.basic(formula = regmodB, data = data_sp, bw = gw.mb, kernel = "bisquare",
 adaptive = TRUE, longlat = FALSE, cv = TRUE)


Dependent (y) variable:  richness_diff
Independent variables:  occlusion_diff pt_dens_diff
Number of data points: 11017
```

```
    **********************************************************************
    *                     Results of Global Regression                  *
    **********************************************************************


    Call:
     lm(formula = formula, data = data)


    Residuals:
        Min        1Q    Median        3Q       Max
    -0.073575 -0.022510 -0.006286  0.015794  0.160506


    Coefficients:
                     Estimate Std. Error t value Pr(>|t|)
    (Intercept)     0.0555791  0.0005661  98.169  < 2e-16 ***
    occlusion_diff -0.0546976  0.0089746  -6.095 1.13e-09 ***
    pt_dens_diff    0.0000471  0.0000306   1.539    0.124


    ---Significance stars
    Signif. codes:  0 '***' 0.001 '**' 0.01 '*' 0.05 '.' 0.1 ' ' 1
    Residual standard error: 0.0319 on 11014 degrees of freedom
    Multiple R-squared: 0.004507
    Adjusted R-squared: 0.004326
    F-statistic: 24.93 on 2 and 11014 DF,  p-value: 1.573e-11
    ***Extra Diagnostic information
    Residual sum of squares: 11.20486
    Sigma(hat): 0.03189414
    AIC:  -44643.57
    AICc:  -44643.57
    BIC:  -55594.12
```

```
***********************************************************************
*          Results of Geographically Weighted Regression          *
***********************************************************************


********************Model calibration information********************
Kernel function: bisquare
Adaptive bandwidth: 78 (number of nearest neighbours)
Regression points: the same locations as observations are used.
Distance metric: Euclidean distance metric is used.

****************Summary of GWR coefficient estimates:****************
                   Min.     1st Qu.     Median     3rd Qu.     Max.
Intercept      -1.8455e-02  3.5706e-02  5.1720e-02  7.3261e-02  0.1942
occlusion_diff -4.4516e+02 -9.0962e-02  7.8198e-03  1.3046e-01 142.2138
pt_dens_diff   -4.0477e-03 -4.1594e-04 -2.0813e-05  4.1464e-04  0.0041
************************Diagnostic information************************
Number of data points: 11017
Effective number of parameters (2trace(S) - trace(S'S)): 1252.648
Effective degrees of freedom (n-2trace(S) + trace(S'S)): 9764.352
AICc (GWR book, Fotheringham, et al. 2002, p. 61, eq 2.33): -73010.54
AIC (GWR book, Fotheringham, et al. 2002,GWR p. 96, eq. 4.22): -74126.56
BIC (GWR book, Fotheringham, et al. 2002,GWR p. 61, eq. 2.34): -77346.38
Residual sum of squares: 0.7087457
R-square value:  0.9370317
Adjusted R-square value:  0.9289527
```
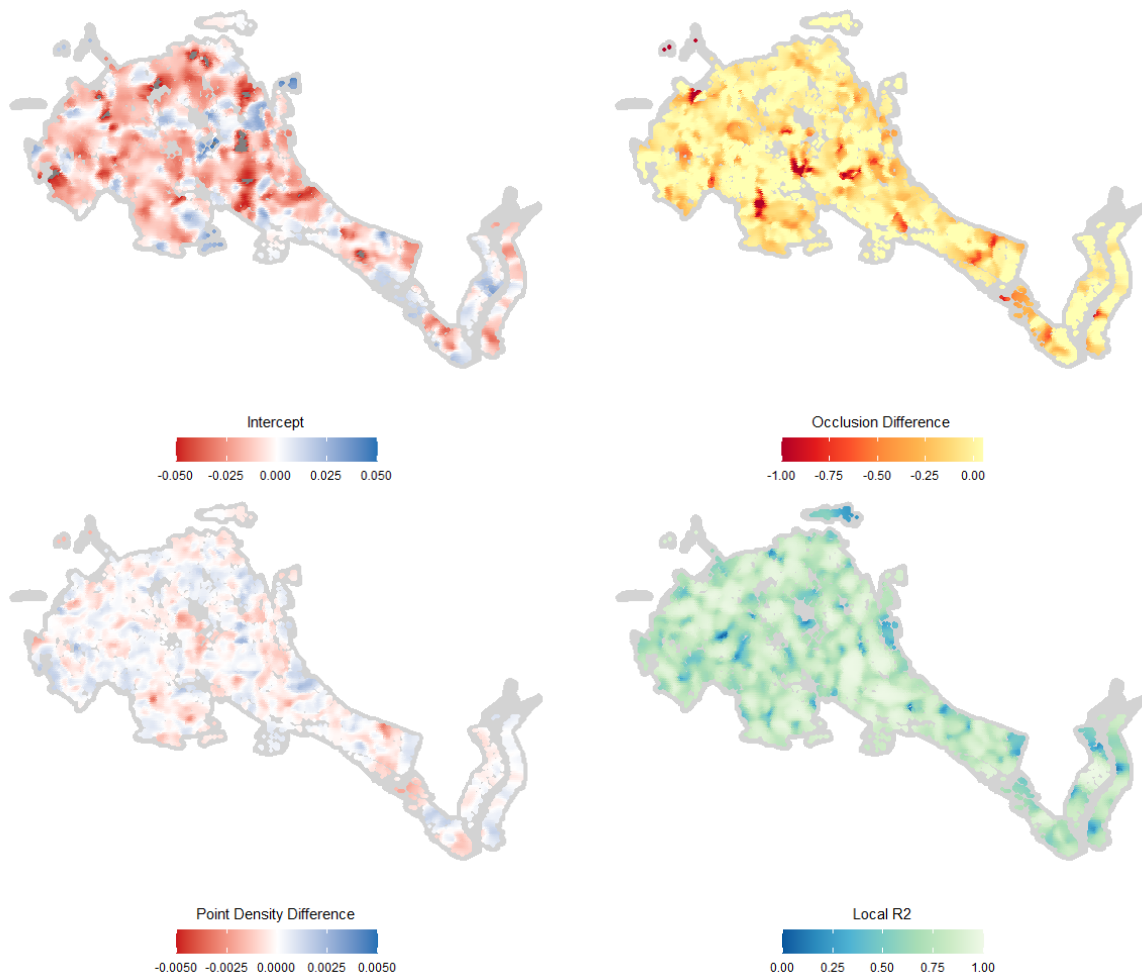
GWR Output of the FDiv Model in Frickberg

Figure B.2: Spatial variation of the local coefficient estimates from the GWR FDiv model in Frickberg.

```
   ***********************************************************************
   *                        Package   GWmodel                           *
   ***********************************************************************
   Program starts at: 2022-07-27 09:51:05
   Call:
   gwr.basic(formula = regmodD, data = data_sp, bw = gw.md, kernel = "bisquare",
    adaptive = TRUE, longlat = FALSE, cv = TRUE)


   Dependent (y) variable:  divergence_diff
   Independent variables:  occlusion_diff pt_dens_diff
   Number of data points: 11017
```

```
********************************************************************
*                      Results of Global Regression              *
********************************************************************


Call:
 lm(formula = formula, data = data)


Residuals:
    Min        1Q    Median        3Q       Max
-0.075579 -0.010019  0.000442  0.010324  0.081416


Coefficients:
                 Estimate Std. Error t value Pr(>|t|)
(Intercept)    -1.073e-02  2.938e-04 -36.518  < 2e-16 ***
occlusion_diff -1.673e-02  4.658e-03  -3.593 0.000329 ***
pt_dens_diff   -6.507e-05  1.588e-05  -4.097 4.22e-05 ***


---Significance stars
Signif. codes:  0 '***' 0.001 '**' 0.01 '*' 0.05 '.' 0.1 ' ' 1
Residual standard error: 0.01655 on 11014 degrees of freedom
Multiple R-squared: 0.00207
Adjusted R-squared: 0.001888
F-statistic: 11.42 on 2 and 11014 DF,  p-value: 1.109e-05
***Extra Diagnostic information
Residual sum of squares: 3.017941
Sigma(hat): 0.01655248
AIC:  -59095.37
AICc:  -59095.37
BIC:  -70045.91
```

```
**************************************************************************
*          Results of Geographically Weighted Regression          *
**************************************************************************


*********************Model calibration information********************
Kernel function: bisquare
Adaptive bandwidth: 78 (number of nearest neighbours)
Regression points: the same locations as observations are used.
Distance metric: Euclidean distance metric is used.

****************Summary of GWR coefficient estimates:*****************
                     Min.     1st Qu.      Median     3rd Qu.      Max.
Intercept      -8.8654e-02 -2.0333e-02 -1.1299e-02 -1.1397e-03   0.0556
occlusion_diff -3.8620e+00 -1.1574e-01 -1.2379e-02  7.2803e-02 146.6376
pt_dens_diff   -3.4939e-03 -4.4084e-04 -4.1222e-05  3.3534e-04   0.0025
************************Diagnostic information************************
Number of data points: 11017
Effective number of parameters (2trace(S) - trace(S'S)): 1252.648
Effective degrees of freedom (n-2trace(S) + trace(S'S)): 9764.352
AICc (GWR book, Fotheringham, et al. 2002, p. 61, eq 2.33): -76198.36
AIC (GWR book, Fotheringham, et al. 2002,GWR p. 96, eq. 4.22): -77314.39
BIC (GWR book, Fotheringham, et al. 2002,GWR p. 61, eq. 2.34): -80534.21
Residual sum of squares: 0.5306708
R-square value:  0.8245252
Adjusted R-square value:  0.8020116
```

C Appendix – List of abbrevations

2D	Two dimensional
3D	Three dimensional
AGIS	Aargauisches Geographisches Informationssystem
ALS	Airborne laser scanning
ANOVA	Analysis of variance
CH	Canopy height
DTM	Digital terrain model
FDiv	Functional divergence
FHD	Foliage height diversity
FR	First returns ratio approach
FRic	Functional richness
GWR	Geographically weighted regression
LiDAR	Light detection and ranging
LAI	Leaf area index
NaN	Not a number
NFI (LFI)	National forest inventory (Landesforstinventar)
NIR	Near-infrared
NR	Nature reserve
PAD	Plant area density
PAI	Plant area index
RTA	Ray-tracing approach
SAR	Synthetic aperture radar
SR	Scaled returns ratio approach
UF	Unprotected forest

Acknowledgements

Personal Declaration

I hereby declare that the submitted thesis is the result of my own, independent work. All external sources are explicitly acknowledged in the thesis.

Location, Date

Wohlen, 5. September 2022

Signature

Charis Moana Gretler